Auditory brainstem response latency in noise as a marker of cochlear synaptopathy

by

Golbarg Mehraei

Submitted to the The Harvard-MIT Division of Health Sciences and Technology
in partial fulfillment of the requirements for the degree of

Doctor of Philosophy in Health Sciences and Technology

at the

MASSACHUSETTS INSTITUTE OF TECHNOLOGY

February 2016

Signature redacted

Author .....
The Harvard-MIT Division of Health Sciences and Technology
November 16, 2015

Signature redacted

Certified by .....
Barbara Shinn-Cunningham, PhD
Director, Center for Computational Neuroscience and Neural Technology/Professor, Biomedical Engineering, Boston University
Thesis Supervisor

Signature redacted

Accepted by .....
Emery N. Brown, MD, PhD
Director, Harvard-MIT Program in Health Sciences and Technology/Professor of Computational Neurosciences and Health Sciences and Technology

Auditory brainstem response latency in noise as a marker of cochlear synaptopathy

by

Golbarg Mehraei

Submitted to the The Harvard-MIT Division of Health Sciences and Technology
on December 11, 2015, in partial fulfillment of the
requirements for the degree of
Doctor of Philosophy in Health Sciences and Technology

Abstract

Communication in environments with multiple competing sound sources can be challenging, even for listeners with normal hearing thresholds (NHT). This difficulty in “normal" listeners is thought to arise from central sites of the auditory system with the assumption that sound encoding at the auditory nerve (AN) is robust. Despite this assumption, growing evidence from animal and human studies suggests that acoustic exposure, too modest to elevate hearing thresholds, can nonetheless cause “hidden hearing loss" that interferes with coding of supra-threshold sound. In animal studies, such noise exposure leads to cochlear synaptopathy (death of auditory nerve fibers or ANFs); however, there is no clinical test of synaptopathy in humans. In animals, synaptopathy reduces the amplitude of auditory brainstem response (ABR) wave-I. Unfortunately, ABR wave-I is difficult to measure in humans, limiting its clinical use.

Here, using behavioral, otoacoustic, and electrophysiological measures in humans and mice in conjunction with computational models of sound processing by the auditory periphery and brainstem, we show that the effect of masking noise on the latency of the more robust ABR wave-V mirrors changes in ABR wave-I amplitude. In our human cohort, the effect of noise on wave-V latency predicts perceptual temporal sensitivity. Further, we show evidence that ABR wave-V latency in forward masking may be affected by ANF loss and is predictive of a listener’s performance in a perceptual task related to speech intelligibility in noise. Our results suggest that measures of the effects of masking on ABR wave-V latency can be used to diagnose ANF survival in humans.

Thesis Supervisor: Barbara Shinn-Cunningham, PhD
Title: Director, Center for Computational Neuroscience and Neural Technology/Professor, Biomedical Engineering, Boston University

Acknowledgments

I would like to start by thanking my advisor, Barbara Shinn-Cunningham, who has taught me many lessons that I could not have learned in any classroom. Barb gave me the freedom to pursue and develop my ideas. Her mentorship and guidance has helped me become a better research scientist and it's difficult to articulate my gratitude of having her as a mentor and friend.

I thank my thesis committee members, Charles Liberman, Bertrand Delgutte, and Dimitrios Pantazis for their valuable feedback and criticism throughout the development of the thesis.

This work has truly been a collaborative effort. First, I would like to thank Ann Hickox for sharing her animal data and guiding me through the analysis. My sincere gratitude to Andreu Parades-Gallardo and Hannah Goldberg for helping me collect data. I would also like to thank Torsten Dau for his mentorship during my time in his lab.

I am very thankful to be part of the Speech and Hearing Bioscience and Technology (SHBT) community, and want to thank the professors and instructors for their dedication to the program and students. My SHBT class, thank you for the support and encouragement through the first couple of years.

To my colleagues at the Auditory Neuroscience Lab, thank you for welcoming me as a friend and showing me that research is supposed to be fun and exciting. I very grateful for all the collaborations and many valuable discussions. I particularly thank Hari Bharadwaj and Sarah Verhulst for paving the way for my thesis through their research. Our many discussions were critical in shaping the ideas in this thesis.

To my dear friends, thank you for all the fun and support throughout the years of our friendship. I have learned so much from you and am grateful to have such amazing friends.

Finally, I want to thank my family for all their love and encouragement. To my parents, Bahar and Parviz, thank you for instilling in me that learning is important and that you must be persistent in your pursuit for answers. To my brother, Payam,

thank you for your love and kindness.

This doctoral thesis has been examined by a Committee of the Department of Health Science and Technology as follows:

Professor M. Charles Liberman .....
Chairman, Thesis Committee
Director, Eaton-Peabody Laboratories

Professor Barbara Shinn-Cunningham .....
Thesis Supervisor
Professor of Biomedical Engineering, Boston University

Professor Bertrand Delgutte .....
Member, Thesis Committee
Professor of Otology and Laryngology, MEEI

Dimitrios Pantazis .....
Member, Thesis Committee
Research Scientist, Director of MEG lab, McGovern Institute for Brain Research

Contents

List of Figures

List of Abbreviations

ABR	Auditory brainstem response
AVCN	Antroventral Cochlear Nucleus
2AFC	Two alternatives, forced choice
AN	Auditory nerve
ANF	Auditory nerve fiber
APD	Auditory processing disorder
BM	Basilar membrane
CF	Characteristic Frequency
CN	Cochlear nucleus
CAP	Compound action potential
CAPD	Central auditory processing disorder
COAE	Click-evoked otoacoustic emissions
DPOAE	Distortion product oto-acoustic emission
EEG	Electroencephalogram
EFR	Envelope following response
ENV	Envelope
ERB	Equivalent rectangular bandwidth
FFR	Frequency following response
HI	Hearing impairment
HL	Hearing level
IHC	Inner Hair Cell
IC	Inferior colliculus
ITD	Interaural time difference

LL	Lateral Lemniscus
ME	Middle Ear
MOC	Medial olivocochlear complex
MPI	Masker to probe interval
MSO	Medial Superior Olive
NHT	Normal hearing thresholds
PCA	Principal component analysis
peSPL	Peak sound pressure level
SNR	Signal-to-noise ratio
SOC	Superior Olivary Complex
SPL	Sound pressure level
SR	Spontaneous (discharge) rate
TFS	Temporal fine structure
UR	Unitary response

Chapter 1

INTRODUCTION AND BACKGROUND

1.1 Acoustic overexposure in the "normal" hearing

Communication in situations where multiple sound sources compete for attention can be challenging, even for listeners who have audiometrically normal hearing threshold (NHT). Indeed, as many as 5-15% of adult patients seeking audiological help for this difficulty turn out to have normal audiometric thresholds [59, 48]. Such listeners are often diagnosed with "central auditory processing disorders" (CAPD/APD, [20]) reflecting the assumption that sound is represented robustly in the AN [48, 78] and that deficits arise from more central processing centers.

In contrast to this assumption, recent animal studies reveal that noise exposure causing only reversible, temporary threshold shifts, can nevertheless produce an immediate and permanent loss (herein referred to as "synaptopathy") of up to 50% of the synapses and cochlear-nerve terminals innervating inner hair cells (IHCs; [58, 36, 68]). Aging also appears to reduce the auditory nerve fiber (ANF) population independent of hair cell loss [106, 107, 73]. Crucially, even large reductions in the number of intact ANFs (e.g. as much as 85% loss) do not seem to affect audiometric thresholds in quiet [71], rendering this loss invisible to traditional clinical evaluations.

Models and recent data suggest that synaptopathy could degrade the coding of both temporal fine-structure (TFS) and temporal envelope (ENV) cues – cues that are important for everyday communication – in clearly audible, supra-threshold sounds [72, 6, 8, 5]. Indeed, recent human data reveals large individual differences in behavioral measures of temporal coding in NHTs listeners. These differences correlate with physiological brainstem measures that may be affected by ANF loss [91, 5]. Furthermore, listeners who have greater noise exposure history show reduced ANF response amplitudes (i.e., ABR wave-I amplitudes; [113]), consistent with the effects of noise-induced cochlear synaptopathy on ABR wave-I in animals.

ANFs with low spontaneous discharge rates (low-SR; SR<20 spikes/s) are particularly susceptible to neuro-degeneration caused by noise exposure and aging [106, 11, 36, 68] . These fibers, by virtue of the fact that they have higher thresholds than high spontaneous rate (high-SR; SR>20 spikes/s) fibers, increase the dynamic range of the auditory periphery [63]. In addition, low-SR fibers are thought to be important for hearing in noisy environments, as they are more resistant to masking by continuous background noise [22]. These facts elucidate why a selective low-SR ANF synaptopathy could lead to hearing loss that only reveals itself through perceptual difficulties when processing supra-threshold sound, even though it has no discernable effect on thresholds.

Motivated by these results, we hypothesize that the number of low-SR ANFs conveying information about supra-threshold sound varies across NHT listeners, resulting in differences in communication ability. AN degeneration may be widespread in humans, evidenced by post-mortem temporal bone analyses [73]. A noninvasive test that reveals the fidelity of the peripheral representation of supra-threshold sound, and that quantifies ANF loss, could have a major impact on evaluation and diagnosis of communication disorders amongst NHT listeners.

1.2 Supra-threshold coding of sound

1.2.1 Encoding of sound via auditory nerve fibers

ANFs are vital for encoding acoustic information about our environment. An ANF contacts a single IHC via a single synapse. At each synapse, an electron-dense ribbon sits near the pre-synaptic membrane surrounded by a halo of glutamatergic vesicles. Environmental sound entering the ear canal is funneled through the tympanic membrane, and middle ear, vibrating the stapes, and leading to cochlear traveling waves. Along the length of the cochlea are sensory cells, the IHCs that detect vibration within the cochlea via stereocilia bundles at their apical surface. The vibrations caused by the cochlear traveling wave deflect IHC stereocilia, opening mechanoelectric transduction channels that lead to a graded change in the IHC membrane potential. This sound-driven receptor potential causes an influx of calcium at the base of the IHC where the ANFs synapse. The calcium influx increases the probability of glutamate release into the synaptic cleft. The release of neurotransmitter leads to the generation of action potentials in an ANF. This AN response to sound then ascends through several nuclei of the brainstem, midbrain and cortex, to eventually elicit an auditory percept [37].

ANFs can be divided into two groups classified by their spontaneous rate (SR; i.e., the spike rate in the absence of intentionally introduced sound). Fibers with low-SR have thinner axons, fewer mitochondria, and predominately innervate the modiolar side of the IHC. In contrast, high-SR fibers, have thicker axons, more mitochondria, and synapse onto the pillar side of the cell [65]. ANF groups also differ in their sensitivity to sound. High-SR fibers have the lowest thresholds, and low-SR fibers have the highest. In quiet environments, high-SR fibers dominate encoding of sounds. However, as sound level increases to 20-30dB above threshold, the average discharge rate of high-SR fibers saturates and low-SR fibers begin to respond. The group-related differences in threshold sensitivity widen the dynamic range and may be important for intensity coding in the auditory system where level discrimination abilities are near-constant over a range of 100dB or more [33, 120].

ANF groups also differ in their contribution to hearing in noisy environments. High-SR fiber activity is relatively easy to mask with continuous noise because these fibers are so sensitive to sound. Their continuous activation even by near-threshold noise may cause vesicle depletion, which prevents them from responding to other signals that might be present [22, 21]. In contrast, by virtue of their higher thresholds, the lower-SR fibers are more resistant to background noise. Thus, with increasing levels of continuous masking noise, lower-SR fibers likely become increasingly important to the encoding of acoustic signals, as they will show the largest changes in average discharge rate in response to transient supra-threshold stimuli [127].

1.2.2 Importance of temporal coding on auditory perception

Although different perceptual attributes of natural sound are encoded by different spectro-temporal cues, many depend on reliable timing information. The AN encodes temporal information in two forms; the temporal fine structure (TFS), corresponding to the timing of the nearly sinusoidal narrowband carrier fluctuations, and the slower temporal envelope of that carrier. ANFs in the low-frequency cochlear regions encode both TFS and temporal envelope; their spike pattern is phase-locked to the carrier and their instantaneous firing rate locked to the envelope. At higher frequencies, ANFs do not phase-lock to the TFS; however, temporal information is conveyed by phase-locking to envelope fluctuations. Such encoding mechanisms are important for the computation of interaural time differences (ITD), used for spatial perception of sound. While perceptually, TFS information in low-frequencies is the dominant perceptual cue determining perceived location [124], for broadband and high-frequency sounds, ITDs can be conveyed by the envelope alone [4]. Additionally, the encoding of the temporal envelope of sound may play a significant role in space perception in everyday settings such as rooms, where reverberant energy distorts TFS cues [7, 25]. The coherence of the temporal envelope across channels helps to perceptually bind together different acoustic constituents of an object in the auditory scene [31, 108]. Coding of pitch and speech formants also may rely on both TFS and envelope temporal

information (see [90], for a review). Thus, a range of temporal features in both TFS and envelopes is necessary to enable a listener to parse mixture of sounds, select a sound source of interest, and analyze its meaning.

In everyday settings, the auditory system is often required to analyze temporal information at supra-threshold sound intensities. Further, everyday settings typically contain competing sound sources and reverberant energy, which degrade the temporal structure of the sound reaching a listener's ear. This degradation may render spatial information about a single source such as ITD diffuse and make speech less intelligible [114, 49].

Given that convergence of multiple fibers underlies an enhancement in the fidelity of temporal coding at higher nuclei along the auditory pathway [50, 86, 52], it is likely that a decrease in the number of fibers making up the auditory nerve population will degrade temporal coding [72] and lead to perceptual difficulties when trying to understand speech in challenging settings. In addition, considering the relative robustness of low-SR fibers to masking [22, 21, 127] and better synchrony to amplitude-modulations at moderate to high sound levels [51], a selective low-SR neuropathy would further increase the likelihood of perceptual difficulties in processing supra-threshold sound.

1.3 Auditory brainstem response

The present study focuses on the ABR as a potential measure of cochlear synaptopathy in humans. The ABR, which is often measured with transient stimuli, is a series of vertex-positive waves that represent far-field activity produced by onset responses of neural elements along the auditory brainstem pathway. The ABR is critically dependent on the synchronous activity of a large number of the responding neural units to produce a detectable and repeatable response. At high stimulus levels, the ABR consists of seven peaks, each attributed to different generator sites along the brainstem, as shown in Fig.1-1 [76, 88]. As such, it is a useful clinical tool for separating peripheral (cochlear-eighth nerve-ABR wave-I) from central

(brainstem) changes [19].

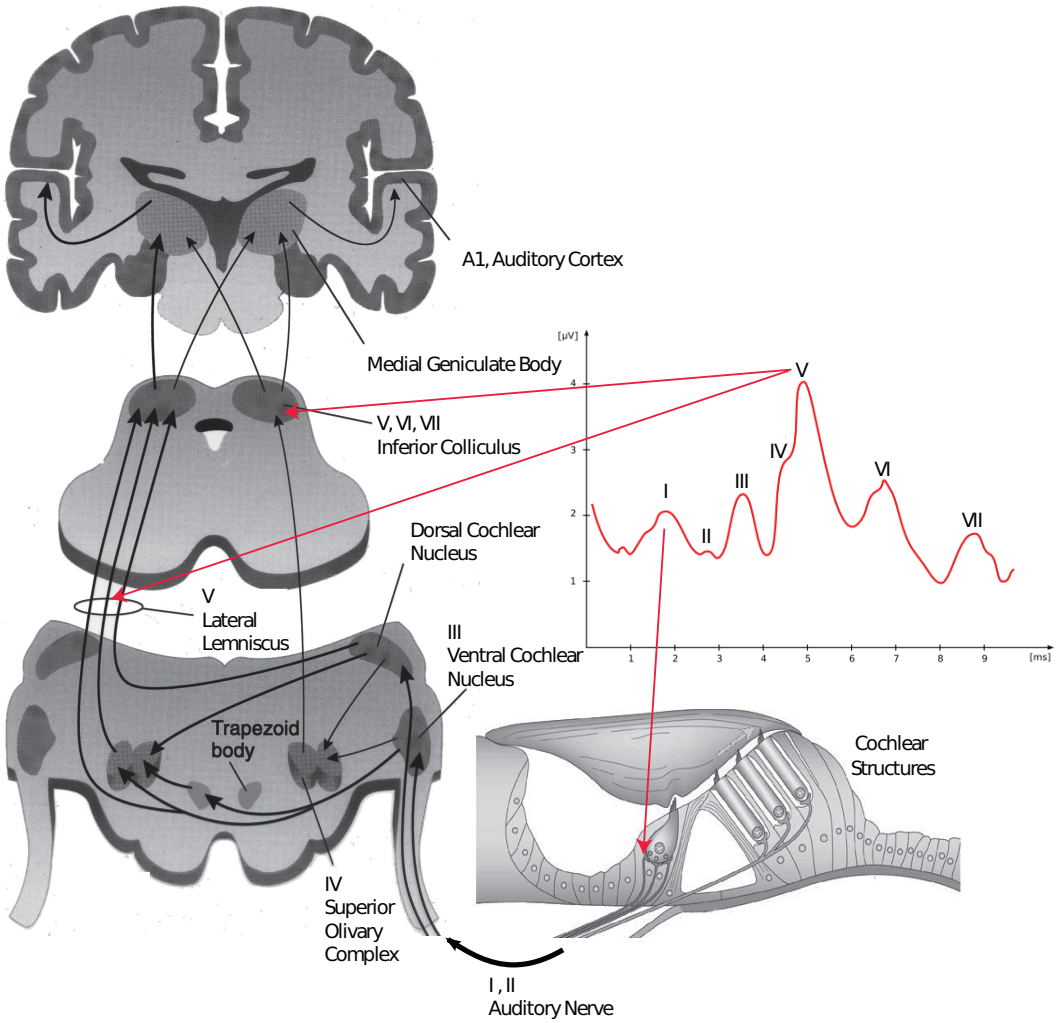

Figure 1-1: Neural generators of the seven waves in the auditory brainstem response. ABR wave-I is often the smallest wave in human measurements as shown and is believed to be generated at the IHC and AN synapse. ABR wave-V, the most robust wave in humans, is generated in the lateral lemniscus and/or inferior colliculus.

In animal studies, changes in supra-threshold amplitudes of ABR wave-I are well correlated with cochlear synaptopathy, so long as the cochlear amplifier is undamaged [58]. Although ABR wave-I amplitude can be a useful objective measure of ANF loss in animals, there is a great deal of within-subject variability in this response in humans; thus, making it challenging to use clinically. One approach to reducing this variability would be to measure the growth rate of wave-I amplitude with stimulus level. Nonetheless, it is difficult to obtain a robust ABR wave-I at low

stimulus levels in humans. In contrast, ABR wave-V, generated in the Lateral Lemniscus and/or Inferior Colliculus (LL, IC; Fig.1-1), is a more robust response in humans and can be recorded at low stimulus levels and in the presence of background noise. However, ABR wave-V magnitude does not seem to be affected by cochlear synaptopathy, potentially due to gain control mechanisms of the central auditory system [107].

Another approach is to evaluate ABR latency, specifically wave-V. In quiet, wave-V latency decreases monotonically with increasing stimulus level [23], in part because cochlear excitation spreads towards high-frequency cochlear regions with increasing level, and high-frequency regions have shorter latencies [83, 46]. In contrast, when a fixed-level ABR-evoking stimulus (e.g., a click), is presented in background noise, mimicking some of the constraints faced by the auditory system in noisy real-world listening conditions, ABR wave-V latency increases with growing background noise level [12, 13, 16]. The underlying mechanisms of this latency shift with noise level are not fully understood, but are ascribed to synaptic and neural processes.

Here, we argue that the ABR wave-V latency shift with increasing noise level could reflect the recruitment of low-SR fibers because 1) the onset response latency of low-SR responses is delayed relative to that of high-SR fibers [100, 79, 11] and 2) low-SR ANFs are more resistant to background noise [22, 127]. If true, a selective loss of low-SR fibers should yield a smaller ABR latency shift with increasing noise level. Furthermore, if this latency measure reflects low-SR ANF loss, the rate at which it changes should correlate with perceptual measures of fine temporal encoding that rely on low-SR responses [5].

1.4 Forward masking ABR

Another systematic difference according to SR is the AN response recovery time to prior stimulation. In forward masking, the response to a stimulus (probe) is decreased by the presence of a preceding stimulus (masker). This type of non-simultaneous masking is believed to arise because of depletion of synaptic vesicles by the masker,

limiting the number of vesicles available to respond to the probe [45]. As the delay between the masker and the probe increases, the probe response recovers to control (i.e., no peceding masker). Animal studies show that low-SR fibers have a longer recovery time (>100ms) than that of high-SR fibers (<100ms) [95]. This difference has not only been shown on a single unit AN level but also on a population level. There is evidence of low and high-SR contribution to the recovery of the compound action potential (CAP, which represents the summed activity of the AN and is equivalent to ABR wave-I amplitude) from forward masking in humans and animal [96, 80]. The recovery of the CAP can be modeled by two separate exponential functions that characterize the fast and slow component of the recovery time course as shown in Fig.1-2. The fast time component of the CAP recovery predominately reflects the recovery of high-SR fibers whereas the slow time component of the CAP recovery function is believed to be low-SR dominated. A selective loss of low-SR fibers with age is shown to yield a faster recovery of the CAP [106].

Changes to CAP/ABR wave-I amplitude in forward masking could prove useful in teasing apart the loss of low-SR fibers. However, as mentioned earlier, ABR wave-I measurements are difficult to obtain and quantify. Thus, we wondered whether the change in wave-V latency as a function of masker to probe interval (MPI) would reflect loss of ANFs. In forward masking, as the probe-elicited ABR wave-I amplitude increases with increasing MPI, the wave-V latency subsequently decreases [57, 13, 9, 121]. We hypothesize that the low-SR contribution to forward masking not only slows down the recovery of the ABR wave-I amplitude but also that this reduced input translates to a wave-V latency that does not shift as much with MPI. Low-SR fibers deafferentation may yield a faster recovery of the probe-elicited ABR wave-I amplitude and thereby a greater change in ABR wave-V latency with increasing MPI. This will be more evident at shorter MPIs where both low and high-SR fibers contribute to the response. Indeed, there is some evidence that older NHT listeners and aged animals have a greater shift in wave-V latency in forward masking at short MPIs, in line with our hypothesis [9, 121].

Here we sought to determine whether individual differences in ABR wave-V

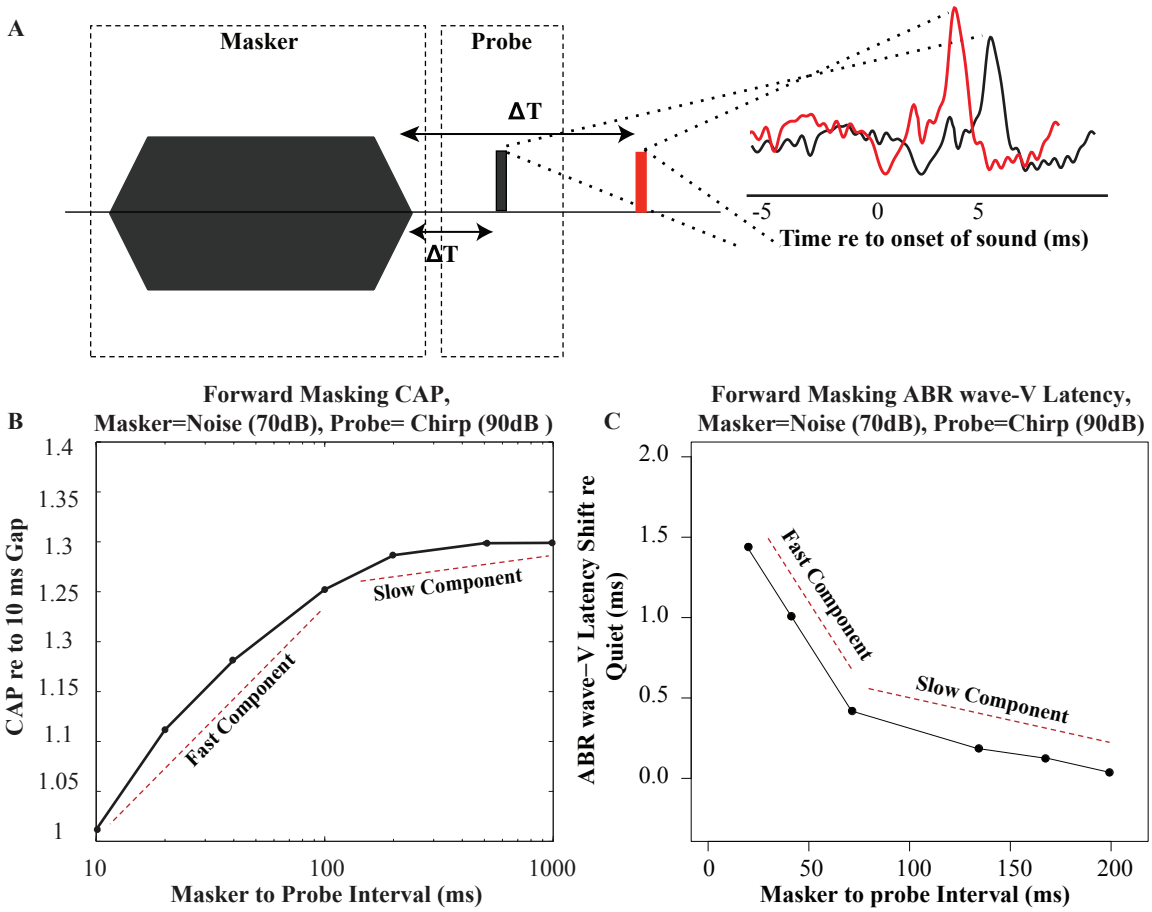

Figure 1-2: A: Forward masking is defined as a decreased probe response, depicted by a reduced CAP, following a preceding masker. At short masker to probe intervals (MPIs), not only is the CAP small but the ABR wave-V latency is delayed relative to the control (no preceding masker). As the gap between the masker and the probe increases, the CAP grows and the wave-V latency decreases. B: Model simulation of the relative change of the CAP with increasing MPI. The forward masking recovery function of the CAP can be characterized by two exponential functions with different time constants. At short MPIs <100ms), the CAP changes more rapidly, reflecting the recovery of the high-SR and low-SR fibers. This portion is defined as the fast time component of the CAP forward masking function. At MPI >100ms, the CAP changes more slowly, following the slow recovery of the low-SR fibers as the high-SRs have fully recovered by a MPI of 100ms. Model used [118]. C: In forward masking, as the MPI increases, the ABR wave-V latency shift relative to quiet decreases (absolute wave-V latency decreases). Similar to the CAP forward masking recovery function, the wave-V latency recovery function has a fast and slow component.

latency changes in young NHT listeners reflects differences in low-SR population size. Selective loss of low-SR fibers may help explain why some listeners have difficulty hearing in noisy environments. As such, to determine whether these differences predict perceptual measures related to temporal coding and speech intelligibility in noise, we chose to measure forward masking behavioral thresholds, a correlate of speech-recognition in interrupted noise [29].

Chapter 2

SPECIFIC AIMS AND RATIONALE

This thesis is dedicated to the study of individual differences in ABR latency in noise and forward masking among NHT listeners and how this timing is affected by ANF loss. The project is divided into two aims: first, characterizing supra-threshold fidelity in listeners with NHTs and comparing to measures of ABR and second, modeling ABR latency changes in noise. The results of the various experiments and modeling efforts provide evidence that a dominant contribution to individual differences in ABR latency in noise likely comes from differences in low-SR ANF population. Additionally, these differences in the ABR latency seem to predict an individual's performance in perceptual tasks that are important when listening in complex environments.

2.1 Aim I. Understanding individual differences in sensory coding of listeners with NHTs

It is evident from past studies that there is large variability in performance on tasks relying on fine spectro-temporal cues in supra-threshold sound in listeners with NHTs [56, 102, 5]. We believe that differences in temporal coding fidelity in ascending ANFs help explain these variations in NHT listeners: such differences may arise due to variation in the population of ANF responding to sound, which may be the result of noise exposure or genetic factors that causes degeneration of ANFs. Our goal here is

to determine whether we can use clinical ABR latencies, specifically wave-V latency, to reveal ANF loss and ultimately predict an individual's listening ability in noisy settings.

Here, we will quantify relationships amongst ABR and perceptual measures of supra-threshold coding for listeners with normal audiometric thresholds. Hypothesis: ABR wave-V latency changes in noise and in forward masking reflect low-SR ANF survival and vary significantly in NHT listeners with normal cochlear mechanics. If so, these individual differences in wave-V latency should be correlated with perceptual differences important for communication in noisy environments. We measured audiograms and click-evoked otoacoustic emission growth functions. In listeners with normal cochlear mechanics, we measured ABRs using clicks in quiet and in noise stimuli. ABRs were also measured using a forward masking paradigm using noise maskers and chirp probes. In the same listeners, we measured envelope interaural timing difference (ITD) sensitivity and forward masking detection thresholds.

2.2 Aim II. Modeling ABR wave-V latency changes in noise

Latencies of ABR wave-V vary with increasing stimulus and noise level. Specifically, the ABR wave-V latency decreases by 1.5-2ms for a stimulus level increase of 40dB [23, 30] and increases by 1ms with growing background noise level over a 50dB range [12]. Past ABR models have largely focused on simulating latency changes with increasing stimulus level [23, 101]. Although they have been able to qualitatively account for latency changes, they underestimate the level dependency of click-evoked ABR wave-V latency [101]. A recent auditory model [118] predicts that wave-V latency is sensitive to the number of responding ANFs. Although this model has been able to successfully capture ABR wave-V latency decrease as a function of increasing stimulus level, model predictions of ABR wave-V latency changes in noise have yet to be accomplished.

Based on recent model predictions and experimental results, we attempted to accurately simulate ABR wave-V latency increase with growing background noise and explore how preferential loss of different fiber types affects the change in latency in noise. Existing models were utilized and altered to simulate single-unit and population responses at different stages along the auditory pathway. Additionally, using the same models, we explored how selective loss of low-SR fibers affects the CAP recovery in forward masking and how that may translate to ABR wave-V latency changes with MPI.

Chapter 3

METHODS

3.1 Measures of ABR, temporal coding, and cochlear mechanics

All measures were obtained with the participants seated in an acoustically and electrically shielded booth (single-walled Eckel C-14 booth, Cambridge, MA). For passive ABR measures, participants watched a silent, captioned movie of their choice, ignoring the acoustic stimuli. A personal desktop computer controlled all aspects of the experiment, including sound delivery and storing data. Special-purpose sound-control hardware (System 3 real-time signal processing systems, including D/A conversion and amplification; Tucker Davis Technologies, Gainesville, FL) presented sound through insert phones coupled to foam ear tips. ER-1 insert phones (Etymotic, Elk Grove Village, IL) were used for ABR wave-I and behavioral ITD measures. ER-10c earphones were used for the ABR in noise measurements to simultaneously record click-evoked otoacoustic emissions (COAE). All sounds were digitized at a sampling rate of 48.828 kHz. For the behavioral experiments, subjects responded by button presses.

3.1.1 Participants

Twenty four (nine female) subjects, aged from 20-40 years (mean=26.95), were recruited from the Boston University and Massachusetts Institute of Technology community. All subjects had pure-tone hearing thresholds better than 20dB HL in both ears at octave frequencies between 250 and 8000Hz. Subjects provided informed consent in accordance with protocols established at Boston University. Subject availability precluded some subjects from completing some measures.

3.1.2 Envelope interaural timing difference

To obtain a binaural measure of temporal coding, detection of ongoing envelope ITD was measured using a transposed tone with a carrier at either 2 or 4kHz and an envelope modulation frequency of 50Hz [4]. The carrier phase was identical in the two ears; the ITD was applied only to the 50Hz envelope. The 450ms stimulus was ramped with a 20ms $\cos^2$ rise-decay (simultaneously in the two ears) to minimize the use of onset cues. The stimulus level was set at 80dB SPL. Off-frequency notched-noise maskers, generated independently in each trial, were presented at an SNR of 10dB (broadband RMS) as illustrated in Fig.3-1, B. The off-frequency masker extended to 20Hz on the low-frequency side and 20kHz on the high-frequency side and served to attenuate off-frequency listening cues, including cues from distortion products. The bandwidth of the notch was set to the equivalent rectangular bandwidth (ERB) of the respective carrier frequency (i.e., ERB at 2kHz=240.58Hz and at 4kHz= 456.46Hz) [38]. To determine whether limiting listeners to use of within-channel timing information enhances individual differences in temporal coding, we tested an additional noise condition for the 2kHz carrier. A diotic noise, low-pass filtered at 1.3kHz, was presented with the stimulus (Fig.3-1, C) to preclude the listener's use of any information at low frequencies such as distortion products [4]. Conditions were presented in alternating blocks. All noises were gated on 400ms prior to the first stimulus interval, and gated off 200ms after the third interval.

Threshold ITDs were determined using a three-interval, two alternative forced

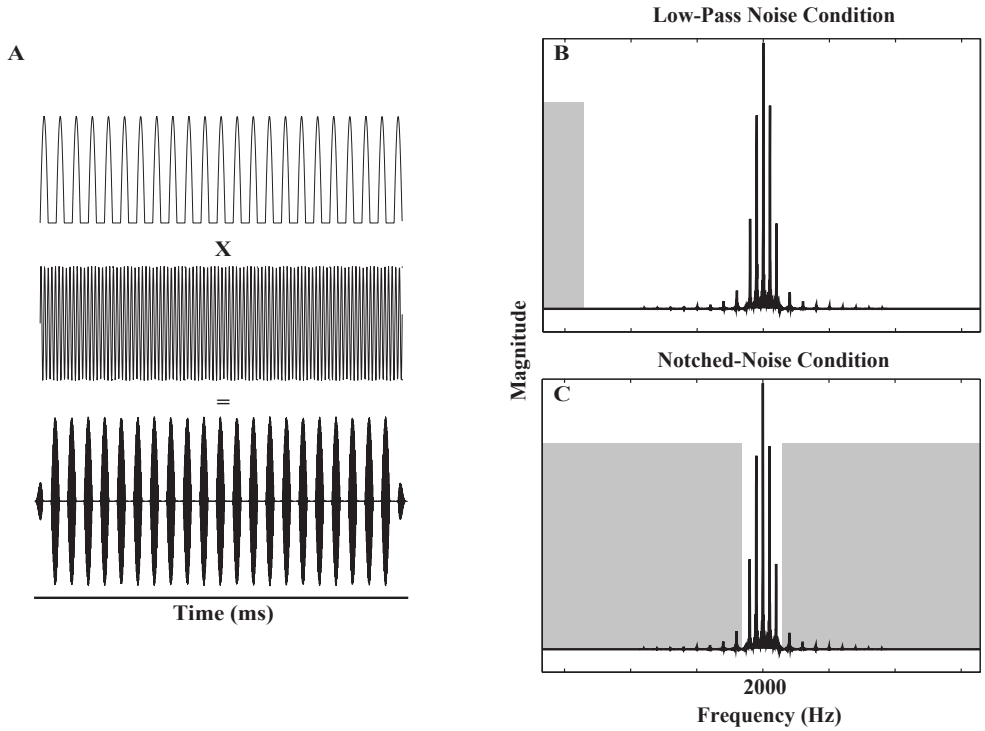

Figure 3-1: A. Schematic representation of the method used to generate transposed stimuli. A 50Hz sinusoid was half-wave rectified, low pass filtered (cutoff=2kHz), and transposed onto 2 or 4kHz carrier. B. Illustration showing the spectrum of the transposed tone presented simultaneously with a low pass noise. This condition was implemented for the 2kHz carrier. C. Spectrum schematic of transposed tone presented simultaneously with notched noise. This condition was used for both 2 and 4kHz carrier.

choice adaptive task (2AFC). Each interval, marked visually by a computer monitor, occurred at intervals of 800ms. The first interval always contained the stimulus with an ITD=0 and served as a reference interval. The listener's task was to detect and identify the presence of an ITD (right ear leading) that was presented with equal probability in the second or third interval. A combination of nonparametric, 2-up 1-down, and parametric, maximum likelihood procedure (MLP) was used to determine the ITD threshold. The 2-up 1-down procedure [62] was used initially for 7 reversals. The listener was presented with a starting ITD of 900μs. The initial step size was 100μs. After 2 reversals, the step size was reduced to 50μs and 25μs after 4 reversals.

The threshold estimation was then switched to the MLP [40]. In this procedure,

a set of psychometric functions with the same slope, attentional lapse rate, and chance level, but different midpoints were hypothesized. After each trial, the subject's responses up to that trial were used to calculate the likelihood of each hypothesis (i.e., each psychometric function). The ITD of the next presented trial was chosen based on the 80.9% correct point on the psychometric function with the highest likelihood. This procedure was repeated until the ITD estimates of the last four trials were within an 80μs range of each other.

Each condition was repeated twice for a total of four blocks in each session. Additional blocks were presented if any of the runs for a condition were off by more than one standard deviation from the mean. The final ITD threshold was defined as the mean of the thresholds, discarding outliers.

3.1.3 Auditory brainstem response measures in noise and quiet

Click-evoked ABRs were measured dichotically using a 32-channel EEG system (Biosemi Active II system, Amsterdam, Netherlands). The better ear was chosen for testing based on the subject's audiogram. If there was no difference between the ears audiometrically, the left ear was chosen. ABRs were collected using a 80μs click presented at a rate of 10Hz via ER-10C insert earphones. A 20ms inter-click jitter was introduced to avoid the accumulation of any stationary interference including the 60Hz power-line noise.

ABR wave-V measures were recorded for five different click levels varying from 50-90dB peSPL in 10-dB steps. ABRs in noise were measured using a click presented at 80dB peSPL in broadband background noise varying from 42-82 dB SPL in 10-dB steps. The bandwidth of the noise was limited by the sampling rate used to generate the stimuli (i.e. 48kHz) and the frequency response of the earphones. Each condition had 3000 repetitions. Conditions were presented in randomly ordered blocks. The 32 channels were referenced to the average of the mastoid channels.

Recorded data sampled at 16.384kHz was passband filtered between 100-2000Hz.

Power line noise (60Hz and harmonics) was removed by applying Thomson's regression method for detecting sinusoids in signals as implemented in the Chronux toolbox [10]. The filtered data were then time-epoched from -10ms to 10ms relative to the onset of the stimulus. Bad channels and trials were removed by analyzing the distribution of the overall amplitude across channels and trials. Specifically, a channel or trial was removed if its cumulative amplitude was two standard deviations away from the mean of the distribution. The number of channels and trials were equalized across conditions for each subject. The averaged epoched response from all good channels were combined to yield an ABR.

The averaged across channel ABR peak-to-baseline amplitude and peak latency of waves-I and -V, respectively, were identified using visual overlay cursors on a computer screen. The slope of the wave-I amplitude with stimulus level, and of wave-V latency change with noise and stimulus level, was computed by fitting a straight line across the conditions in which the waveforms were identifiable. A minimum of three conditions where the ABR waves-I and V were clear was required for the linear fits.

3.1.4 Click-evoked Otoacoustic Emissions

To obtain an objective correlate of cochlear-mechanical compression, COAE were measured simultaneously with the ABR measurements using $80\mu s$ clicks at levels of 50-90dB peSPL in 10dB increments. Each click level was presented 3000 time. COAES were filtered using a 250-6000Hz bandpass filter as they are most reliable from 1000 to 3000Hz [34]. To obtain estimates that are robust to artifacts, trials were combined by calculating the sample by sample median instead of the mean. The spectrum of the COAE was computed and the magnitude was compared to the spectrum of the noise floor, defined as the difference between the odd and even trials (Fig.3-2).

To provide more frequency-specific information, CEOAE responses were band-filtered in octave-bands centered at 1000, 2000 and 4000Hz and the signal power was calculated for each band. The COAE growth function at each band is defined as the difference between the COAE power (in dB) and the input level. Across listeners, reliable COAEs were obtained at least in one octave-band at click levels greater than

60dB peSPL. As such, the amount of compression in each frequency band, defined as the slope of the COAE growth function using a linear fit on log-scale, was determined using COAEs at click levels of 70, 80, 90dB peSPL.

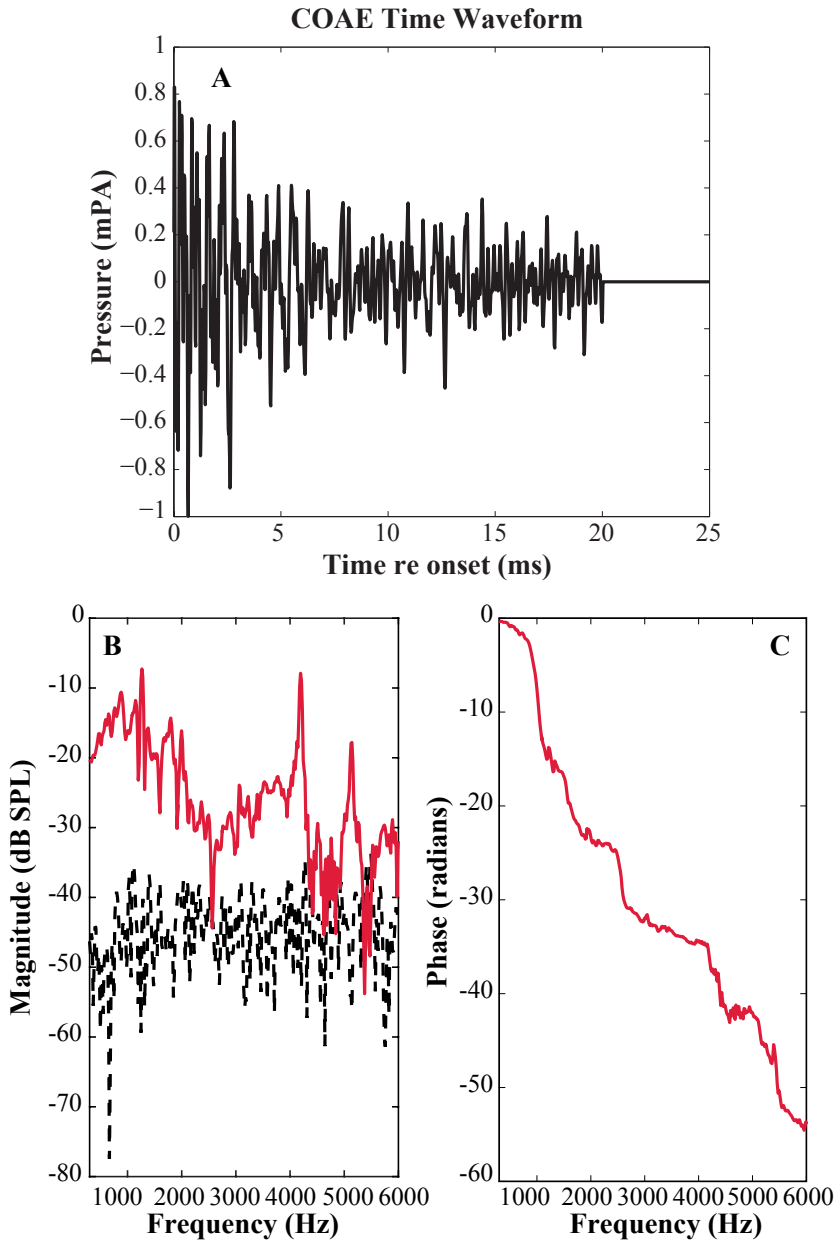

Figure 3-2: Sample COAE of a 90dB peSPL click. A: Time waveform of COAE. B: Spectrum of COAE depicted in red and the noise floor in black. Notice that the COAE are strongest around the 1 to 2kHz frequency region. C: Phase of the COAE.

3.2 Animal measurements

The animal measurements were conducted by Ann Hickox during her PhD with Dr. M.Charles Liberman and were generously given to me to analyze. The animal subjects and methods have been previously described in detail in Hickox and Liberman (2014; [47]). In brief, CBA/CaJ male mice (Jackson Laboratories) were exposed in groups to moderate-level noise at 16-18 wks of age, and cage-mates served as unexposed age- and sex-matched controls. Measures of both cochlear and auditory neural function were recorded to assess the degree of recovery from noise exposure. Counts of synaptic ribbons per inner hair cell confirmed noise-induced loss of cochlear synapses. An additional assay, the masked ABR, was recorded in subsets of exposed and unexposed mice to investigate new physiological indicators of noise-induced cochlear synaptopathy, reported for the first time here. All procedures were approved by the Institutional Animal Care and Use Committee of the Massachusetts Eye and Ear Infirmary.

3.2.1 Noise exposure

Mice were exposed for 2 hours to octave-band noise (8-16kHz) at one of two levels, 100 or 94dB SPL. The 100dB "neuropathic" exposure in these mice, causes only transient threshold elevation and extensive cochlear synaptopathy and neural loss in the basal half of the cochlea [58]. The 94dB "non-neuropathic" exposure was designed to cause similar transient threshold elevation and no ANF loss [47], providing a control group for non-specific exposure-related effects. Mice were placed, awake and unrestrained, in an acoustically transparent cage within a small reverberant chamber. The noise waveform was digitally generated (fifth-order Butterworth filter), amplified (Crown Power Amplifier D75A), and presented with a compression driver (JBL model 2446H) through an exponential horn in the roof of the chamber.

3.2.2 Physiology: Auditory brainstem response and distortion product otoacoustic emission

ABRs and DPOAEs were measured in the left ear of each mouse 6-10 weeks post-exposure, under ketamine/xylazine anesthesia (100mg/kg and 20mg/kg, respectively, via i.p. injection). A custom acoustic assembly containing two miniature dynamic speakers and an electret condenser microphone (Knowles FG-23329-P07) was placed within millimeters of the tympanic membrane for delivery of all stimuli and recording of DPOAEs. The assembly was calibrated using a 1/4-inch condenser microphone (Bruel & Kjaer), and each recording session began with in-ear calibrations. Stimulus generation and data acquisition were controlled by custom LabVIEW software on a National Instruments PXI system (16- or 24-bit sound cards).

To assess outer hair cell-based cochlear function, DPOAEs were recorded using primary frequencies f1 and f2 (f2/f1 = 1.2), where f2 = 8-45.3kHz in half-octave steps. For each set of primaries, levels L1 and L2 (L1-L2 = 10dB) were swept from L2 = 10-80dB SPL in 5-dB steps. Amplitude of the cubic distortion product 2f1-f2 was extracted from averaged ear canal spectra. DPOAE threshold was interpolated from amplitude input/output functions at 2f1-f2 = 5dB SPL.

To assess auditory brainstem function in quiet, ABRs were recorded using 4-ms tone-pips (0.5 ms $\cos^2$ rise-fall, alternating polarity, 40/s) at 32kHz. Levels were swept from 15-80dB SPL in 5-dB steps. At each level average waveforms were generated from 1024 presentations (512 stimulus pairs), amplified 10,000X, band-pass filtered from 0.3-3kHz and stored for offline analysis. Responses were differentially recorded from subdermal needle electrodes at the vertex and ventral edge of left pinna, with ground at the base of the tail. ABR wave-I growth functions were constructed using peak 1 amplitude at each level, defined as the difference between a 1-ms average of the pre-response baseline and the wave-I peak (with additional high-pass filtering to remove low-frequency baseline shifts).

Masked ABRs were recorded as for ABRs in quiet, using 32kHz tone pips at 60 and 80dB SPL. Broadband masking noise was generated and played with each tone-

pip presentation. The magnitude spectrum of the masking noise compensated for the CBA/CaJ mouse audiogram constructed from single-unit ANF thresholds, such that a particular noise level would have a similar masking effect across ANFs of different characteristic frequencies regardless of their absolute thresholds. This method was implemented using average ANF threshold data binned according to characteristic frequency in half-octave bands centered at 4-45.3kHz in half-octave steps (with linear interpolation between points). Masking noise was swept from -5-85dB SPL in 5-dB steps. Wave-IV peak latency was defined through visual analysis by two judges, and wave-IV latency slope was calculated as for human data.

3.2.3 Histology: synaptic ribbon counts

Left inner ears were extracted from three mice for each group (100dB neuropathic exposure, 94dB non-neuropathic exposure, unexposed controls), selected as representative ears based on ABR wave-I amplitude. Ears were extracted following intracardiac perfusion (4% paraformaldehyde) while deeply anesthetized, and were postfixed for 2 hours at room temperature. Following decalcification in EDTA for 2-3 days, the cochlear spiral was microdissected into six whole-mount pieces that were immunostained with the following: primary antibodies overnight at 37 (mouse anti-CtBP2 at 1:200, BD Transduction Labs; rabbit anti-Myosin VIIa at 1:200, Proteus Biosciences no. 25-6790), and secondary antibodies for 1 hour at 37 (biotinylated donkey anti-mouse at 1:200 followed by streptavidin-conjugated Alexa Fluor 568 at 1:1,000; Alexa Fluor 647-coupled donkey anti-rabbit at 1:200).

Whole-mount pieces were imaged using confocal microscopy (Leica TCS SP2) at specific cochlear frequency-locations that were identified using a reconstruction of the cochlear frequency map across pieces (custom ImageJ plug-in). For a given location, two adjacent regions were captured as z-stacks using an oil-immersion x100 objective (1.4 NA) with x2 digital zoom and a z-step of $0.25\mu m$. Z-stacks of the inner hair cell base area were analyzed offline as 3D reconstructions in Amira (Visage Imaging). Individual ribbons (anti-CtBP2 puncta) were quantified and expressed as synaptic ribbons per number of inner hair cells in the stack (anti-Myosin VIIa cytoplasmic

label).

3.3 Forward masking

The forward masking behavioral and ABR measures were carried out at Technical University of Denmark in Lyngby, Denmark. During the experiments, subjects were seated in an acoustically and electrically shielded booth (double-walled from IAC). For the forward masking ABR measures, participants watched a silent, captioned movie of their choice, ignoring the acoustic stimuli. A desktop computer outside the booth controlled all aspects of the experiment, including triggering, sound delivery and storing data. The stimuli were presented via Fireface UCX (RME, Haimhausen Germany) and triggers were sent from a RME ADI-8 trigger box (RME, Haimhausen Germany). A headphone driver presented sound through ER-2 insert phones (Etymotic, Elk Grove Village, IL). All sounds were digitized at a sampling rate of 44.1kHz. For the forward masking behavioral experiments, subjects responded using a touch screen in the booth. All tests were measured in the left ear with the exception of one subject.

3.3.1 Participants

Twenty (four female) subjects, aged from 20-40 years (mean=26.95), were recruited from Technical University of Denmark in Lyngby, Denmark. All participants had pure-tone hearing thresholds better than 20dB HL in the tested ear at octave frequencies between 125 and 8000Hz shown in Fig.3-3. Subjects provided informed consent in accordance with protocols established at Technical University of Denmark.

3.3.2 Pure Tone Thresholds

Pure-tone thresholds were measured for each subject using a three-interval alternative forced choice task (AFC; the psychophysical-measurement package for MATLAB, University of Oldenburg, Germany). Thresholds were collected in the tested ear at

octave frequencies between 125 and 8000Hz, each 100ms in duration. On each trial, the presentation of each interval was indicated by highlighting the interval button on the screen. The listener was asked to identify which of the three intervals contained the pure-tone signal. Intervals were separated by 201ms and trials were separated by 660ms. A nonparametric, 2-up 1-down adaptive procedure was used to obtain thresholds [62]. Pure-tone level started at 50dB SPL and was reduced by 5, 2, and then 1dB in the tracking procedure to reach threshold. The step-size was changed after each upper reversal. Threshold was defined as the mean of the last six reversals. This measure was repeated twice for each pure-tone. If a threshold was a standard deviation away from the mean of the two repetitions, an additional threshold would be measured for the pure-tone(s) condition(s). Outlying thresholds were not used in the analysis.

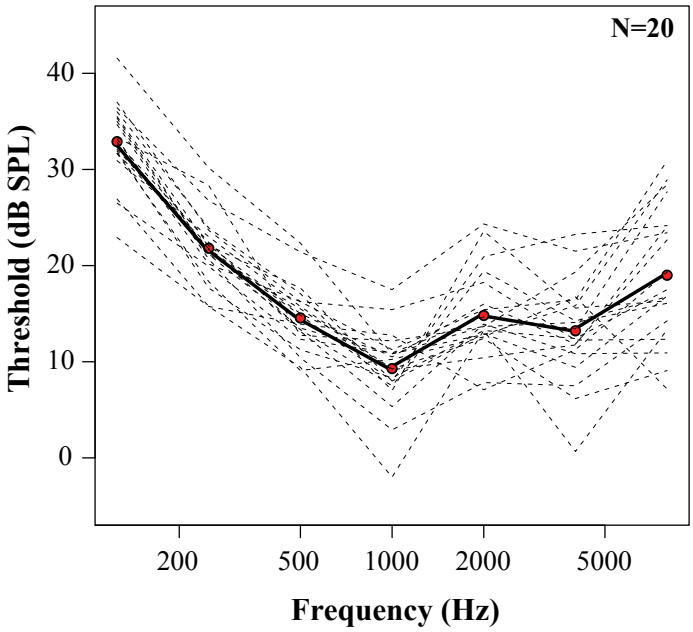

Figure 3-3: Pure-tone thresholds expressed in dB SPL for each participant of the forward masking study. Solid line represents mean threshold at each tested frequency. Dashed lines depict individual pure-tone thresholds.

3.3.3 Forward masking behavioral experiment

The same AFC package described above was used to measure forward masking detection thresholds. The masker was a 100ms broadband noise presented at a level of 35 and 70dB SPL. The noise was ramped with a 20ms $\cos^2$ rise-decay to minimize the use of onset cues. The bandwidth of the noise was limited by the sampling frequency (i.e., 44.1kHz) and the frequency response of the ear phones. The probe was a flat-spectrum, broadband, "synchronized" chirp spanning the frequency of 0.08-20kHz [24]. This chirp is designed to account for the group delay observed in the traveling wave along the cochlea by first presenting low- and then high-frequency components in time [24]. As illustrated in Fig.1-2, the probe was presented following the masker at MPIs of 20, 40, 72, 132, 168, and 201ms. On each trial, two of the three intervals contained only the masker and one interval presented the masker followed by the probe at a fixed MPI. Listeners were asked to identify the interval in which the probe was present. For each MPI and masker level condition, the probe level was varied to obtain detection threshold. The probe level started at 70dB peSPL and was adaptively changed using the same step-sizes in the pure-tone threshold procedure. Conditions were randomly presented in blocks and two repetition of each condition was implemented. A third repetition was acquired if any of the thresholds were a standard deviation away from the mean across repetitions.

Additionally, chirp thresholds (i.e. without a preceding masker) were measured using the same experimental design. Subject's were asked to identify the chirp in one of three intervals on each trial. The chirp level started at 50dB peSPL and was varied adaptively.

3.3.4 Forward masking ABR

Forward masking ABRs were recorded in the left ear using a 5-channel EEG system (Biosemi Active II system, Amsterdam, Netherlands). The 5-channel configuration included channels, Pz, Cz, Fz on the 32-channel cap along with the left and right mastoids. ABR was measured using the same masker and probe as in the forward

masking behavioral task (i.e. masker=100ms broadband noise at 35 and 70dB SPL, probe=synchronized chirp). In contrast to the forward masking detection task, the probe level was fixed at 90dB peSPL to elicit a strong response from low and high-SR fibers. A repetition rate of 2Hz, measured from onset of masker in the previous trial to onset of masker in the current trial, was used to limit adaptation and fatigue in the ANFs. In addition, a 20ms jitter was introduced in the repetition rate to avoid the accumulation of any stationary interference including the 50Hz power-line noise.

Forward masking ABR was recorded for MPIs of 20, 40, and 201ms at different masker levels (35 and 70dB SPL) yielding a total of 6 stimulus conditions. Each condition had 1500 repetitions presented randomly. Additionally, chirp-ABR (without a preceding masker) was recorded for the control condition using the same chirp level and repetition rate. The channels were referenced to the average of the mastoid channels. The ABR wave-V was best identified using the Cz to average mastoids; thus, we used this configuration for wave-V latency analysis.

Recorded data sampled at 16.384kHz was filtered between 100-2000Hz. Power line noise (50Hz and harmonics) was removed by applying Thomson's regression method as implemented in the Chronux toolbox [10]. The filtered data were then time-epoched from -10 to 10ms relative to the offset of the chirp. Bad trials were removed by analyzing the distribution of the overall amplitude across trials. The number of trials was equalized across conditions for each subject. Peak latency of wave-V was identified using visual overlay cursors on a computer screen. The change in wave-V latency was defined as the difference in the wave-V latency across tested MPIs .

3.4 Statistical tests

Unless otherwise specified, statistical inference was performed by fitting mixed-effects models to the data and adopting a model comparison approach [3]. Fixed-effects terms were included for the various experimental factors whereas subject-related effects were treated as random. In order to not over-parameterize the random effects, models were compared with and without each term using the Akaike information criterion [89].

All model coefficients and covariance parameters were estimated using restricted maximum likelihood as implemented in the lme4 library in R. An F approximation for the type-II scaled Wald statistic was employed to make inferences about the fixed effects [54]: this approximation is more conservative in estimating Type I error in contrast to the Chi-squared approximation and performs well even with complex random-effects covariance structures [104]. The p-values and F-statistics based on this approximation are reported.

Chapter 4

EXPERIMENTAL RESULTS

4.1 ABR in noise

The purpose of this study was two-fold: to determine 1) whether noise-induced cochlear synaptopathy in animals influences how ABR wave-V latency shifts with increasing background noise level and 2) if ABR wave-V latency shifts are related to individual differences in supra-threshold temporal coding in a group of young NHT human listeners.

Methods and measures were designed to reveal the contributions of low-SR fibers, which have been shown to be vulnerable to noise exposure [106, 36, 68] and may be important for coding in acoustic scenes with multiple talkers and background noise [8, 5]. Specifically, we employed:

1. High sound levels, where the contribution of low-SR fibers to the overall population response is greater, in contrast to low sound intensities where the response is high-SR dominated [63].

2. Broadband noise maskers for our ABR measures, to highlight the resistance of low-SR fibers to background noise [22, 127].

3. Off-frequency maskers for our psychophysical measures, to reduce the contribution of off-frequency high-SR fibers to encoding of the target stimulus.

Envelope ITD sensitivity was chosen as the target task because sound localization based on timing information relies on the time-locked synchronous response of ANFs.

We specifically studied sensitivity to envelope ITD with carrier frequencies of 2 and 4kHz because noise-induced threshold shifts often present as notches around 4kHz, and because ABR wave-V arises from mid to high frequencies [1].

4.1.1 Click-evoked otoacoustic emissions

Fig.4-1 shows the mean COAE spectral power growth rate relative to input click level in each frequency band. The growth rate (i.e., slope) of the COAE spectral power relative to the input level (i.e., COAE spectral power-click level) represents the amount of compression in those frequency regions, which likely reflects OHC function [110, 109]. If there is OHC damage, the COAE is expected to grow more linearly with click level. The growth function was fitted on a log scale; thus, a slope of 0 would mean that the COAE spectral power grew linearly with increasing stimulus level while a negative slope depicts a compressive growth.

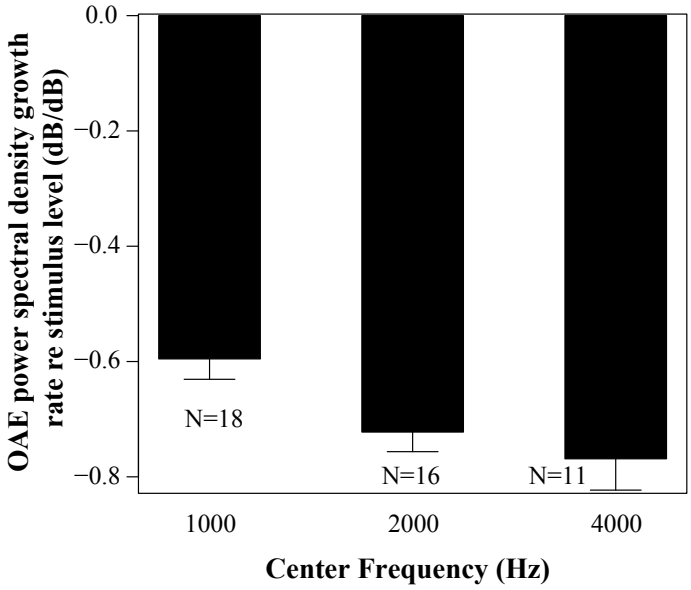

Figure 4-1: Mean COAE spectral power growth rate with increasing stimulus level for each frequency band. Growth rate is the slope of the normalized COAE spectral power as a function of the stimulus level. COAE spectral power is normalized to the stimulus level. Error bars depict standard error. Notice that the number of subjects varies for each frequency band as not all subjects had reliable COAE in each frequency band.

There appears to be larger compression in the higher frequency bands and moderate variability across subjects, as depicted by the standard error. However, we found no significant correlation between the individual differences in this measure and that of the envelope ITD thresholds or the ABR wave-V latency shifts with noise. Thus, the differences we observe in the ABR and ITD measure do not seem to be significantly affected by changes in cochlear mechanics.

4.1.2 Wave-V latency, wave-I amplitude and temporal acuity in humans

Click-evoked ABRs recorded with scalp electrodes showed a robust wave-V in both quiet and noise-masked conditions. Responses to stimuli in quiet showed a clear decrease in wave-V latency with increasing stimulus level, consistent with earlier reports (e.g., [23]). This effect is likely due to the broadening of peripheral auditory filters with level, yielding shorter impulse responses and an excitation pattern that peaks more basally along the basilar membrane [83, 46]. In contrast, masked ABRs showed evidence of increasing wave-V latency with background noise level Fig.4-2 (A-D). Measuring the slope of this latency vs. masker-level function, as calculated by linear fit, helps normalize for inter-subject differences in the timing of this wave due to gender, age and anatomy [77]. As seen in Fig.4-3, wave-V latency shift varied over a wide range for our NHT subjects from, 0.0018-0.0464ms/dB. From here on we will refer to this slope as the "ABR wave-V latency shift".

Concomitantly, we found large individual differences in the binaural measure of temporal coding fidelity, like that observed in prior studies [5, 102]. When an off-frequency masker was used, envelope ITD thresholds for carrier frequencies of 2 and 4kHz varied over a wide range across our NHT listeners, from about 200μs to 800μs, Fig.4-3 (B and D). This range is greater, and the threshold values are higher, than past reports (e.g., [27]). These difference may arise because, unlike previous studies, we 1) presented our stimuli at a relatively high intensity, 2) introduced off-frequency maskers, and 3) tested a lower envelope modulation rate. When the

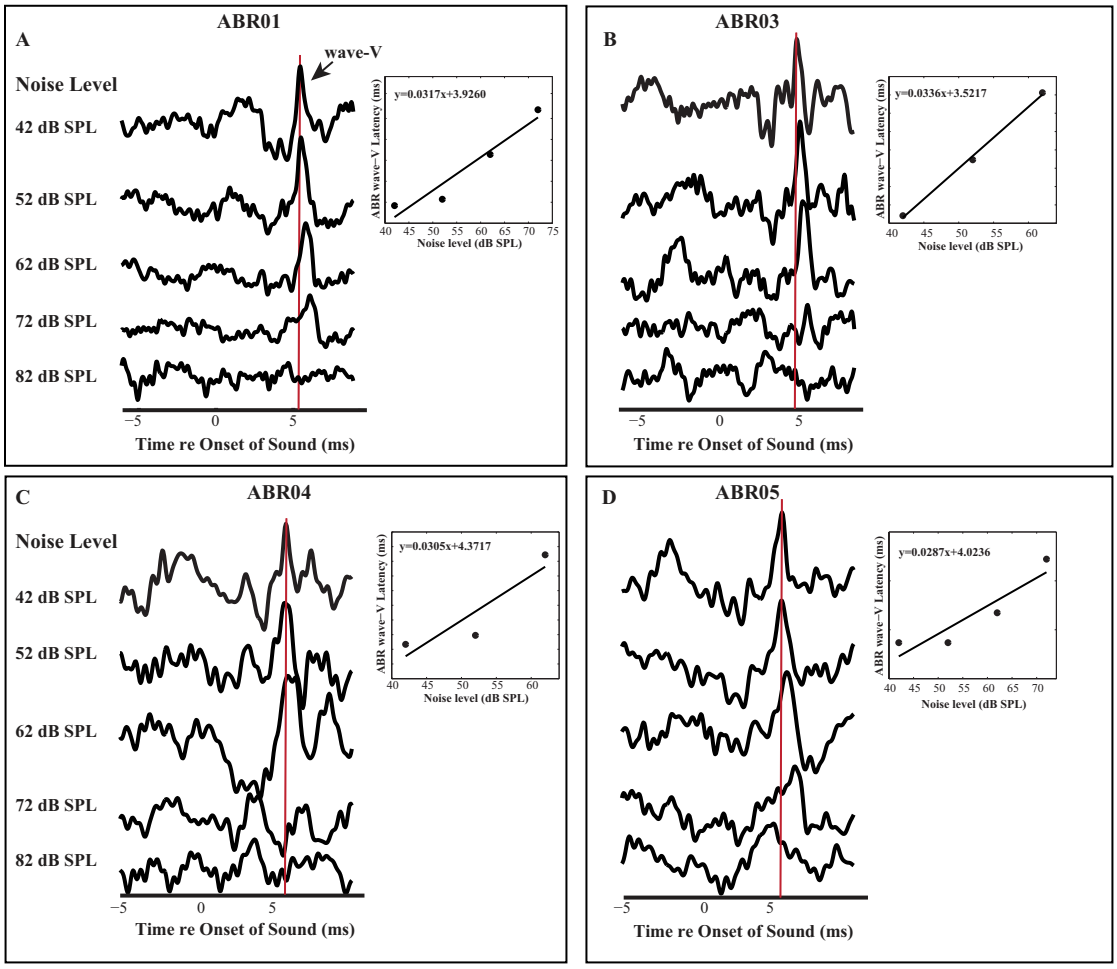

Figure 4-2: Sample human ABRs in noise using a 80dB peSPL click at different background noise levels for 4 listeners. Note how wave-V latency shifts with increasing noise level. At each noise level, peak ABR wave-V latency was defined and a linear regression was fitted to all noise level conditions where ABR wave-V was identifiable for each listener (inset in each plot). The slope of each fit was used for analysis.

stimulus is presented with a low-pass noise alone Fig.4-3 (C), the envelope ITD thresholds improve and the variability decreases, suggesting that listeners benefit from recruitment of off-frequency high-SR fibers in this temporal encoding task.

To evaluate the relative contributions of different factors to envelope ITD discrimination, we used a linear mixed-effects regression model. The model included fixed-effect terms for age, pure-tone thresholds at 2 and 4kHz, gender, carrier frequency, and ABR wave-V latency shift. Although the 2 and 4kHz pure-tone thresholds were correlated with envelope ITD threshold, their respective contributions to ITD sensitivity cannot be disentangled from each other. However, because neither is correlated with the ABR wave-V latency shift, discarding them does not affect inferences about how the ABR wave-V latency shift is related to envelope ITD coding. The main effect of the ABR wave-V latency shift was significant for predicting the envelope ITD thresholds [$F(1,14.671)=15.16$, $p=0.0015$].

Post-hoc analysis revealed that the smaller the wave-V latency shift, the poorer the listener was at detecting changes in envelope ITD in the presence of off-frequency masking noise (Fig.4-3 B and D). This correlation was significant for both the 2kHz ($r=-0.538$, $p=0.0098$) and 4kHz carrier frequencies ($r=-0.636$, $p=0.0019$). However, when off-frequency cues were not masked (i.e., only low-pass masking noise is used), the two measures did not correlate ($r=-0.418$, $p=0.0605$, Fig.4-3, (C). Further, the amount that the notched noise affects a listener's ITD threshold relative to the low-pass noise condition was correlated with the ABR wave-V latency shift ($r=-0.476$, $p=0.046$): listeners who were hurt more by the notched noise had a smaller wave-V latency shift, as shown in Fig.4-4. This is consistent with the interpretation that the individual differences in envelope ITD sensitivity in notched noise (Fig.4-3, B and D) are driven primarily by the contribution of on-frequency ANFs and reflect the temporal encoding of low-SR fibers. At higher stimulus levels, as tested here, the low-SR fibers are relatively more synchronized to the envelope modulation of the acoustic signal than high-SR fibers [8]. Thus, the timing difference in the envelope of our stimulus may largely but not entirely be encoded by the low-SR fibers.

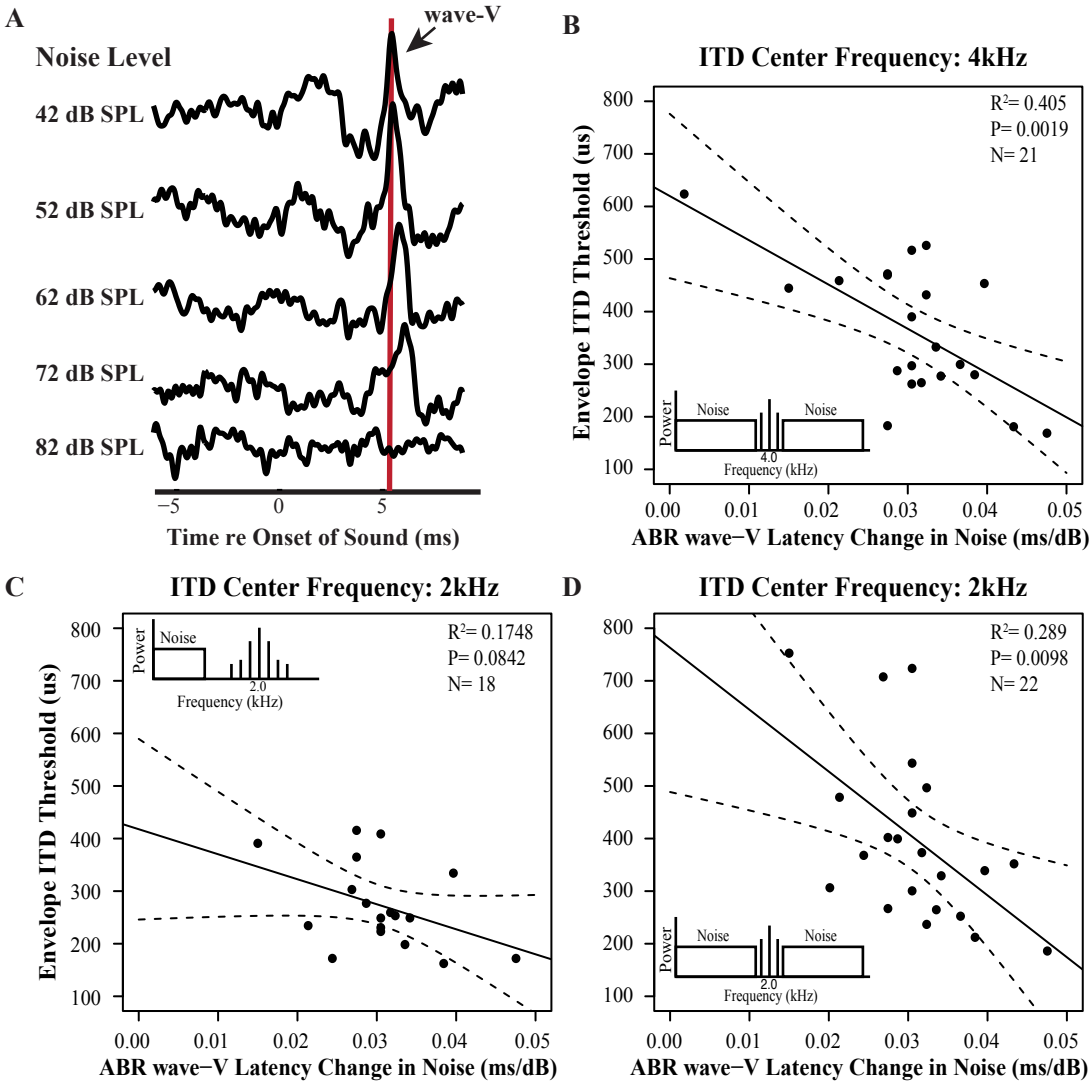

Figure 4-3: ABR wave-V latency change in noise correlates with perceptual performance on temporal-cue tasks. A: Sample masked human ABRs using a 80dB peSPL click at different background noise levels. The rate of change of the wave-V latency with noise level was compared to envelope ITD sensitivity measured using a transposed tone with center frequency of B: 4kHz and D: 2kHz presented with notched noise. Notch width was equivalent to the ERB of the used center frequency. X-axis in plots depicts the slope of each fit. There is a significant correlation between sensitivity to envelope ITD and the slope describing ABR wave-V latency change with noise level when the ITD sensitivity is measured using notched noise. When the transposed tone was presented with a low-pass noise, allowing off-frequency listening (C), the envelope ITD sensitivity did not correlate with the masked ABR wave-V latency rate of change.

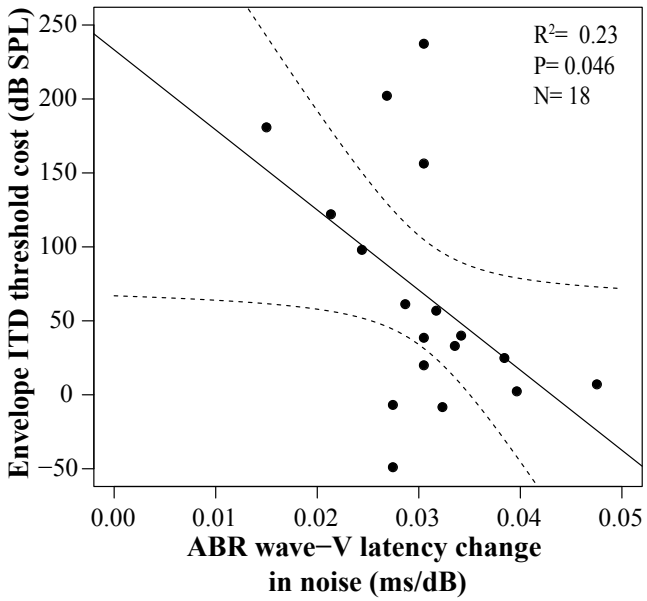

Figure 4-4: ABR wave-V latency shift in noise correlates with the cost of ITD thresholds at a 2kHz carrier. The ITD threshold cost is defined as the difference between ITD thresholds in notched noise vs. in low pass noise. The higher the cost (i.e. larger the threshold difference), the smaller the ABR wave-V latency shift and vice versa.

To better understand the underlying mechanisms of the ABR wave-V latency shift in noise, we compared the individual differences in the wave-V latency shift with how wave-V latency changed with stimulus level (in quiet). These two measures did not correlate, suggesting that the wave-V latency shift is not due to changes in the cochlear excitation pattern with overall level. Furthermore, no significant relationship was found between ABR wave-V latency shift and how wave-V amplitude changes with either the stimulus level (in quiet) or the noise level. The results are consistent with our hypothesis and suggest that a loss of low-SR fibers yields sound coding deficits that affect both hearing in background noise and in coding temporal information important for the ITD task.

Because wave-V is dominated by the IC or LL [81], it is unclear whether the differences in ABR wave-V latency shifts are a direct consequence of differences in AN response or from a later stage of processing. To investigate this, we measured ABR wave-I to high-level clicks (60-100dB SPL) using ear-canal electrodes ("tiptrodes"),

positioned closer to the AN generators. As shown in Fig.4-5, there was a significant relationship between wave-I growth and ABR wave-V latency shift (r=0.66, p=0.036): listeners with a steeper ABR wave-I growth curve had larger wave-V latency shifts. This is consistent with our hypothesis that differences in ABR wave-V latency shift arise from changes in the ANF response. In contrast, there was no correlation between wave-I amplitude growth and wave-V amplitude growth in quiet (r=-0.1801, p>0.05), consistent with the idea that after cochlear damage, there are compensatory increases in gain in the auditory central pathway that maintain the magnitude of the wave-V response [105, 107].

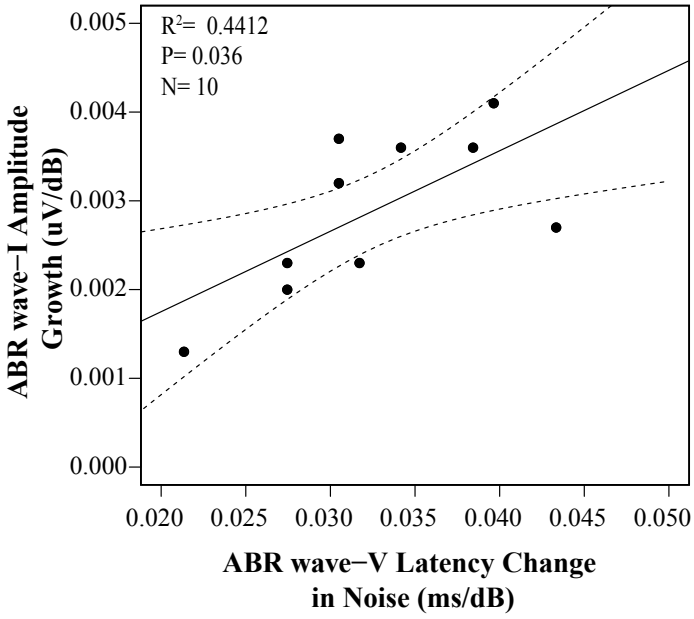

Figure 4-5: Human ABR wave-I amplitude growth correlates with ABR wave-V latency shift with noise level in 10 NHT listeners. ABR wave-I amplitude was defined by peak amplitude relative to 5ms baseline. ABR wave-I amplitude growth slope with click level was calculated using a linear regression.

4.1.3 Wave-IV latency, wave-I amplitude and cochlear synaptopathy in mice

Although our human data suggest that individual differences in the wave-V latency shift in NHT listeners arise from changes in AN responses, studying masked ABRs

in mice with noise-induced AN degeneration allows a more direct test of the hypothesis. Mice were divided into three groups: 1) unexposed (controls), 2) exposed to octave-band noise (8-16kHz) at 94dB SPL designed to cause only transient threshold elevation and no ANF loss (non-neuropathic group) and 3) exposed to the same noise at 100dB SPL, causing transient threshold elevation, and no hair cell loss, yet marked degeneration of AN synapses (neuropathic group). Cochlear synaptopathy was assessed by immunostaining with an antibody to a major protein in the presynaptic ribbon, present at each synaptic contact between an ANF and the hair cell it contacts [47]. The neuropathic group showed a significant reduction in ribbons per hair cell compared to unexposed controls (44%) and to the non-neuropathic mice, whereas the non-neuropathic group showed ribbon counts statistically indistinguishable from controls (Fig.4-6, A). Prior work has shown that the loss of synaptic connections is associated with a corresponding decrease (36%) in the supra-threshold amplitude of ABR wave-I [47]. The wave-I amplitude growth was reduced in the neuropathic group by 50% relative to the control, whereas the non-neuropathic mice showed a reduction which was statistically insignificant compared to the control (Fig.4-6, B).

To evaluate ABR latency shifts in noise, we examined wave-IV in the mice because it is robust and reliable wave [47], and because waves I-IV in animals are approximately equivalent to waves I-V in human [81, 74]. As with the human data, the ABR wave-IV latency in mice increased with increasing noise level. The mean slope of the latency vs. noise level functions was smaller in the neuropathic group relative to control and non-neuropathic animals (Fig.4-7). A linear model with group and probe level as predictors yielded significant main effects of group [$F(2,51)=4.2$, $p=0.02$] and probe level [$F(1,51)=12.09$, $p=0.001$] on wave-IV latency shift with noise level. Post-hoc one-tailed t-tests revealed significant differences between the neuropathic and control mice at both probe levels (60dB, $p=0.0045$; 80dB, $p=0.0365$). There was also a significant difference between the non-neuropathic and neuropathic groups at 80dB SPL ($p=0.0328$). In contrast, no significant differences were found in the wave-IV latency shift between the control

and non-neuropathic group at either probe level.

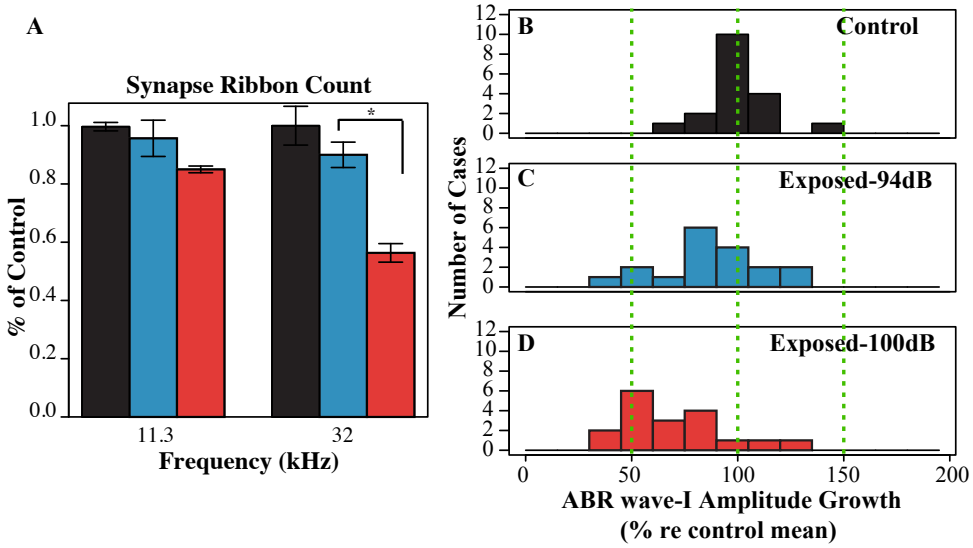

Figure 4-6: Reduced synaptic ribbon counts and ABR wave-I amplitude growth are observed in mice following neuropathic noise exposure. A: mean presynaptic ribbon counts per IHC across exposure groups, expressed as percent of unexposed control means. The Exposed-100dB group (red) showed a significant reduction in ribbon counts at the 32kHz cochlear frequency-location relative to the other groups. Histograms of ABR wave-I amplitude growth with stimulus level for B: control C: Exposed-94dB (non-neuropathic) and D: Exposed-100dB (neuropathic) group. Abscissa depicts percentage of wave-I growth relative to the control mean.

To evaluate outer hair cell function, we measured distortion product otoacoustic emissions (DPOAEs). Mean thresholds were similar between the control ears and the neuropathic group, with a hint of threshold elevation at the highest test frequency (Fig.4-8) suggesting mild outer hair cell damage. To examine whether the differences in ABR latency shift are ascribable to slight differences in cochlear thresholds, we designed a linear model including group, probe level, DPOAE thresholds at 32kHz (where ABRs were measured), DPOAE thresholds at 45kHz, and their interactions as predictor variables of wave-IV latency shift. This model revealed only main effects of probe level [$F(1,48)=12.14$, $p=0.0011$] and group [$F(2,48)=3.26$, $p=0.04$]; the DPOAE thresholds were not a significant predictor [$F(1,48)=0.49$, $p=0.58$]. These results support the idea that the differences between the neuropathic and control mice wave-IV latency shift arise from the loss of AN synapses, rather than changes in cochlear mechanics.

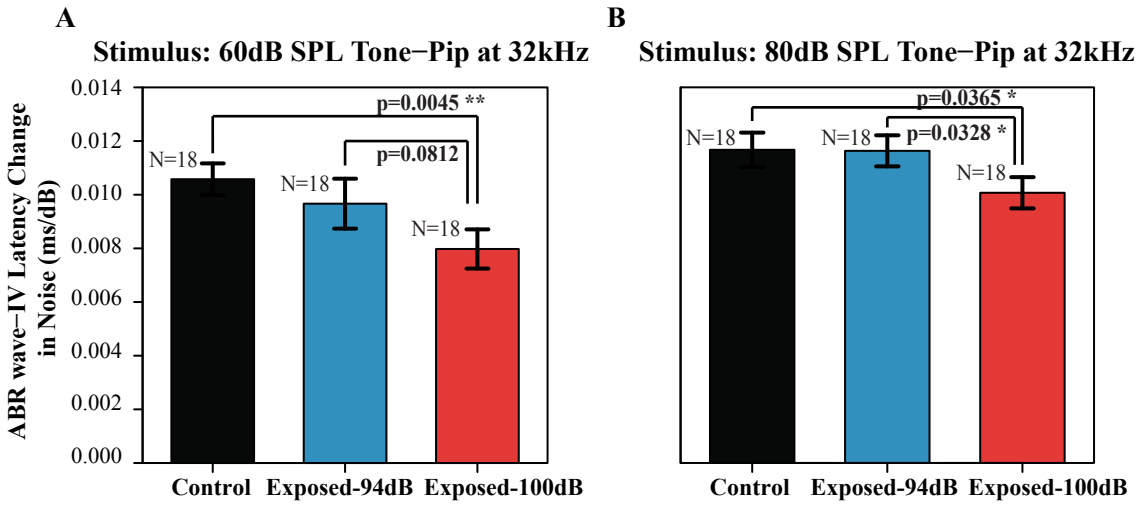

Figure 4-7: In mice, ABR wave-IV latency rate of change with noise level is reduced following neuropathic noise exposure. Similar to the human ABR wave-V latency slopes, wave-IV latency was defined as peak latency, and the change in latency was fitted with a linear regression model. ABR measurements were recorded with a A: 60dB SPL and B: 80dB SPL tone-pip at 32kHz. The neuropathic mice (Exposed-100dB) showed a significant reduction in mean wave-IV latency rate of change relative to the control and non-neuropathic groups.

Similar to the human data, wave-IV latency shifts were correlated with wave-I amplitude growth. To compare the wave-I amplitude growth and wave-IV latency shift, we pooled across all animals (N=54). The animals form a continuum of noise-exposure phenotypes (Fig.4-6, A) without large differences in thresholds (Fig.4-8), similar to the human subjects in the current study who all had thresholds within the "normal" audiometric range (<20dB HL). Using a mixed effect linear-model with wave-I amplitude growth, probe level, DPOAE thresholds at both 32 and 45kHz, and their interactions, we find significant main effects of only wave-I amplitude growth [$F(1,50)=5.187$, $p=0.027$] and probe level [$F(1,50)=11.75$, $p=0.0011$]. This analysis further supports the idea that cochlear synaptopathy, reflected in ABR wave-I amplitude growth, underlies the ABR wave-IV latency shift differences between the groups of mice.

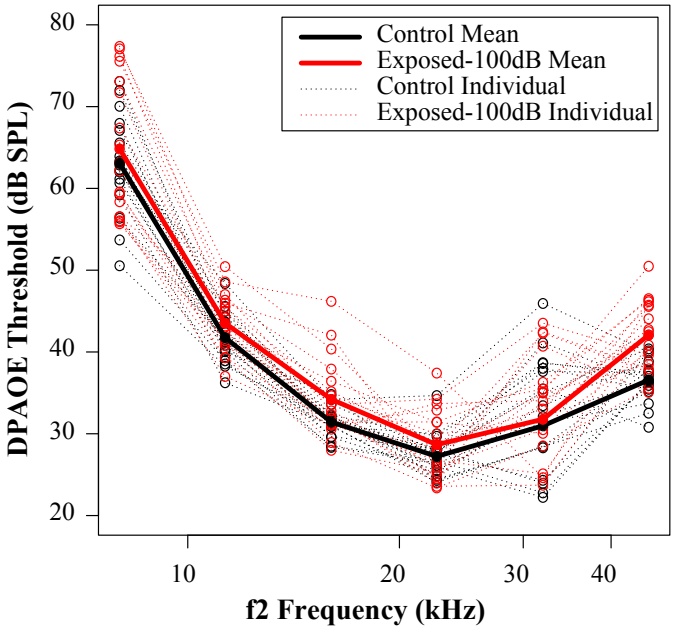

Figure 4-8: Like the range of thresholds encountered in the NHT listener subject group (<20dB HL), noise-exposed mice with cochlear synaptopathy show cochlear thresholds within a "normal-hearing" range (within 20dB of controls). Mice exposed to neuropathic (100dB) noise (red) showed a modest mean elevation in cochlear thresholds in the 45kHz region compared to unexposed controls (black). Analysis with a statistical linear model suggests that noise-induced differences in DPOAE thresholds, and thus cochlear mechanics, do not account for ABR wave-IV latency changes with background noise level (see text). Data for individual mice are shown with dotted lines and open symbols; data for group means are shown with solid lines and filled symbols.

4.2 Forward masking

Forward masking at the neural level describes the phenomenon whereby the presence of a preceding stimulus (masker) decreases the response to a subsequent stimulus (probe) presented within a couple of hundreds of milliseconds following the termination of the masker. The phenomenon is thought to arise because the masker depletes the pool of readily releasable vesicles at the IHC/AN synapse, with the recovery behavior of the probe response reflecting the restocking of that pool [45].

Recovery from forward masking can be evaluated using CAP responses [98, 97], where previous work has suggested that the selective loss of low-SR fibers can be detected via changes in the CAP forward masking functions [96, 9]. Since we were

unable to successfully measure the CAP/ABR wave-I in our forward masking experiment, we hypothesize that the differences in the CAP forward-masking function may be mirrored in the recovery function of the ABR wave-V latency. Missing low-SR fibers should reduce the slowly recovering nerve population, leaving the ABR wave-V latency recovery dominated by the rapidly recovering high-SR fibers. In addition to recovering more slowly relative to high-SR fibers, low-SR fibers have higher thresholds, larger dynamic ranges, smaller effective response areas (narrower bandwidths), and are better able to preserve timing information and amplitude modulation (see review in Schmiedt et al., 1996, [106]). These characteristics may provide low-SR fibers with an increased resistance to the effects of masking. Loss of low-SR fibers may as such increase perceptual forward masking detection thresholds. This may be more evident at shorter MPIs where the high-SR have not fully recovered and the resistance to masking characteristic of low-SR fibers may be important for encoding the stimulus.

4.2.1 Behavioral vs. physiological forward masking

Sample ABR recordings are shown in Fig.4-9 for two subjects. When the masker is presented at 35dB SPL, the wave-V latency changes very little, if at all, with increasing MPI (Fig.4-9, A and B). However, at the higher noise level, there is a monotonic decrease of the wave-V latency with increasing MPI (Fig.4-9, C and D). The ABR wave-V latency and behavioral results of NHT subjects for the two masker levels are summarized in Fig.4-10. Each line represents an individual listener and all data is normalized to the control to reduce differences in external factors that can affect detection thresholds and ABR. The peak ABR wave-V latency is plotted as the amount of latency shift relative to control (no preceding masker) as a function of MPI. Similarly, the forward masking detection thresholds are represented as the shift in thresholds in the presence of a preceding masker (i.e., threshold with preceding masker-threshold without masker). We did not measure control ABR in four of our participants and hence, the plots show data for only 16 of our listeners.

At a masker level of 35dB SPL, little effect of forward masking was observed on

either the ABR wave-V latency (Fig.4-10, A) or forward masking thresholds (Fig.4-10, B). The forward masking function, in general, was quite flat for both the wave-V latency and detection thresholds as a function of MPI across subjects. One listener had shorter ABR wave-V latencies in the forward masking experiment relative to the control. This may be because slight differences in the stimulus repetition rate of the chirp in the forward masking vs. the control experiment affected the ABR wave-V latency [18, 14, 15]: the inter-stimulus interval in the forward masking experiment was defined from onset to onset of the masker. Although this was fixed to 2Hz, the chirp presentation rate slightly varied as the MPI differed from trial to trial. In contrast, the repetition rate of the chirp in the control experiment was fixed to 2Hz. Nevertheless, the modest effect of forward masking observed could be because this masker level was insufficient to elicit a strong response from both SR fiber types. Yet the high level chirp induced a strong response from all SR fibers, as the vesicles had not been depleted due to the preceding masker.

In contrast, we observed a stronger effect of forward masking in the ABR and detection thresholds when the masker level was increased to 70dB SPL (lower panel; Fig.4-10, C and D). This masker presumably elicited a response from both high and low-SR fibers. The vesicle depletion due to the masker maybe more prominent in the high-SR ANF because of the smaller synaptic ribbon at their synapse [69]. Hence, the probe response may be dominated by low-SR fibers.

Large individual differences were observed in the shift in the ABR wave-V latency and the detection thresholds, especially at MPIs <72ms. Further, the forward-masking recovery function of the ABR wave-V latency and detection thresholds with MPI varied from subject to subject. As seen in past studies, the forward-masking recovery function consists of a fast and slow time component and can be modelled as a sum of two exponential functions [96, 80]. In the forward masking detection task, the fast time component was defined as thresholds for MPI<72ms. In our forward masking ABR, the fast time component of the wave-V latency recovery function was defined by MPI< 40ms as we did not record ABR at a 72ms gap. At longer MPIs, t-test reveals no significant differences in detection thresholds and thus, we

define this segment as the slow time component for the forward-masking function. In both experiments, we presume that the fast time component of the forward-masking function has contribution from both SR fiber groups.

To derive a single metric of forward masking for each listener, detection thresholds at MPIs between 20-70ms were fitted using a power law function. This fit yielded a single exponential constant for the fast component of the forward masking recovery function that describes how quickly the forward masking detection thresholds decreased with MPI. We opted to compare this fit to the change in peak ABR wave-V latency from 20 to 40ms MPI because we were limited to the few MPI conditions we measured.

To evaluate the relative contribution of different factors to forward masking threshold recovery function at short MPIs, a linear regression model was implemented. The model included the fixed-effect terms for the ABR wave-V peak latency shift from 20 to 40ms MPI, and gender. Additionally, we wanted to look at the contribution of the pure-tone thresholds measured for the seven tested frequencies since broadband stimuli were used in the experiment. However, these thresholds were correlated with each other. To disentangle their respective contribution, principle component analysis (PCA) was used. The first two components of this analysis, which roughly accounted for 75% of the variance in the pure-tone thresholds, were also used as predictors in the model. The main effect of the ABR wave-V latency shift form 20 to 40ms MPI was the only significant predictor for the forward masking threshold recovery function at short MPIs [$F(1,14)=6.0232$, $p=0.0278$).

Fig.4-11 shows the post-hoc comparison between the wave-V peak latency shift from 20 to 40ms MPI and the time constant of the fast component of the forward masking threshold recovery function. We observed a significant relationship between the amount of change in wave-V latency and forward masking detection thresholds at short MPIs [$r=0.6164$, $p=0.0053$]: listeners with a larger change in wave-V latency also had greater change in forward masking detection thresholds at short MPIs. This relationship remained when simply comparing the change in ABR wave-V latency to

the change in forward masking detection thresholds from 20 to 40ms MPI [r=0.6612, p=0.005]. This is consistent with our hypothesis of a selective loss of low-SR fibers: the recovery of the CAP will be dominated by rapidly recovering high-SR fibers in listeners with low-SR loss thereby resulting in a faster change both in CAP and wave-V latency with increasing MPI.

Further, we find that the listeners with a larger decrease in wave-V latency from 20 to 40ms MPI are perceptually hurt more by a preceding masker at the 20ms MPI (i.e., higher thresholds, Fig.4-12) [r=0.5348, p=0.0151]. Interestingly, the listeners who were affected more by the preceding masker at 20ms MPI also showed greater shifts in detection thresholds at the longest tested MPI (201ms) relative to control [r=0.6, p=0.0052]. In the ABR measruements, listeners whose ABR wave-V latencies are shifted more by a preceding masker at 20ms MPI, also exhibit a larger decrease in wave-V latency from 20 to 40 ms MPI. Although this may be trivial, this relationship holds for all MPIs tested and emphasizes the importance of low-SR fibers' resistance to masking. A loss of these high-threshold fibers may lead to a larger effect of the preceding masker on the probe response at short MPIs. The increased effect of masking with AN loss may result in higher detection thresholds and ABR wave-V latency shift as observed in this data.

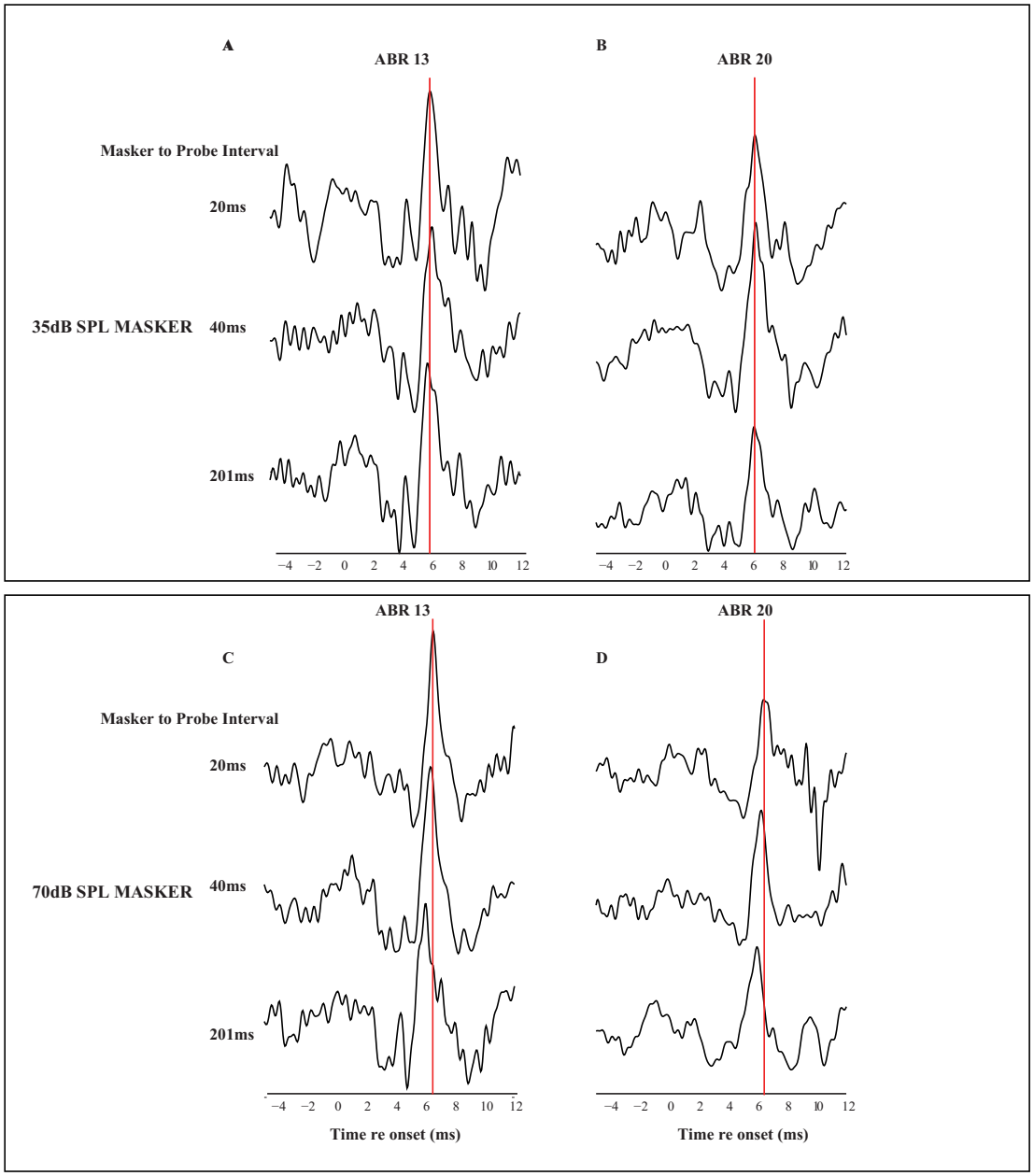

Figure 4-9: Sample ABR recordings in forward masking for 2 subjects at both 35 dB (top panel) and 70dB (bottom panel) masker level.

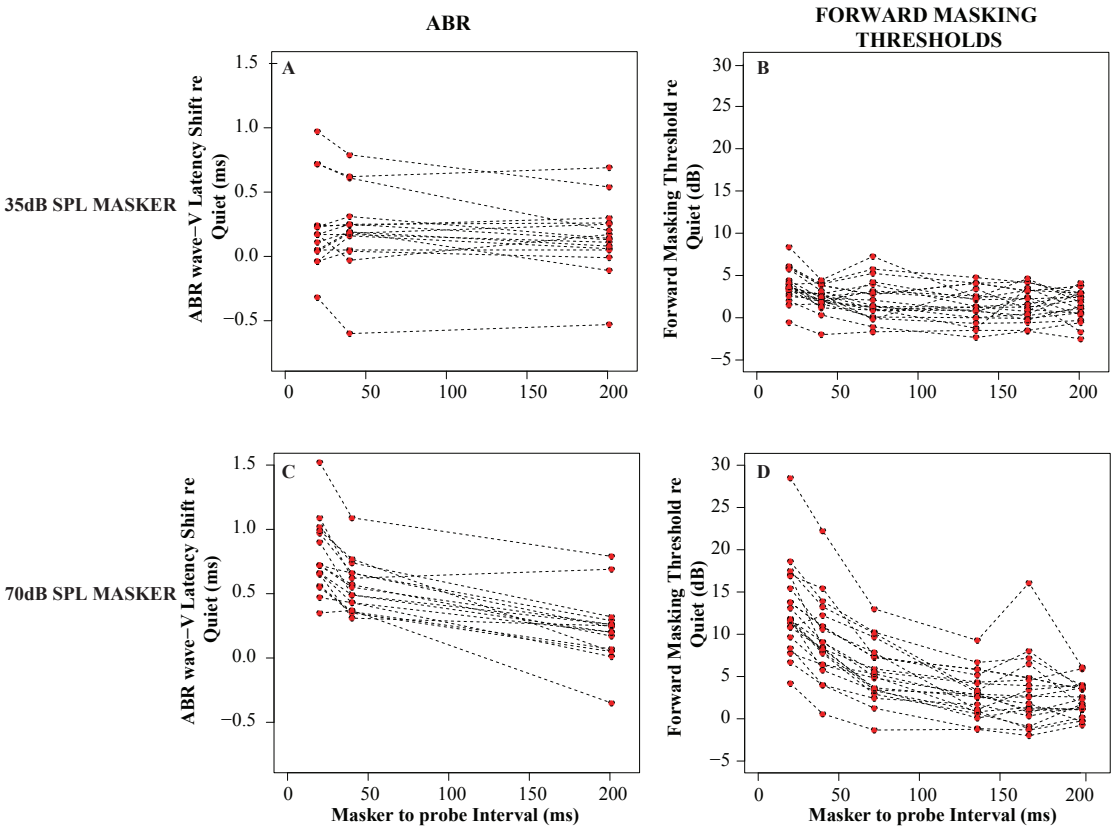

Figure 4-10: ABR wave-V latency shifts re to control in the presence of a 35dB SPL (A) and 70dB SPL (C) preceding masker as function of MPI. Forward masking detection thresholds re to control with a 35dB SPL (B) and 70dB SPL (D) masker at different MPIs. ABR wave-V latency is defined as the peak latency of the wave and is plotted as the shift in latency relative to control where there is no preceding masker. Similarly, forward masking thresholds are shown as the amount of forward masking relative to thresholds in the absence of a preceding masker (control). Each line presents a subject.

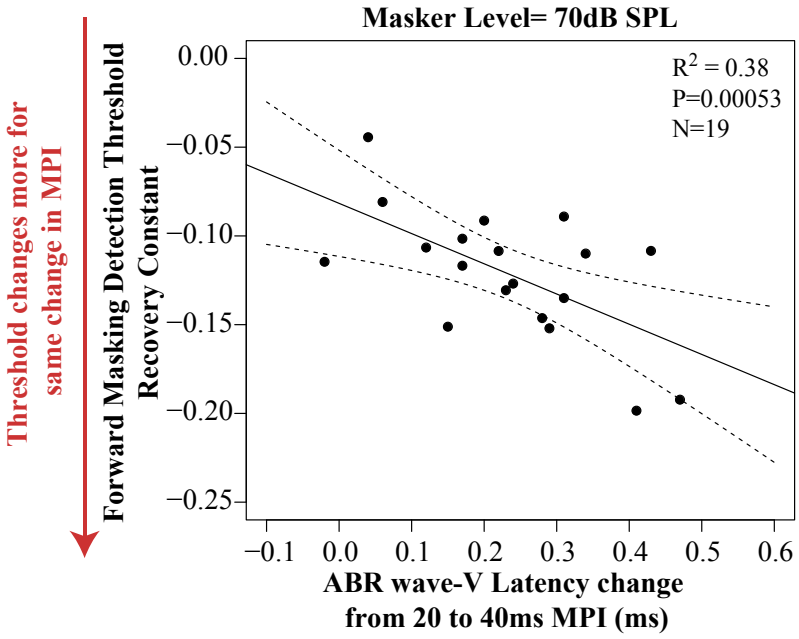

Figure 4-11: Comparison of the change in ABR wave-V latency from 20 to 40ms MPI was significantly correlated with the time constant that described the recovery of the forward masking thresholds at MPI<72ms. As indicated by the arrow, a more negative time constant depicts a faster recovery/change in forward masking detection thresholds with MPI.

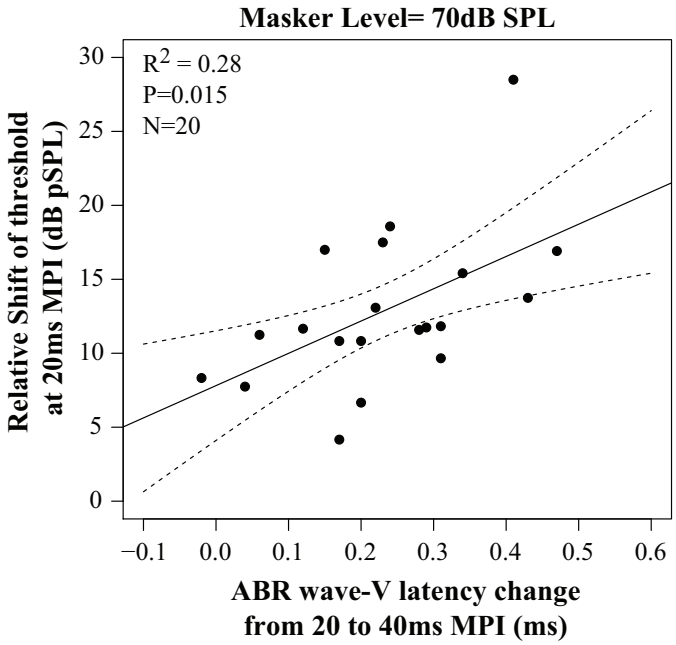

Figure 4-12: The change in ABR wave-V latency from 20 to 40ms MPI was also a significant predictor of the amount of masking on forward masking thresholds at a 20ms MPI. The large the decrement of forward masking thresholds at a 20ms MPI (higher threshold), the larger the change in ABR wave-V latency.

Chapter 5

MODELING ABR IN NOISE AND FORWARD MASKING

5.1 Background and motivation

We have thus far shown through experimental results that ANF loss affects ABR wave-V latency in noise and perhaps in forward masking. Although a considerable body of work, including the work in this thesis, describes the phenomenology of population responses like the ABR, not much is known about their relationship to single neuron responses. More importantly, it is still unclear whether a general loss of ANFs or a selective degeneration of low-SR fibers affects wave-V latency in noise and in forward masking. Thus, computational modeling is necessary to understand the neural mechanisms underlying the effects we observe in ABR wave-V latency in different masking paradigms.

Most existing functional ABR models have focused on simulating latency changes with increasing stimulus level [23, 101, 118] and until recently, they failed to adequately account for the latency shift with level. The most recent model by Verhulst et al. (2015; [118]) has successfully captured the ABR wave-V latency decrease of 1.2-2ms for a stimulus level increase of 40 dB [23, 30, 115]. Unlike previous models that use single-unit AN models to drive population responses in parallel auditory filterbanks [130, 133, 132], the Verhulst model uses a transmission

line to capture level-dependent features of the cochlear processing in combination with single-unit models of AN fibers, cochlear nucleus (CN) and IC neurons.

Although ABR wave-V latency changes with stimulus level have now been successfully simulated, model predictions of ABR wave-V latency changes in noise and in forward masking have to yet to be implemented. Here, we try to simulate ABR wave-V latency in noise using AN models that have a parallel filter bank cochlea [132] and a transmission line cochlea [118]. The Zilany et al. (2014; [132]) model is a well accepted phenomenological model of the auditory system; however, the fundamental issue with a parallel filter bank model of the cochlea is that the relative latency of responses across frequencies is mostly determined by free model parameters, rather than being constrained by the physics of the cochlear mechanics. As a result, the model introduces arbitrary frequency dependence in the gain of the IHC response driving the AN and in the AN threshold parameters in order to fit experimental data. The frequency dependence imposed on the AN thresholds does not match the AN physiology literature: AN thresholds are SR-dependent and frequency-independent. Motivated by this, we used the Verhulst et al. (2015, [118]) model, which overcomes these limitations by using a nonlinear transmission-line model of the cochlea. This traveling wave model inherently captures the across-frequency mechanics of the cochlea without introducing frequency-dependence at subsequent stages. Importantly, this model adjusts the AN synapse parameters to be SR-dependent and the immediate permeability of the synapse to be level dependent.

To validate our hypothesis of increasing low-SR contribution in noise, we explore how preferential loss of different SR fibers affects AN, CN, and IC latency and amplitude in background noise. Additionally, the effects of low-SR fibers on the CAP recovery function in forward masking are simulated. Both models show that with increasing background noise level, the contribution of low-SR fibers increases; however, the models fail to quantitatively capture the latency increase with noise level.

5.2 Model descriptions

5.2.1 Acoustic Stimulus

To simulate ABR in background noise, a click train consisting of a 100, 80μs clicks in broadband noise was used. Click level was fixed at 80dB peSPL while the background noise level varied from 42-82dB SPL in 10dB steps matching our experimental stimuli. The click repetition was 10Hz.

For the forward masking simulations, a 100ms broadband noise followed by a "synchronized" flat spectrum chirp was used [24]. The masker (i.e., broadband noise) was presented at 70dB SPL while the chirp level was kept constant at 90dB peSPL. The chirp contained frequency components ranging from 0.08-20kHz. Further, the simulations was implemented using MPI of 0, 10, 20, 40, 100, 500, 1000ms with a control condition without a preceding masker. All stimuli were generated at a 100kHz sampling rate.

5.2.2 Auditory nerve model

Simulations were implemented using two models: 1) a parallel filter bank cochlear model coupled to a humanized AN model [132] and 2) a transmission line model of the cochlea combined with an AN synapse model [118]. Detail descriptions of the two models can be found in Zilany et al. (2006, 2009, 2014; [131, 133, 132]) and Verhulst et al. (2015, [118]). From here on out, for brevity we will refer to the first model as the Zilany model and the second model as the Verhulst model.

The structure of the Zilany model is shown in Fig.5-1. This AN model calculates the instantaneous discharge rate for individual AN fibers in response to a given acoustic stimulus defined in pascals. The parameters of this model are set to estimate human responses. Detailed descriptions of the model stages are provided in Zilany and Bruce 2006, 2009, 2014, [131, 133, 132]. The input to the middle ear (ME) is an instantaneous pressure waveform of the stimulus in pascals sampled at 100kHz. The ME filter is followed by three parallel filter paths: the C1 and C2 filters in the signal

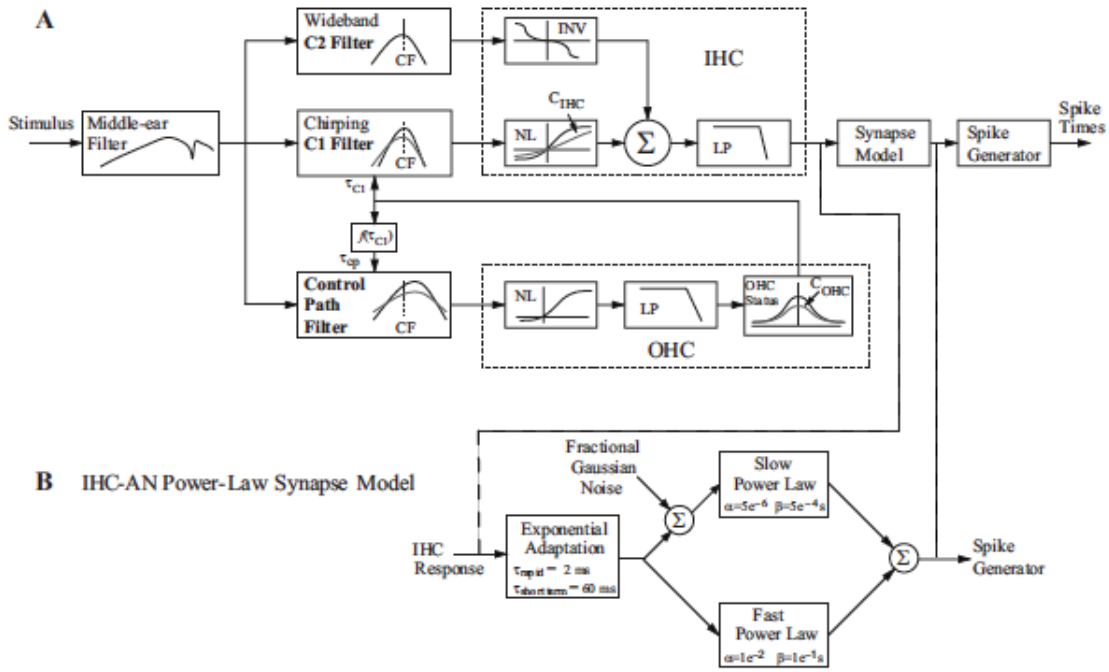

Figure 5-1: Overview of the Zilany et al. 2014 model [132]

path and the broadband filter in the control-path. The control-path regulates the gain and bandwidth of the C1 filter to account for several level-dependent properties in the cochlea [130]. The C1 filter produces the tuning properties for the model BM response that provides input to the C1 IHC transduction function. The C2 filter is implemented based on the two-factor cancellation hypothesis [55]. The combined response of the transduction functions following the C1 and C2 filters provides the input to a seventh-order IHC lowpass with a 3kHz cutoff frequency. The IHC output drives the model for the IHC-AN synapse, which is described by the time-varying three-store diffusion model of Westerman and Smith (1988, [123]) followed by a power-law adaptation that captures the adaptation properties of the AN [133]. We bypass the spike-generator in this model and use the synapse output for our simulations and analysis. Thus, the simulations shown here do no take into account refractoriness observed in AN post-spike timing histograms because we focus on onset responses, where this effect is not critical.

Fig.5-2 provides an overview of the different processing stages in the Verhulst model. In this model, the stimulus pressure passes through a 4kHz low-pass and 0.6kHz high-pass filter with a pass-band gain that matches those of the human ME transfer function [94]. The filtered stimulus enters a nonlinear transmission-line model of the cochlear partition [119], after which basilar membrane (BM) velocity is translated to IHC bundle deflection. The deflections at each characteristic frequency (CF) is passed through a compressive nonlinear function and a second-order 1kHz cutoff low-pass filter to account for the degradation of TFS phase locking. The filter order of this model is smaller than that of the Zilany and thus, the alternating to direct current ratio rolls off more slowly with CF. Nevertheless, the lower cutoff frequency (1 instead of 3kHz in Zilany model) qualitatively matches the model response to data [87].

The AN stage of the model is based off of the Zilany AN model but differs in that the AN thresholds were made SR-dependent. Further, SR-dependence in this three-store diffusion synapse model was implemented [123, 129]. The immediate permeability in the diffusion model was the only level-dependent parameter in the AN synapse [118]. This model also uses the synapse output rather than AN spikes as input to the brainstem model.

In both models, the response of the different SR fibers were weighted at each CF according to the known population size. Here, we assigned 47% of the population of ANFs as low-SR (includes med-SR) and the remaining 53% as high-SR ANFs. This distribution is based on the ANF recordings of Furman et al. 2013 in guinea pigs [36]. At each CF, the weighted instantaneous firing rates of AN fibers are summed and used as the input to the CN model stage described below.

5.2.3 Brainstem model

To obtain ABR wave-V, a functional inhibition/excitation model of the spherical bushy cells in the ventral cochlear nucleus (VCN) and IC was adopted [84]. Details of this model can be found in Nelson and Carney (2004, [84]). The model was designed to account for the common band-pass shaped modulation transfer functions of chopper

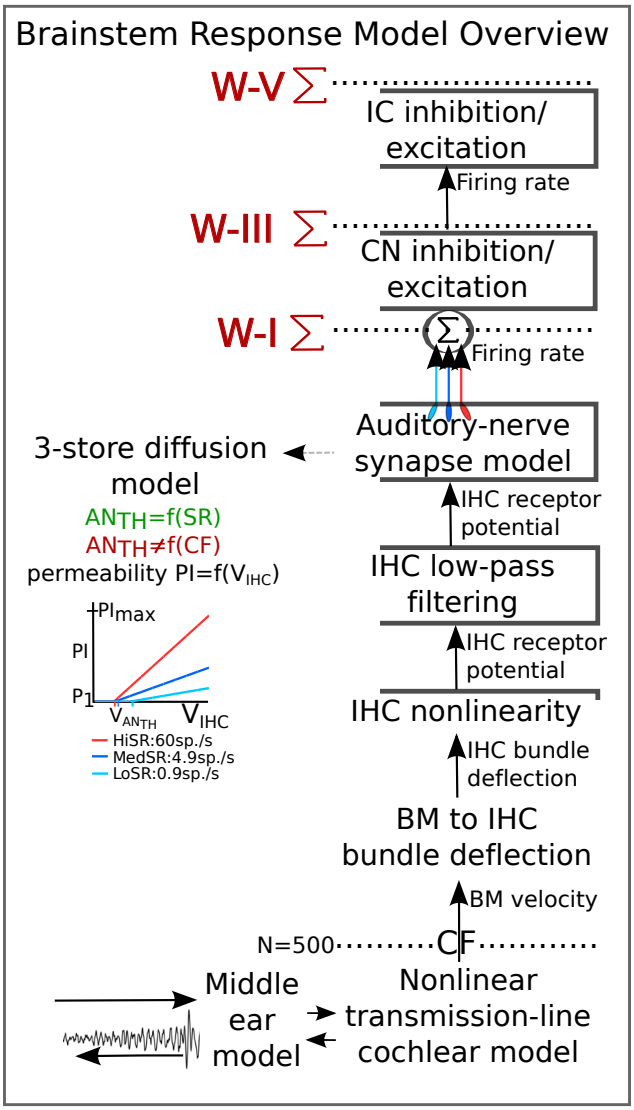

Figure 5-2: Overview illustration of the Verhulst et al. 2015 auditory model [118]

and onset neurons [35]. Although this model is designed to simulate the amplitude-modulation properties of CN and IC neurons, it may also be well suited for modeling onset response such as the ABR because the neurons with the strongest sensitivity to amplitude-modulation characteristics also have onset responses with sharp temporal precision [35].

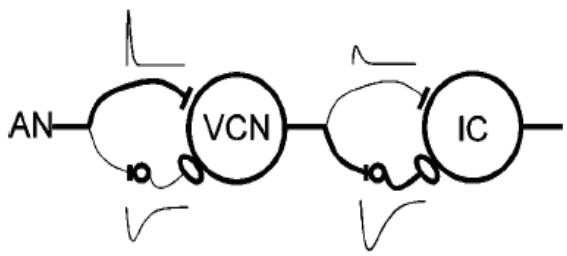

Figure 5-3: A CN and IC schematic from Nelson and Carney (2004 ; [84]). In both stages, the inhibition time-course is slower than that of the excitation. Further, the inhibition is weaker relative to the excitation at the level of the CN and vice-versa in the IC.

In brief, the model is comprised of a simple inhibition/excitation network for the CN and IC stage. The networks are defined by the time constants associated with excitation and inhibition and the synaptic delays associated with the CN and IC. As shown in Fig.5-3, the inhibition is weaker relative to the excitation in the CN and vice versa in the IC. The AN instantaneous firing rate was used as the input to this brainstem model.

5.3 ABR in noise model simulations

For both models, simulated population responses were obtained by summing the instantaneous firing rate across cochlear sections either at the level of the AN (ABR wave-I), at the level of the CN (ABR wave-III), and at the level of the IC (ABR wave-V). It was assumed that there are no additional latencies introduced by tissue volume, which is justified for responses below about 10kHz where the brain/ scull/scalp tissues are purely conductive [44]. In the transmission line model, only cochlear frequency channels above 175Hz were included in the summation. Similarly, the population

response of the Zilany model included channels above 500Hz. This is in line with ABR measurements which show that contributions of the mid- and high- frequency tonotopic sections of the cochlea dominate ABRs [26]. In order to explore the full frequency range of the neural responses, the simulated ABR responses were not low-pass filtered, even though experimental studies often focus exclusively on low-frequency portions of the responses and filter ABRs with a low-pass cutoff frequency between 1.5 and 3kHz. The instantaneous firing rate of the models has been baseline corrected to analyze the click response rather than the click+noise response of the models.

5.3.1 Auditory nerve

Fig.5-4 shows the AN population response for each SR fiber group for the Zilany model. The click level is fixed at 80dB peSPL where as the noise level differs in each subplot. At a low noise level of 42dB SPL (Fig.5-4, A), the high-SR response dominates the overall population response. However, as the noise level increases (Fig.5-4, A-D), the low-SR response systematically increases relative to the high-SR fibers and dominates the population response at the highest noise levels (Fig.5-4, C, D). Notice that there are additional peaks in the response following that of the onset peak. These peaks are a result of the phase dispersion in the low CF regions. The relative contribution of the low-SR ANFs to that of the combined AN response (i.e., high+low-SR fiber response) is summarized in Fig.5-5 for both models. Like the Zilany model which shows a 23% increase in low-SR contribution with a 30dB increase in noise level, the Verhulst model shows a 28% increase in low-SR contribution. Additionally, the overall contribution of the low-SR fibers in the Verhulst model is smaller than that of the filter-bank model. Nevertheless, the model simulations here are consistent with our hypothesis of low-SR recruitment with increasing noise level. In the Zilany model, there is an apparent SR-dependent latency difference as shown in Fig.5-4: the low-SR peak response is delayed to that of the high-SR response consistent with previous data showing first spike timing difference between fiber types using pure-tone stimuli [100, 11]. This latency difference is fixed despite noise level

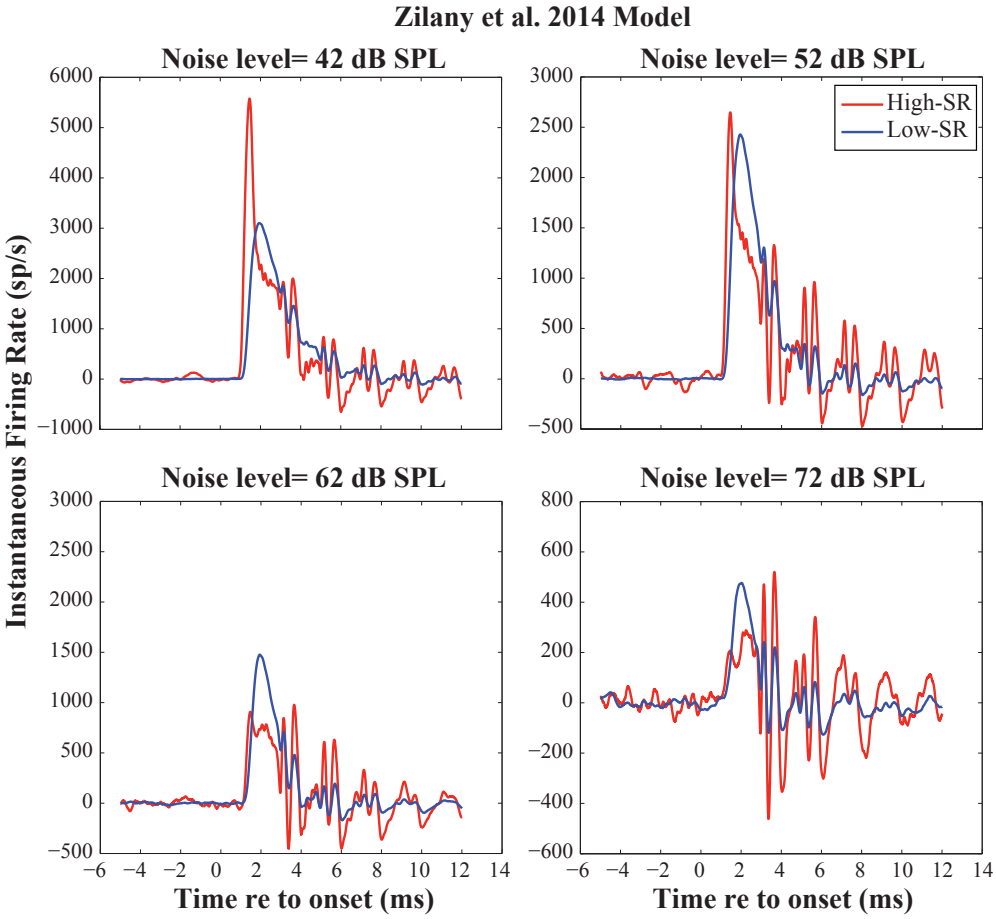

Figure 5-4: Population response (sum acrossed all CFs) of low/med-SR (red) and high-SR (black) fibers to 80dB peSPL click stimulus in varying background noise level (A-D). Simulations were done using Zilany et al. 2014 auditory model [132]

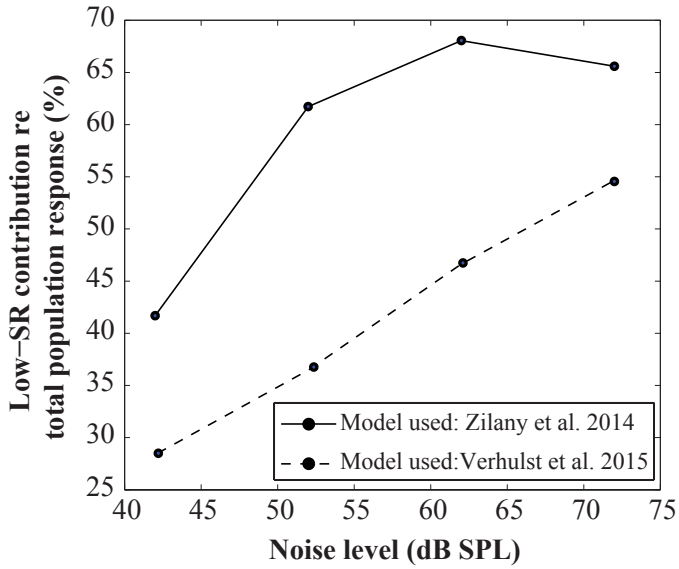

Figure 5-5: Percentage of low-SR fiber contribution to the total AN population response with increasing noise level. The low-SR contribution increases in both models with noise level.

increase (Fig.5-6, A). As the low-SR contribution increases with noise level, the peak population response latency progressively reflects the latency of the low-SR fibers (Fig.5-6, A: red trace) consistent with our hypothesis. Note, that this latency shift of approximately 0.61ms is too small compared to our experimental results that show ABR wave-V latency shifts of 0.8-1.2ms with a 40dB SPL increase in noise level. Nevertheless, this trend is consistent with what we observe in our data and previous studies [12, 13, 17, 15]. Furthermore, the latency shift in the AN response diminishes with a complete loss of low-SR fibers (Fig.5-6, A: blue trace). Partial loss of low-SR fibers has a small effect on the latency shift as shown in the dashed traces in Fig.5-6 (A). In fact, the reduced latency shift with noise level becomes apparent when there is 75% and 85% low SR loss. In contrast to the Zilany model, the Verhulst model does not show the SR-dependent onset latency difference. Thus, the latency increase with noise level is not observed in this model (Fig.5-6, B). A marked difference between the two models, is the excitation pattern along the cochlea (Fig.5-7). In quiet, the strongest AN click response arises at frequency regions >2kHz (Fig.5-7, A) in the Zilany model in contrast to the Verhulst model that yields a peak response around the

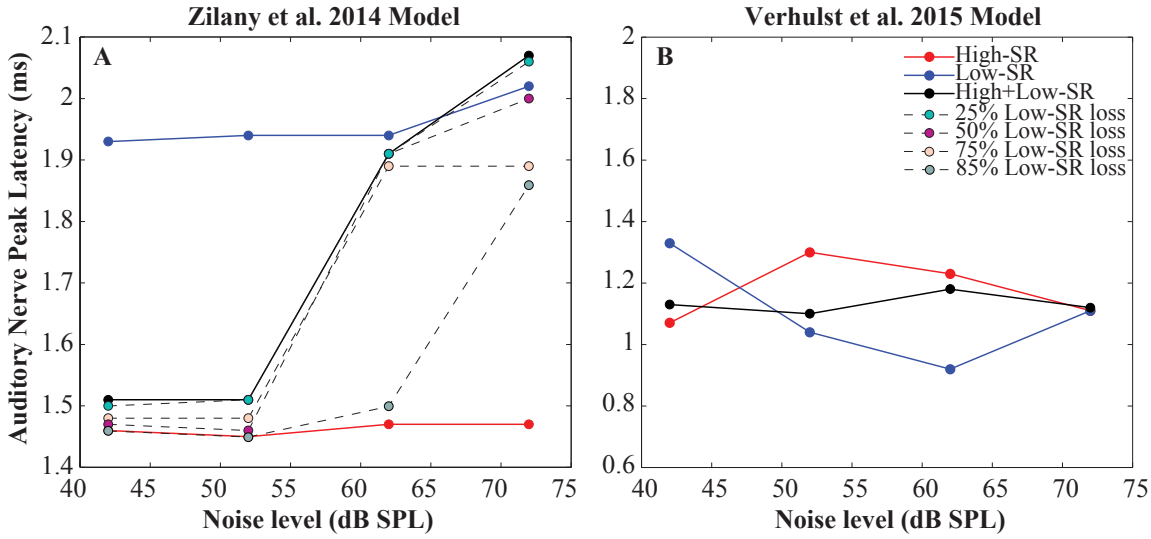

Figure 5-6: AN peak latency of the A) Zilany and B) Verhulst model as a function of noise level. The AN latency begins to reflect the low-SR latency at higher noise levels in the Zilany model (A). Systematic loss of these fibers reduces the shift in AN latency with noise level. The AN peak latency in the Verhulst model does not change with noise level and little SR-dependent latency difference is observed (B).

1kHz cochlear region (Fig.5-7, B). The addition of background noise reduces the high-frequency response in the Zilany model; therefore, there is an apical shift in response with increasing noise level. The Verhulst model, however, shows an overall reduction in response with noise level. One can argue that perhaps the latency increase with noise level we observe in (Fig.5-6, A) is due to an apical shift in the peak response on the cochlea. However, this contradicts past studies that show that the latency shift in noise is due to neural/synaptic mechanisms [12, 13, 17, 15]. Additionally, the model shows that the loss of low-SR fibers has an effect on the latency shift despite this excitation pattern change.

5.3.2 ABR simulation using unitary response

To simulate ABR responses, the convolution model of ABR generation described in Rønne et al. 2012 [101] was used. The generation of ABR was first described as a summation of individual brainstem cell potentials in response to a given stimulus [76].

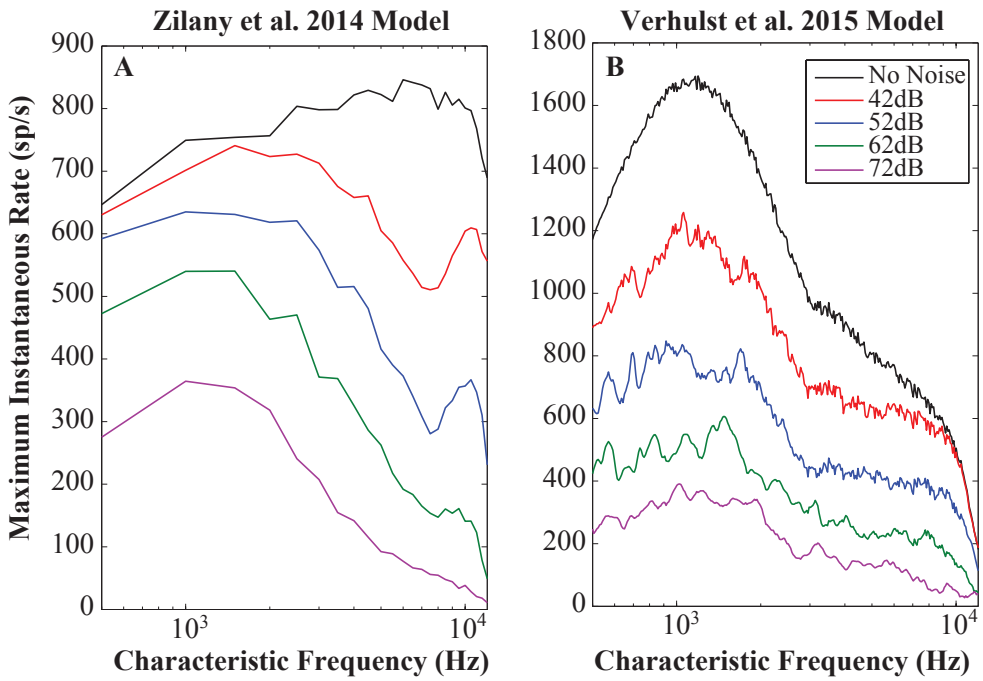

Figure 5-7: AN response to click stimuli in noise at various noise levels for each simulated characteristic frequency in the Zilany (A) and Verhulst (B) model.

The potential of a cell in response to a given acoustic stimulus can be determined by a convolution between the instantaneous firing rate of that cell and a unitary response (UR) function. The UR function is defined as the potential produced between the electrode positions on the scalp each time the cell discharges. To obtain an ABR using the convolution method, all cells need to be considered individually. However, Melcher and Kiang (1996, [76]) suggested that cells can be grouped by the physio-anatomical type of the cell and all cells of a population described are assumed to have the same UR, as they have the same morphological and electrical properties. Following this suggestions, Dau (2003, [23]) assumed that the instantaneous firing functions of the medial superior olive (MSO), antroventral cochlear nucleus (AVCN) are the same as in the AN and thus, have the same UR function. As such, the generation of the ABR (specifically waves I, III and V) using this method is thus represented as the sum of the instantaneous firing from all cells, convolved with a UR that is dependent on the electrode location on the scalp but assumed to be independent of cell type, efferent influence, and stimulus. The UR from Rønne et al. (2012; [101]) used

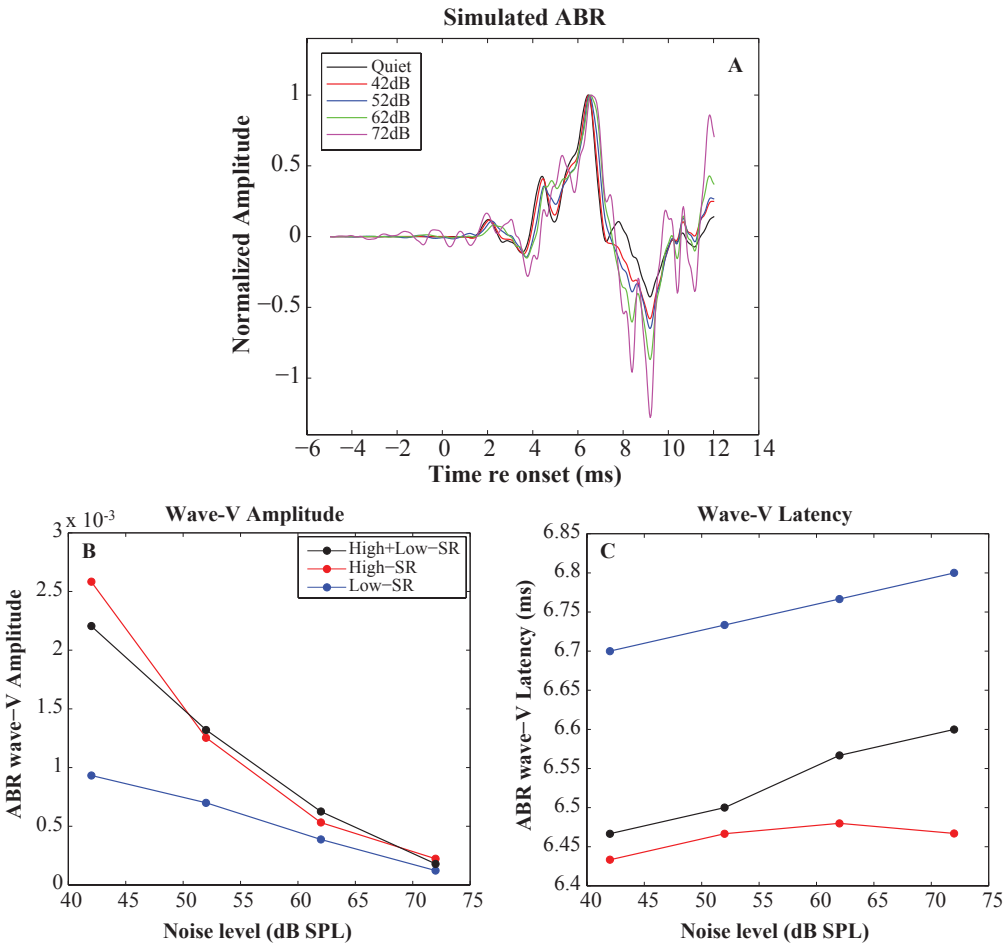

Figure 5-8: Computed ABR to click in noise using unitary response (A). Wave-V peak amplitude decreases differentially with increasing noise level with different SR fiber loss (B). Similarly, the simulated ABR wave-V peak latency increase with noise level differs with SR-dependent loss of ANFs (C).

here was obtained by deconvolving a "template" click-evoked ABR with the summed neural activity pattern generated by the Zilany (2006) AN model [131] in response to a click stimulus. Here, we convolved this UR with the AN output of the Zilany model in response to the click stimulus in various levels of noise. Fig.5-8 (A) shows the simulated ABR for the different noise levels. The simulated ABR, normalized to its peak, captures wave-I, III and V. Similar to the AN response, as the noise level increases, the wave-V latency slightly increases and its amplitude decreases as summarized in Fig.5-8 (B and C). The latency shift is much smaller than observed in the AN response because of the filtering process.

The different SR ANFs differentially affects the ABR wave-V amplitude and latency in noise as observed in Fig.5-8 (B and C). The complete loss of low-SR fibers has little effect on the ABR wave-V amplitude (red vs. black trace in Fig.5-8, B). However, the latency increase with noise level is reduced with low-SR loss (Fig.5-8,C). In contrast, a complete loss of high-SR ANF loss reduces the overall wave-V amplitude (Fig.5-8,B) and delays the overall latency but leaves the latency growth with noise level intact.

5.3.3 Brainstem response

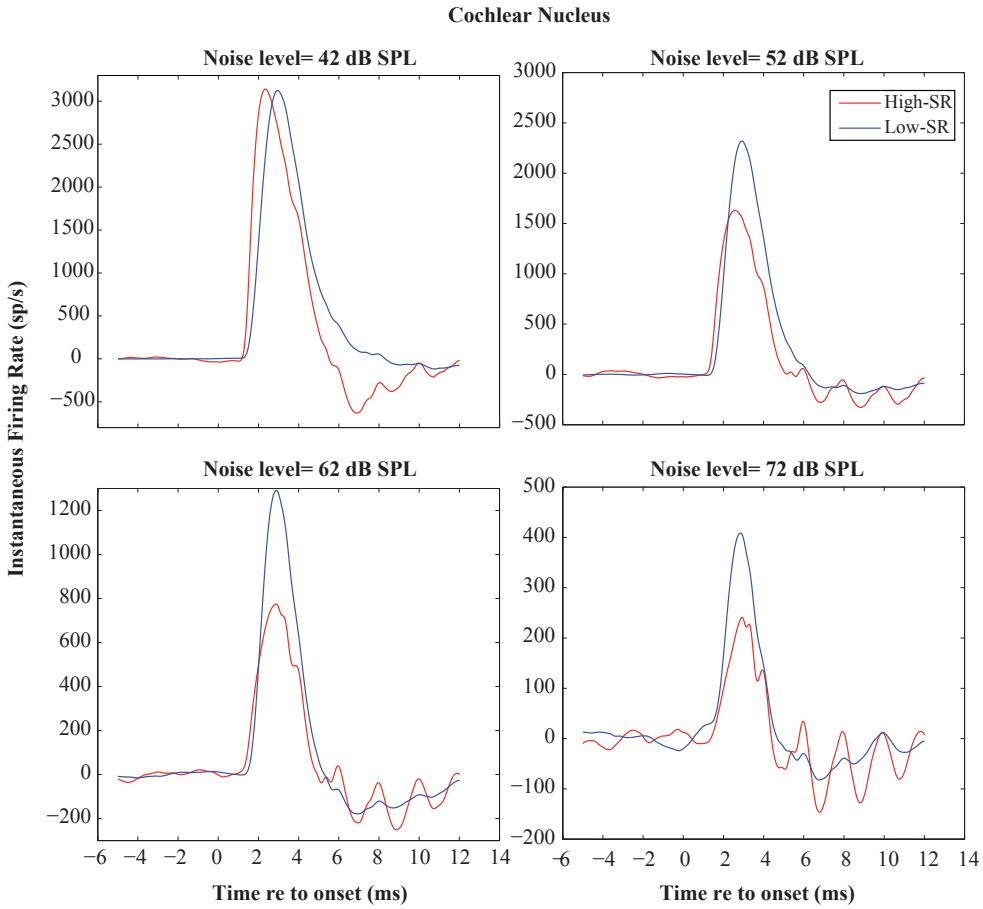

Figure 5-9: Population response (sum acrossed all simulated CFs) of the CN with only low/med-SR (blue) and high-SR (red) fibers input. CN response is to a 80dB peSPL click stimulus in varying background noise level (each panel). AN response of the Zilany model was used as the input to the CN.

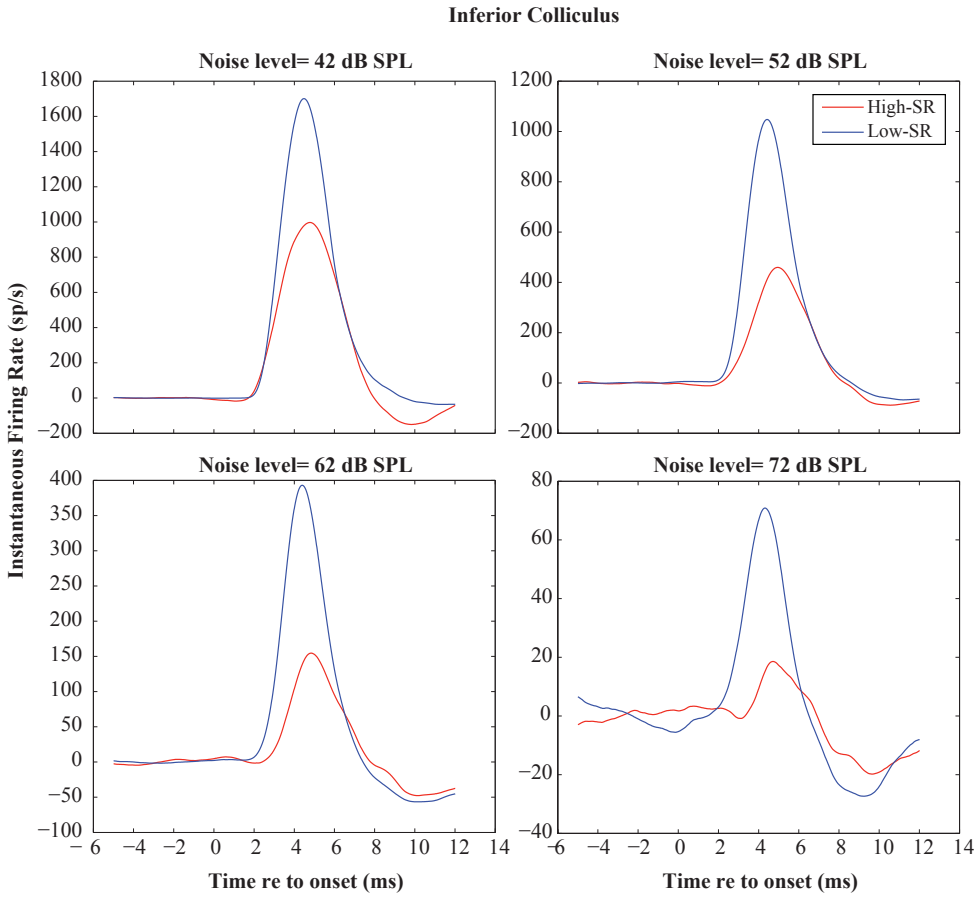

Figure 5-10: Population response (sum acrossed all simulated CFs) of the IC with only low/med-SR (red) and high-SR (black) fibers input. IC response is to a 80dB peSPL click stimulus in varying background noise level (each panel). AN response of the Zilany model was used as the input to the CN which was then used as the input to the IC.

In the previous section, we showed that ABR wave-V generation using the AN response does not capture the latency shift that is observed in experimental data. As such, we turn to a functional brainstem model [84] to simulate ABR wave-III and wave-V. The inhibition and excitation dynamics of this brainstem model may perhaps alter the differences seen at the AN. ABR wave-III is defined as the summed output of the CN and wave-V is the summed output of the IC stage in this model. Fig.5-9 and Fig.5-10 shows that the low-SR response dominates at higher noise levels, reflecting the trend seen in both AN models. When the Zilany AN response is used as input to the brainstem model, the SR-dependent difference in peak latency is maintained

(i.e. low-SR input produced delayed peak re to high-SR input, Fig.5-9) in the CN. However, the IC output that is only driven by high-SR fibers is delayed relative to that of the IC response driven by low-SR fibers (Fig.5-10) in contrast to the AN and CN stage of the model. As illustrated in the neurogram of Fig.5-11, at the level of the AN, high-SR response is strongest at low- to mid- frequency cochlear regions while low-SR response is driven by a broader frequency region. However, the low frequency response does not sum up optimally due to phase dispersion across low- to mid- frequency channels in the model (Fig.5-11, A) thereby resulting in a peak AN response that is largely driven by high-frequency channels. The bandpass behavior of the IC model smoothes out these phase differences to yield a strong IC response in the low- to mid- frequency regions (Fig.5-11, B). Thus, yielding a delayed peak IC response with high-SR ANF input. When using the Zilany AN response as the input to the brainstem model, the peak latency of the CN and IC stage of the model increase with noise level by 0.58 and 0.27ms respectively (Fig.5-12). This latency shift is not enough to capture the experimental ABR latency increase in noise. Further, the Verhulst cochlear model fails to capture even the trend of latency increase with noise level. In fact, when using the Verhulst model as input to the brainstem model, the CN and IC latency decreases with noise level as shown in Fig.5-12. This is likely due to the change in excitation pattern with increasing noise level in which the response of the low frequency channels become equivalent to that of the high frequency regions with increasing noise level (Fig.5-7). Nevertheless, the brainstem model simulation coupled with the Zilany AN model show the right trend. The loss of low-SR fibers in this model diminishes the little latency increase observed in the IC consistent with our hypothesis. However, the model simulations suggest that the mechanism underlying the latency shift comes from the change in cochlear frequency region contribution rather than the SR-dependent differences in the onset latency. It is unclear at this time to what extent these proposed mechanisms are valid.

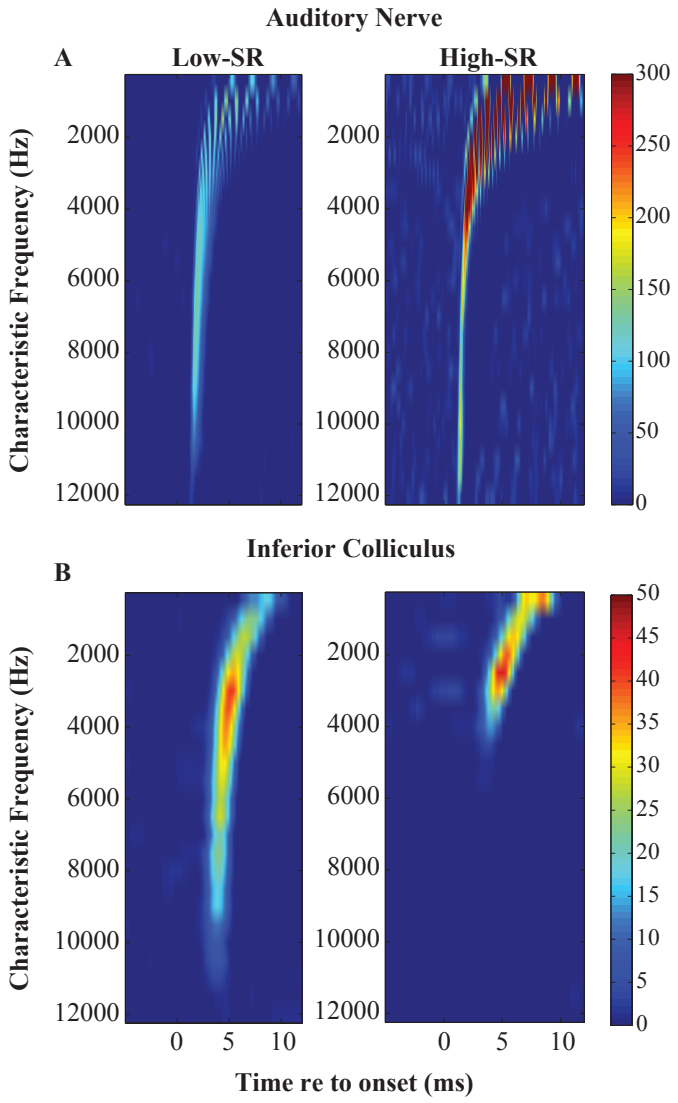

Figure 5-11: Model simulation to click in noise stimulus at the level of the Zilany AN (top panel) and IC (bottom panel) for different SR fibers at different CFs. The color scale indicates the normalized instantaneous firing rate to the click. 80dB peSPL click in 62dB SPL noise was used as the acoustic input to the model.

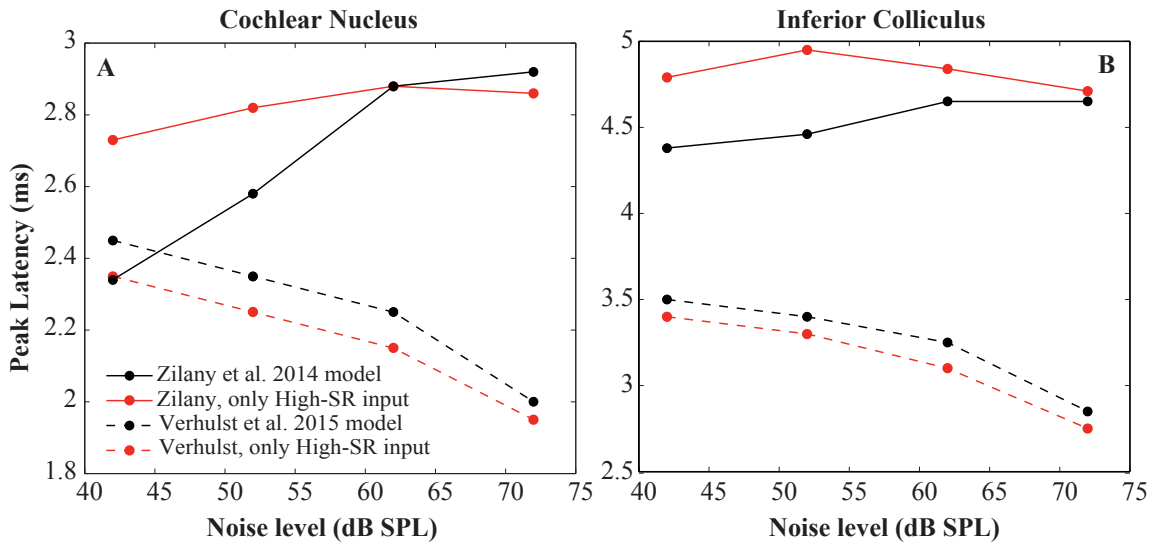

Figure 5-12: CN (A) and IC (B) peak latency as a function of noise level using either the Zilany (solid) or Verhulst (dashed) AN model response as input to the brainstem model.

5.4 Forward masking ABR model simulations

To better understand the observed effects in the forward masking data discussed in section 4.2, the AN response was simulated in a forward masking paradigm. The Verhulst model was used for the simulations as it better captures the across-frequency mechanics of the cochlea likely important for broadband signals such as the chirp. Further, the Zilany model failed to capture the effects of forward masking when using the broadband masker and probe inconsistent with our data. Although we analyzed the ABR wave-V latency in the forward masking experiment, here we only look at how the AN population response (i.e., CAP/wave-I) changes with MPI because there is currently no appropriate model that captures the ABR latency effects in masking paradigms. Low-SR neuropathy in the model should 1) have a larger effect on the CAP at short MPI (i.e. larger reduction in CAP) 2) cause the CAP to recovery/grow more quickly with increasing MPI. These effects at the level of the AN may potentially translate to 1) a larger shift in ABR wave-V latency at short MPI and 2) larger change of the ABR wave-V latency in forward masking with MPI.

5.4.1 Auditory nerve

Fig.5-13 shows the model AN response in forward masking for high-SR (A), low-SR (B), and combined fibers (C). Consistent with physiological studies, the probe-elicited AN response of the high-SR fibers in the model grows more rapidly with increasing MPI than the low-SR fiber response [95]. The low-SR probe response is less affected by the preceding noise than the high-SR response (Fig.5-13, A, B). The combined AN response (Fig.5-13, C) tends to reflect the high-SR response because of their higher firing rate. These observations are summarized in Fig.5-14, which shows the AN peak response to the probe normalized to the control (i.e., no preceding masker). Notice that the AN response is almost fully recovered by 200ms MPI, consistent with our forward masking experimental data, which generally shows a full recovery of the wave-V latency and detection thresholds by 201ms. Also, in the model, the low-SR response to the probe goes above that of the control. This is an artifact and is likely because of the grouping of the low- and medium-SR fibers, which have different recovery times in the model (i.e., medium-SR have a fast recovery compared to the low-SR). When there is a selective loss of low-SR fibers, the relative growth of the AN probe response (i.e., CAP/ABR wave-I) is faster than the combined response of both low- and high- SR fibers, as shown in Fig.5-15. Additionally, to determine whether peripheral changes affects the forward-masking time course of the AN CAP, we simulated hearing impairment (HI) in the model by reducing the compression and broadening the tuning of the cochlear channels. This was motivated by studies that have used changes of forward masking detection thresholds as a measure of cochlear compression [92]. Shown by the dashed traces in Fig.5-15, the reduced cochlear compression and broader tuning in the HI model accentuate the SR-dependent differences in the CAP growth with MPI: the high-SR fiber CAP grows more quickly whereas the CAP growth of the low-SR fibers is reduced relative to the NH model. However, the combined response of these fibers in the HI model does not significantly differ from that of the NH model, suggesting that peripheral changes alone do not impact the forward masking time course of the CAP growth. The SR-dependent changes in the CAP may translate to

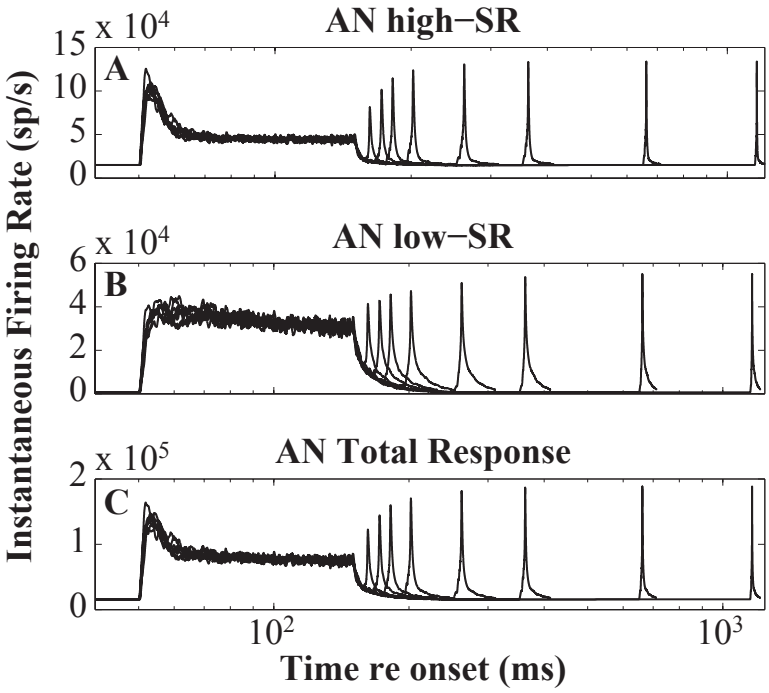

Figure 5-13: Simulated forward masking response of high-SR (A), low-SR (B), and combined (C) ANFs. The AN probe response increases faster for the high-SR than the low-SR with increasing MPI.

differences in how ABR wave-V latency changes in forward masking: if we consider a simple integrate-and-fire neuron as representative of brainstem cell units, a reduced input to the model (i.e., smaller CAP) would delay the neural response. However, this model does not differentiate between low vs. high-SR loss. Thus, at this time, it is unclear whether a selective loss or a general loss of ANFs affects ABR wave-V latency in forward masking. Modelling of the brainstem would help answer this question.

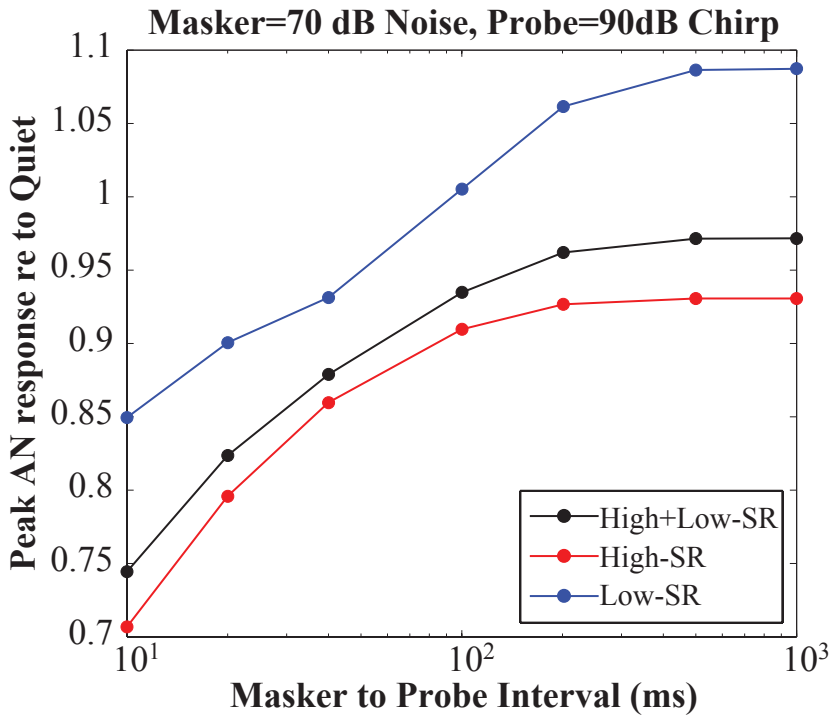

Figure 5-14: The effect of preceding masker on the AN probe response for different SR fibers as a function of MPI. Peak AN response is normalized to peak response with no preceding masker.

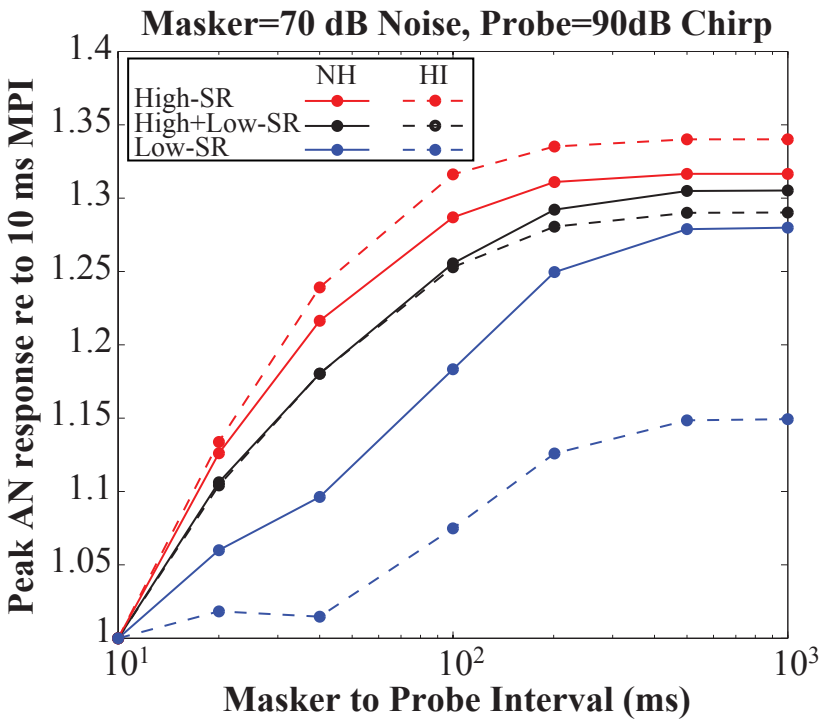

Figure 5-15: Simulated probe-elicited CAP as a function of MPI for different SR fibers for NH (solid lines) and HI (dashed lines) model. The CAP is normalized to the response at a 10ms MPI.

Chapter 6

DISCUSSION

Recent animal studies have shown that both moderate noise exposure and aging can produce significant degeneration of the synaptic connections between ANFs and hair cells without changes to the hair cells themselves [58, 73, 107, 36]. This synaptopathy, which can occur immediately after noise exposure, is followed by a slow degeneration of the entire auditory nerve cell. However, once the synapse is lost, each ANF is silent, whether or not its cell body and central axon survive. This diffuse neural loss likely degrades aspects of supra-threshold auditory processing, because it appears to be selective for the subset of ANFs with high thresholds and low-SRs [36, 68], but it does not elevate thresholds as measured by conventional audiometry. Given these characteristics, this damage has been called "hidden hearing loss" [105].

6.1 ABR in noise

Motivated by the animal studies, we and others have looked for correlates of this "hidden" hearing loss in human listeners. A growing number of studies suggest that inter-subject differences in humans with NHTs measured both behaviorally and using electrophysiological measures (such as ABR wave-I amplitudes and the envelope following response or EFR) can be explained by ANF loss [113, 5]. Here, we show that compared to those with small latency shifts, the NHT listeners showing large wave-V latency shifts with increasing masker level are the listeners who perform better on a

sound localization task that requires discrimination of interaural timing differences in sound envelopes. In mice, we show that noise-induced cochlear synaptopathy reduces an analogous measure of ABR latency shift. In both mice and human subjects, the masking-noise latency shift correlates with the growth of ABR wave-I amplitude with stimulus level, but not with measures of hair cell function (helping to rule out dysfunctions involving cochlear mechanics). Taken together, the data suggest that the latency shift in masked ABRs could be a useful metric of ANF loss in human subjects.

It is difficult to compare our human results with previous studies because 1) until recently, effects typically have been investigated on a group, rather than individual level and 2) there has been more focus on absolute rather than relative measures. Evidence of a reduced latency shift in humans has been previously seen in older NHT human listeners [16]; however, this effect was only seen when the older listeners were divided into "better" and "worse" listeners based on audiogram thresholds and was also quite small. Generally, ABR wave-V latency increases with age [16]. This is in contrast to what we observed in the few listeners we tested who were over the age of 35: their absolute masked ABR latencies were short relative to the ABR latencies in our other listeners, who were all under the age of 30 (not shown). Furthermore, little difference was found in the ABR wave-V latency in quiet at the tested click levels.

6.1.1 Mechanisms of ABR wave-V latency shift in noise

The results here corroborate previous findings that implicate a neural rather than cochlear-place mechanism underlying ABR wave-V latency shifts in noise. Using a high-pass subtractive masking technique and varying broadband noise level, Burkard and Hecox (1987; [13]) showed that wave-V latency changes were greater than could be explained on the basis of shifts in cochlear region of excitation. Additionally, there was an interaction between stimulus repetition rate and noise level on wave-V latency [12, 13, 15]. Higher repetition rates results in a decrease in rate-induced ABR peak latency shift in the presence of masking noise, suggesting an overlap in the synaptic/neural mechanisms underlying masking-induced and rate-induced latency

shifts.

Studies suggest that the ABR wave-V latency shift with noise level is linked to neural desynchronization either originating from presynaptic events involving the synaptic vesicle cycle, or from decreased probability of discharge in post-synaptic events [12, 13, 17, 15]. Building on this neural hypothesis, we note that the degree to which noise desynchronizes ANFs is greater in high-SR than low-SR fibers, perhaps because high-SR fibers have a low response threshold and smaller dynamic range [63, 99]. In contrast, low-SR fibers, with their higher thresholds, are more resistant to masking by background noise [22] and as such, their relative contribution to the total neural response increases as noise level increases.

6.1.2 Effects of central auditory changes to ABR latency

While cochlear synaptopathy likely affects ABR wave-V latency shift with noise level, alterations in brainstem/central auditory activity may also influence the ABR latency. Hyperactivity in the central pathways has been seen after moderate noise exposure and may explain why the ABR wave-V/I amplitude ratio increases [41, 105]. At the level of the inferior colliculus (IC), older mice have a smaller response latency to amplitude-modulated sounds, perhaps due to a decrease in inhibition strength with aging [112]. Decreased inhibition at the level of the IC may also explain why the high-frequency cut-off of the EFR is lowered in humans with aging [93]. Separately, following carboplatin administration, the absolute wave-V latency increases, albeit without any changes in the slope of the latency vs. noise-level curve [17]. Carboplatin causes significant changes in the auditory periphery, including loss of IHCs at low doses. The loss of IHCs reduces the strength of ANF input to higher auditory centers, which can cause changes to central pathway processing. Further, Burkard et al. (1997; [17]) did not observe differences in the slope of the wave-V latency vs. noise level, likely because the damage caused by carboplatin was not selective to a low-SR but rather caused a general loss of ANFs. Nevertheless, this reduced input may not only lead to delayed responses but also degraded coding of temporal information [72]. Thus, it is unclear if and how central changes affect the ABR wave-V latency shift

with noise level and how those effects are related to synaptopathy; more systematic investigation is necessary.

To disambiguate the effects of central vs. auditory nerve changes on ABR, we investigated the ABR wave-IV latency shift with noise level in mice with two types of noise exposure. Both exposures caused significant temporary threshold shifts; neither caused significant loss of sensory cells; yet only one caused significant loss of ANFs [47]. Consistent with our hypothesis, only the neuropathic exposure led to a significant reduction in the wave-IV shift. These results provide empirical evidence that the reduction in wave-IV latency shift with noise level after acoustic injury is due to the loss of ANFs rather than a direct effect of noise exposure on the central auditory system.

6.2 Cochlear synaptopathy of low-SR fibers

Although we do not show direct proof of a preferential loss of low-SR fibers in our mice, there is growing evidence that low-SR ANFs are more susceptible to deafferentation with noise exposure and age. In aged gerbils, low- and med-SR fibers in the high CF regions declined from 57% to 29% of the population [106]. Similarly, following 2 hr exposure in guinea pigs, Furman et al. (2013; [36]) observed a drop in the percentage of ANFs that had low SR, from 47% to 29%. In addition to the single-unit population studies, recent histological analysis in mice reveals a selective low-SR loss with noise exposure [68].

Low-SR fibers may have certain physical disadvantages that make them more vulnerable to excitotoxic terminal swelling. The dendritic endings of low-SR fibers tend to be long and thin, as little as half the diameter of high-SR fibers [65, 39], with similarly smaller synaptic endings. Having physically smaller cell membranes may reduce the ability of a low-SR terminal to survive the physical swelling that results after noise exposure. Furthermore, low-SR fibers contain fewer mitochondria than high-SR fibers, a difference that presumably reflects the relative demand on Na^+/K^+ pumping, depending on discharge rate [64]. Studies of glutamate

excitotoxicity in central neurons suggest that Ca^{++} entry is an important event in the excitotoxicity cascade, and that mitochondria are a crucial component of Ca-buffering machinery [116]. As such, it is plausible to interpret the reduction in the wave-IV latency rate of change in our neuropathic mice as arising from the loss of low-SR fibers.

6.3 Forward Masking

6.3.1 Effects of low-SR fiber deafferentation on the CAP forward masking recovery function

On a single-unit level, animal studies have shown differences in forward masking between low and high-SR fibers [95, 36]. Generally, fibers with less than 100ms recovery time are high-SR and fibers with greater than 100ms recovery time are mostly low-SR [36]. The clear separation between SR types would suggest that contributions from different SR types should be separable with gross physiology such as ABR or CAP.

Loss of low-SR fibers may increase masking at very short intervals and a complete loss may yield a full recovery of the CAP (i.e. ABR wave-I) by 100ms, at which point high-SR fibers have fully recovered to the unmasked response. Indeed, previous work shows a faster recovery of the CAP in forward masking with deafferentation of low-SR fibers [106]. However, Furman et al. (2013; [36]) did not observe the same effect with a partial loss of low-SR fibers. They explained that when considering group mean responses, when some low-SR fibers are missing, the remaining 60% of low-SR fibers seem sufficient to provide unchanged, normalized CAP responses to forward masked stimuli. Further, they suggest that one may see differences in the CAP forward masking on an individual basis before and after exposure.

Although we could not obtain reliable recordings of the ABR wave-I/CAP in forward masking in this study, we can infer that there are individual differences in the CAP forward masking recovery function based on the individual differences we see

in the ABR wave-V latency forward masking function and our modelling simulations (see chapter.5). It is plausible to propose that changes at the level of the AN affect the timing of later auditory pathways, since we showed in Fig.4-5 that the change in ABR wave-V latency with noise level is predicted by the growth of ABR wave-I both in humans and animals. Therefore, a greater shift in wave-V latency at short MPI would translate to increased masking of the CAP at these short intervals, potentially due to the loss of low-SR fibers. Additionally, the large decrease in wave-V latency with increasing MPI suggests a faster recovery of the CAP.

6.3.2 Effects of forward masking on ABR wave-V latency

In our cohort of young NHT listeners, we observed an increase in the wave-V latency at short forward-masking intervals. As the forward-masker interval increased, the wave-V latency systematically decreased reaching baseline latency by 201ms MPI. A decrease in ABR peak latency with increasing forward-masker interval has been reported previously in humans [61, 57, 13, 60, 121], gerbils [9] and mice, using tone-burst maskers and probes [122], noise-burst maskers and probes [9], and noise-burst maskers and click probes [61, 57, 13, 60, 121]. As forward-masking recovery time appears to depend on the acoustic characteristics of the probe and masker [60], comparison across studies of forward masking recovery times will not be done here. Further, although our choice of masker intensities and duration have an affect on the wave-V latency, these acoustic characteristics were kept fixed across subjects in the ABR experiment so as to target underlying neural rather than cochlear mechanisms involved with forward masking. Indeed, previous work has shown that human ABR recovery of peak latency to click stimuli from a noise forward masker is similar for a range of probe and masker level as long as the relative level of the probe to the masker is held constant [61].

The greater wave-V latency shifts that we observe in our subjects who perform relatively poorly in the forward masking detection task has been shown in studies of aging in humans [121] and animals [9, 122]. Walton et al. (1999) reported greater wave-V latency shifts at short MPI in older listeners with NHTs relative to the young

NHT group. This effect was observed only in high frequency regions, where animal studies suggest larger low-SR fiber innervations [117]. The greater wave-V latency shifts at short MPIs in the older NHT listeners subsequently yielded larger changes in wave-V latency with MPI compared to the young listeners [121].

Boettcher et al. (1996; [9]) reported that aged gerbils showed greater ABR wave-IV latency shifts than young-adult gerbils in response to a second noise-burst when preceded by a noise-burst forward masker. They argued that the prolongation of ABR wave-IV latency in aged gerbils was the result of changes in the brain of aged animals and not due to peripheral changes, because the CAP showed no age-dependent change in forward masking-induced latency shift or recovery rate. Similarly, middle-aged mice demonstrated greater wave-V latency in forward masking conditions while the CAP showed no such age-dependent latency shift [122]. This is in contrast with some previous work and our current hypothesis that aging, similar to noise exposure, would result in a selective loss of low-SR fibers. This loss would in turn cause a faster recovery of the CAP in forward masking, resulting in larger decrease in wave-V latency with increasing MPI. The animal studies described here do not show a difference in CAP recovery in forward masking between the young and aged groups. One reason may be that in both studies, the aged animals had cochlear hearing loss and thus, the peripheral changes may have masked the effects of ANF loss on the CAP recovery rate.

6.3.3 Forward masking detection thresholds

Psychophysical forward masking detection thresholds have previously been shown to be significantly correlated to speech intelligibility in interrupted noise [28, 29]. As forward masked thresholds increase (get worse), speech recognition in interrupted noise degrades. Interestingly, age related differences have also been observed in this relationship. Older listeners with NHTs show an increase in forward masking thresholds at short MPIs that correlates with a degradation of speech recognition performance in noise [28, 29]. This finding may be linked to age-related decline of ANFs that may affect how well the auditory system recovers from prior stimulation

and speech performance in noisy environments.

Here we show that individual differences in how ABR wave-V latency changes with increasing MPI in young NHT listeners is related to not only to differences in the recovery of behavioral forward masking detection thresholds (Fig.4-11), but also to how much a listener's detection threshold is affected by a preceding masker at a short MPI (i.e., cost, Fig.4-12). The change in both the wave-V latency and detection thresholds in forward masking is linked to the effect of a preceding masker ("cost") at short MPIs: greater shifts in the ABR wave-V latency and the detections thresholds at 20ms MPI went hand in hand with a larger change not only in the wave-V latency but also in the forward masking detection thresholds as function of MPI. Although this may suggest a faster recovery in both thresholds and wave-V latency, our analysis suggests that this effect of preceding masker is consistent across MPIs: if a listener was hurt more by a preceding masker at 20ms, they also showed larger thresholds and wave-V latency shifts at 201ms MPI. This is similar to previous work on older NHT listeners [28, 29], who showed larger effects of forward masking (higher thresholds) relative to young controls. Further, we find that the change in wave-V latency is related to the "cost" of forward masking at short MPI: the greater the amount of masking (higher threshold shifts) at a 20ms MPI, the larger the change in wave-V with increasing MPI.

In our cohort of subjects, the differences we observed in the psychophysical forward masking measure is largest at the shortest MPIs and may reflect the contributions of different SR fibers: at a very short MPI, the probe may be encoded more robustly by low-SR fibers as their response is resistance in the presence of masking noise [22]. A loss of these fibers would presumably increase forward masking detection thresholds. Indeed, a model of the auditory periphery closely approximates human psychophysical forward masking data when high- and low-SR types are combined [75]. Additionally, because the low-SR fibers are a major input to the olivocochlear reflex [66, 82], which serves an "antimasking" role [53], a loss of these fibers should cause deficits in experiments such as forward masking.

6.3.4 Neural correlates of forward masking

Although it may be tempting to try to explain the forward masking effects we observe both in the ABR wave-V latency and behavioral thresholds in terms of the adaption properties of different SR fibers, there are other neural factors that significantly contribute to the effects seen in forward masking. For instance, forward masking can be observed in cochlear implant patients where hair cell physiology may not be relevant [70]. The inhibitory networks of the brainstem and cortex may also significantly contribute to forward masking. It is already known that the efferent inhibitory mechanisms, for instance, influence the CN response to forward masking [111]. In the cortex, responses of cortical neurons to forward masking in guinea-pigs showed threshold shifts larger than in the AN, CN, and IC, suggesting that their is central contribution to forward masking [2]. However, the threshold shifts observed in the cortical neurons were larger than observed psychophysically. By recording forward suppression in marmoset IC neurons, Nelson et al., (2009;[85]) suggested that psychophysical forward masking may arise from forward masking at the level of the IC and involves inhibitory mechanisms from within the IC or from earlier auditory processing stages [85].

Our results may indeed be explained by differences in inhibition at the brainstem level, especially since the ABR wave-V is generated in the LL and IC [81, 76]. However, a more recent study has shown that forward-masking suppression in the ventral cochlear nucleus (VCN) of the guinea-pig closely resembles forward-masking threshold shifts observed in humans [125]). Data from VCN lends support to the idea that different ANFs differ in their rate of recovery from forward masking. Specifically, comparing primary-like and primary-notch neurons of the VCN, Winter et al. found that low-SR neurons took longer to recover from forward masking than high-SR neurons, just as in AN studies [125]. As such, although it is unclear which site of the auditory brainstem produces the forward masking effects we observes in human data, it is plausible to believe that a differential loss of different ANF types will influence brainstem mechanisms that are responsible for forward masking.

6.4 Modelling Efforts

The model simulations presented in this thesis reveal the capabilities and limitations of current auditory models when trying to capture ABR latency effects in noise. Comparison of two models showed rather different effects. At the level of the AN, both the Zilany and Verhulst models showed an increased contribution of low-SR fibers with increasing noise level, reflecting the low-SR resistant to masking. The growing contribution of the low-SR fibers with noise level yielded a trend of increasing AN response latency in the Zilany model. In contrast, the Verhulst did not show a latency increase as the influence of the low-SR ANFs increased. One of the fundamental differences in these two models, other than the differences in the excitation pattern illustrated in Fig.5-7, is the latency difference between the low and high-SR AN populations. Single-unit recordings show a delay of approximately 1ms in the first spike in low-SR fibers relative to high-SR fibers [100]. These recordings were completed using tone-pips, different from the broadband stimuli used in the experiments and model simulations in this thesis. Further, the tone-pips were not presented in noise. In the Zilany model, the latency difference between the SR population is present not only at the onset of the background noise but also at each subsequent click presentation. As such, when the AN response is epoched to the click stimulus and averaged, the latency difference between the low- and high-SR population is preserved and the overall AN population response latency increases as low-SR responses become more influential. However, the latency difference between the two SR populations is only apparent at the onset of the noise in the Verhulst model. This difference is not preserved in response to the additional click stimuli. As a result, the click-evoked AN response latency does not increase with the recruitment of the low-SR fibers in the Verhulst model. At this time, it is unclear whether the onset latency difference between low and high-SR ANF populations is preserved when an additional stimulus is added to noise: to our knowledge, there are no published single-unit AN recordings that analyze and compare the onset latency between low and high-SR ANFs types in response to the stimuli in noise. Thus, future work should involve recording and

analyzing the onset response latency of different SR fibers using stimuli in noise.

The output of the brainstem model also demonstrates contrasting results when using the AN response of the Verhulst and Zilany model as input. In the Zilany model, the CN and IC peak response latency increases with noise level, reflecting the effect seen at the level of the AN. The Verhulst model shows a decrease of the CN and IC peak response latency with growing noise, contradicting experimental results. The loss of low-SR fibers had little effect on the growth of the latency both at the level of the CN and IC for the Verhulst model, whereas the latency shift with noise level was reduced in the Zilany model. This difference is likely due to how the contribution of the different frequency regions changes in the models as the noise level is increased. As the noise level increases, the peak response slightly changes to the high frequency regions-where the group delay is shorter- in the Verhulst model in contrast to the apical shift observed in the Zilany model. This basal shift in the Verhulst model presumably is a result of the level-dependent tuning of the cochlear mechanics [118]: as the noise level is raised, the cochlear filter becomes broader, causing a basal shift in the peak AN response. The apical shift in the Zilany model is due to the masking of the high-frequency regions by the noise. Although it is true that ABR wave-V has frequency contributions from low frequencies [1], there are a number of studies that show that the wave-V latency increase with noise level is not due to changes in the cochlear excitation pattern [12, 13, 17, 15]. Therefore, the effect of the excitation pattern changes on the brainstem response in the models warrants further investigation.

Despite differences in the models and potential confounds, the Zilany model shows a trend of increasing latency with noise level that is attributable to the recruitment of low-SR fibers. The observed latency shift seen at all levels of the Zilany auditory model is too small compared to that of ABR data, which show a wave-V latency shift of 0.8-1.2ms with a 40dB increase in noise level. At the level of the IC, one of the sites where the ABR wave-V is generated [81, 76], the shift in the model is only 0.27ms. This small shift suggests that low-SR recruitment may not be the only mechanism causing wave-V latency to increase with increasing noise level. Changes

in the brainstem may also contribute to this phenomena. Modelling, for instance, how the CN or IC inhibition and excitation strength changes with noise level or how cochlear synaptopathy affects these properties may further elucidate why the ABR wave-V latency increases with noise level.

The underestimation of the latency shift may also suggest a need to improve the brainstem model as it is quite crude compared to that of the Zilany peripheral model. The current brainstem model uses a simple linear filter to model the synapse at the CN and IC and is based on only two cell types (chopper and onset neurons) out of many different types of neural units in the brainstem. The model is also missing the superior olivary complex (SOC) and the LL, located between the CN and IC in the brainstem. The neural units in SOC are thought to be the driving input into the LL, one of the generator sites of ABR wave-V [76]. Further, the brainstem model was designed for steady state rather than onset stimuli. As such, it is necessary to expand on this model to capture the effects we observe in data.

Similar to the ABR in noise model simulations, preliminary forward masking simulations using the Verhulst model showed a trend that is consistent with our hypothesis and previous animal data [9]: the loss of low-SR fibers results in a faster growth of the CAP (i.e., AN population response) with increasing MPI. However, we have yet to show how this change at the AN translates to ABR wave-V latency changes in forward masking. Furthermore, it is unclear how this would affect forward masking detection thresholds. Future work will include simulating ABR wave-V latency in forward masking and the effects of ANF loss on forward masking detection thresholds and wave-V latency recovery.

An important part of the auditory system that has not been implemented in either model is the medial olivocochlear (MOC) efferent system. The MOC innervates OHCs and has an "antimasking" effect: activation of the MOC reduces the resistance of the OHC basolateral membrane, effectively shunting the OHC receptor potential and reducing the "gain" of the cochlear amplifier [37]. This effect has been shown to be important for detection and discrimination of signals in noise [128] and likely plays a strong role in our experimental measurements, both in the ABR in noise and forward

masking ABR and behavioral task. Indeed, click stimuli at high sound levels elicit efferent activity [42].

The integrity of low-SR fibers could be important for efferent activation because of their central projections. Low-SR fibers give rise to substantially larger axonal arborizations within the AVCN compared to that of high-SR fibers [32, 82]. The long branches emitted by low-SR fibers synapse onto the small cell cap units [67, 103]. These units have been shown to send axons to neurons belonging to the MOC efferent system [126]. Thus, in this context, the low-SR ANFs play an important role in the efferent feedback circuit to the inner ear.

Moreover, MOC-induced inhibition on low-SR fibers may be important at the high intensity levels we implement in our experiments. For high-SR fibers, the MOC-induced inhibition is greatest at low sound levels, but for low-SR fibers, this inhibition peaks at mid-to-high-sound levels [43]. Although it may seem that the MOC effects of the low-SR fibers could be ignored because of their small population size, their response at high levels and in noise most likely plays an outsized role in behavioral tasks and ABR. Consequently, a selective loss of low-SR fibers may reduce MOC-induced inhibition in the AN, thereby reducing the signal-to-noise ratio of stimuli presented in noise and potentially in forward masking. As such, it is important to model the MOC-efferent system and analyze the effects on the ABR and forward masking thresholds.

Chapter 7

CONCLUSION

We conclude that a substantial population of the individual differences observed in NHT listeners, both in perceptual abilities and in ABR wave-V latency shift with noise level or with MPI in forward masking, reflects different degrees of ANF loss. Unlike absolute ABR peak amplitude and latency analyses, where inter-subject variability in signal-to-noise ratio is large and depends on numerous factors independent of coding fidelity, we show that the relative change in latency in noise or in forward masking could be a robust measure of cochlear synaptopathy. The testing conditions we adopted (utilizing target signals presented with simultaneous/forward maskers) stress good temporal coding of sound that is clearly audible, mimicking some of the challenges experienced in everyday settings, where many middle-aged listeners report communication difficulties.

Future studies should focus on simultaneously measuring ABR wave-I with wave-V in noise and in forward masking. Recording wave-I will allow for direct comparison of changes in ABR peak latencies and amplitude of both a measure emanating from the auditory nerve (wave-I) and the brainstem (wave-V). This will aid in the determination of whether the present results are due to changes in the auditory periphery or from more central auditory regions. Further, studies should also explore the precision of these measures in noise-exposed human cohorts. It is also important to expand on the preliminary modeling work presented here to better understand the underlying neural mechanisms of ABR wave-V latency changes in masking and its

relationship to perception.

List of Journal Abbreviations

Acta Otolaryngol	Acta Otolaryngologica
Acta Otolaryngol Suppl ...	Acta Otolaryngologica Supplementum
Acta Otorhinolaryngol Belg	Acta Acta Otorhinolaryngologica Belgica
Am J Ind Med	American Journal of Industrial Medicine
Am J Otolaryngol	Americal Journal of Otolaryngology
Am J Phys Med Rehabil ...	American Journal of Physical Medicine and Rehabilitation
Anesth Analg	Anesthesia and Analgesia
Ann Stat	Annals of Statistics
Arch Intern Med	Archives of Internal Medicine
Audiol Neurotol	Audiology and Neurotology
Behav Brain Res	Behavioural Brain Research
Br J Audiol	British Journal of Audiology
Clin Neurophysiol	Clinical Neurophysiology
Curr Biol	Current Biology
Ear Hear	Ear and Hearing
Front Biosci	Frontiers in Biosciences
Front Int Neurosci	Frontiers in Integrative Neuroscience
Front Neurosci	Frontiers in Neuroscience
Front Syst Neurosci	Frontiers in Systems Neuroscience
Hear Res	Hearing Research
Hum Brain Mapp	Human Brain Mapping
Int J Audiol	International Journal of Audiology
Int J Lang Commun Disord	International Journal of Language and Communication Disorders
J Acoust Soc Am	Journal of the Acoustical Society of Americal
J Am Acad Audiol	Journal of the American Academy of Audiology
J Am Med Assoc	Journal of the American Medical Association
J Assoc Res Otolaryngol ...	Journal of the Association for Research in Otolaryngology
J Clim Appl Meteorol	Journal of Climate and Applied Meteorology
J Comp Neurol	The Journal of Comparative Neurology
J India Inst Speech Hear ..	Journal of the All India Institute of Speech and Hearing
J Laryngol Otol	The Journal of Laryngology and Otology

J Neurophysiol	Journal of Neurophysiology
J Neurosci	Journal of Neuroscience
J Neurosci Meth	Journal of Neuroscience Methods
J Occup Environ Med	Journal of Occupational and Environmental Medicine
J Speech Hear Res	Journal of Speech, Language and Hearing Research
Nat Neurosci	Nature Neuroscience
Noise Health	Noise and Health
Physiol Rev	Physiological Reviews
Proc IEEE	Proceedings of the IEEE
Proc Meet Acoust	Proceeding of Meetings on Acoustics
Proc Natl Acad Am U S A	Proceedings of the National Academy of Sciences of the United States of America
Psychophysiol	Psychophsyiology
Sig Proc IEEE	IEEE Signal Processing Magazine
Trend Cogn Sci	Trends in Cognitive Sciences
Trends Neurosci	Trends in Neurosciences

Bibliography

[1] C. Abdala and R.C. Folsom. The development of frequency resolution in humans as revealed by the auditory brain?stem response recorded with notched?noise masking. *Acoust. Soc. Am.*, 98(2):921–930, 1995.

[2] A. Alves-Pinto, S. Baudoux, A.R. Palmer, and C.J. Sumner. Forward masking estimated by signal detection theory analysis of neuronal responses in primary auditory cortex. *J Acoust Soc Am*, 11(3):477–494, 2010.

[3] R. H. Baayen, D. J. Davidson, and D. M. Bates. Mixed-effects modeling with crossed random effects for subjects and items. *J Mem. and Lang.*, 59(4):390–412, 2008.

[4] Leslie R Bernstein and Constantine Trahiotis. Enhancing sensitivity to interaural delays at high frequencies by using "transposed stimuli". *J Acoust Soc Am*, 112(3):1026–1036, 2002.

[5] H. M. Bharadwaj, S. Masud, G. Mehraei, S. Verhulst, and Barbara Shinn-Cunningham. Individual Differences Reveal Correlates of Hidden Hearing Deficits. *J Neurosci*, 35(5):2161–2172, 2015.

[6] H. M Bharadwaj, S. Masud, and B. G. Shinn-Cunningham. Bottom-up and top-down contributions to individual differences in auditory spatial attention task performance. Presented at the Abstracts of the Midwinter Meeting of the ARO XXXVI: #887, San Diego, CA, 2013.

[7] H. M. Bharadwaj, S. Masud, and B. G. Shinn-Cunningham. The role of high-frequency cues for spatial hearing in rooms. In *Proc Meet Acoust*, volume 19, page 015049. Acoustical Society of America, 2013.

[8] H. M. Bharadwaj, S. Verhulst, L. Shaheen, M. C. Liberman, and B. G. Shinn-Cunningham. Cochlear neuropathy and the coding of supra-threshold sound. *Front Syst Neurosci*, 8:26, 2014.

[9] F.A. Boettcher, J.H. Mills, J.L. Swedloff, and B.L. Holley. Auditory evoked potentials in aged gerbils: responses elicited by noises separated by a silent gap. *Hear Res.*, 102(1):167–178, 1996.

[10] H. Bokil, P. Andrews, J. E. Kulkarni, S. Mehta, and P. P. Mitra. Chronux: a platform for analyzing neural signals. Journal of neuroscience methods. *J Neurosci Meth*, 192(1):146–151, 2010.

[11] J. Bourien, Y. Tang, A. Batrel, C .and Huet, M. Lenoir, S. Ladrech, and J. Wang. Contribution of auditory nerve fibers to compound action potential of the auditory nerve. *J Neurophys*, 112(5):1025–1039, 2014.

[12] R. Burkard and K. Hecox. The effect of broadband noise on the human brainstem evoked response. I. Rate and intensity effects. *J Acoust Soc. Am*, 74:1204–1213, 1983.

[13] R. Burkard and K. Hecox. The effect of broadband noise on the human brainstem auditory evoked response. III. Anatomic locus. *J Acoust Soc. Am*, 81:1050–1063, 1987.

[14] R. Burkard, J. McGee, and E. Walsh. Effects of stimulus rate on the feline brain-stem auditory evoked response during development. I. Peak latencies. *J Acoust Soc. Am*, 100(1), 1996.

[15] R. Burkard and D. Sims. The Human Auditory Brainstem Response to High Click Rates: Aging Effects. *Am J Audiol*, 10:53–61, 2001.

[16] R. Burkard and D. Sims. A comparison of the effects of broadband masking noise on the auditory brainstem response in young and older adults. *Am J Audiol*, 11:13–22, 2002.

[17] R. Burkard, P. Trautwein, and R. Salvi. The effects of click level, click rate, and level of background masking noise on the inferior colliculus potential (ICP) in the normal and carboplatin-treated chinchilla. *J Acoust Soc. Am*, 102(6), 1997.

[18] R. Burkard and H. Voigt. Stimulus dependencies of the gerbil brainstem auditory evoked response BAER. I. Effects of click level, rate and polarity. *J Acoust Soc. Am*, 85:2514–2525, 1989.

[19] R.F. Burkard, J. J. Eggermong, and M. Don. *Auditory Evoked Potentials: Basic Principles and Clinical Application*. Lippincott Williams and Wikins, 2007.

[20] G. D. Chermak and F. E. Musiek. *Central auditory processing disorders: New perspectives*. San Diego: Singular publishing group, 1997.

[21] J. A. Costalupes. Representation of tones in noise in the responses of auditory nerve fibers in cats. I. Comparison with detection thresholds. *J Neurosci*, 5(12):3261–3269, 1985.

[22] J. A. Costalupes, ERIC D Young, and DANIEL J Gibson. Effects of continuous noise backgrounds on rate response of auditory nerve fibers in cat. *J Neurophysiol*, 51(6):1326–1344, 1984.

[23] T. Dau. The importance of cochlear processing for the formation of auditory brainstem and frequency following responses. *J Acoust Soc Am*, 113(2):936–950, 2003.

[24] T. Dau, O. Wenger, V. Mellert, and B. Kollmeier. Auditory brainstem responses with optimized chirp signals compensating basilar-membrane dispersion. *J Acoust Soc Am*, 107(3):1530–1540, 2000.

[25] M. Dietz, T. Marquardt, N. H. Salminen, and D. McAlpine. Emphasis of spatial cues in the temporal fine structure during the rising segments of amplitude-modulated sounds. *Proc Natl Acad Sci U S A*, 110(37):15151–15156, 2013.

[26] M. Don and J. J. Eggermont. Analysis of the click?evoked brainstem potentials in man using high?pass noise masking. *Hear Res*, 63(4):1084–1092, 1978.

[27] A.A. Dreyer and J. Oxenham, A. Effects of level and background noise on interaural time difference discrimination for transposed stimuli. *J Acoust Soc Am*, 123(1):EL1–EL7, 2008.

[28] J. R. Dubno, A. R. Horwitz, and J. B. Ahlstrom. Benefit of modulated maskers for speech recognition by younger and older adults with normal hearing. *J Acoust Soc Am*, 111(6):2897–2907, 2002.

[29] J. R. Dubno, A. R. Horwitz, and J. B. Ahlstrom. Recovery from prior stimulation: masking of speech by interrupted noise for younger and older adults with normal hearing. *J Acoust Soc Am*, 113(4):2084–2094, 2003.

[30] C. Elberling, J. Callo, and M. Don. Evaluating auditory brainstem responses to different chirp stimuli at three levels of stimulation. *J Acoust Soc Am*, 128(1):215–223, 2010.

[31] M. Elhilali, L. Ma, C. Micheyl, A. J. Oxenham, and S. A. Shamma. Temporal coherence in the perceptual organization and cortical representation of auditory scenes. *Neuron*, 61(2):317–329, 2009.

[32] D.M. Fekete, E.M. Rouiller, M.C. Liberman, and D.K. Ryugo. The central projections of intracellularly labeled auditory nerve fibers in cats. *J Comp Neur*, 229(3):432–450, 1984.

[33] M. Florentine, S. Buus, and C. R. Mason. Level discrimination as a function of level for tones from 0.25 to 16 kHz. *J Acoust Soc Am*, 81(5):1528–1541, 1987.

[34] D. J. Franklin, M. J. McCoy, G. K. Martin, and B. L. Lonsbury-Martin. Test/retest reliability of distortion product and transiently evoked otoacoustic emissions. *Ear and Hear*, 13(6):417–429, 1992.

[35] Robert D Frisina, Robert L Smith, and Steven C Chamberlain. Encoding of amplitude modulation in the gerbil cochlear nucleus: I. A hierarchy of enhancement. *Hear Res*, 44(2):99–122, 1990.

[36] A. C. Furman, S. G. Kujawa, and C. M. Liberman. Noise-induced cochlear neuropathy is selective for fibers with low spontaneous rates. *J Neurophysiol*, 110(3):577–586, 2013.

[37] D. C. Geisler. *From sound to synapse: physiology of the mammalian ear*. Oxfored University Press, 1998.

[38] Brian R Glasberg and Brian CJ Moore. Derivation of auditory filter shapes from notched-noise data. *Hear Res*, 47(1):103–138, 1990.

[39] O. Gleich and S. Wilson. The diameters of guinea pig auditory nerve fibres: distribution and correlation with spontaneous rate. *Hear Res*, 71:69–79, 1993.

[40] M. Grassi and A. Soranzo. MLP: a MATLAB toolbox for rapid and reliable auditory threshold estimations. *Beh. Res. Meth.*, 41(1):20–28, 2009.

[41] J.W. Gu, B.S. Hermann, R.A. Levine, and J.R. Melcher. Brainstem auditory evoked potentials suggest a role for the ventral cochlear nucleus in tinnitus. *J Assoc Res Otolaryngol*, 13:819–833, 2012.

[42] J.J. Guinan, B.C. Backus, W. Lilaonitkul, and V. Aharonson. Medial olivocochlear efferent reflex in humans: otoacoustic emission (OAE) measurement issues and the advantages of stimulus frequency OAEs. *J Assoc Res Otolaryngol*, 4(4):521–540, 2003.

[43] J.J. Guinan Jr. *Physiology of olivocochlear efferents. In The cochlea*. New York: Springer, 1996.

[44] Matti Hämäläinen, Riitta Hari, Risto J Ilmoniemi, Jukka Knuutila, and Olli V Lounasmaa. MagnetoencephalographyâĂŤtheory, instrumentation, and applications to noninvasive studies of the working human brain. *Reviews of modern Physics*, 65(2):413, 1993.

[45] D.M. Harris and P. Dallos. Forward masking of auditory nerve fiber responses. *J. Neurphys*, 42(4):1083–1107, 1979.

[46] J. Harte, G. Pigasse, and T. Dau. Comparison of cochlear delay estimates using otoacoustic emissions and auditory brainstem responses. *J. Acoust. Soc. Am.*, 126:1291–1301, 2009.

[47] A. Hickox and M.C. Liberman. Is noise-induced cochlear neuropathy key to the generation of hyperacusis or tinnitus? *J Neurophys*, 111(3):552–564, 2014.

[48] S. E. Hind, R. Haines-Bazrafshan, C. L. Benton, W. Brassington, B. Towle, and D. R. Moore. Prevalence of clinical referrals having hearing thresholds within normal limits. *Int J Audiol*, 50(10):708–716, 2011.

[49] S. Jørgensen and T. Dau. Predicting speech intelligibility based on the signal-to-noise envelope power ratio after modulation-frequency selective processing. *J Acoust Soc Am*, 130(3):1475–1487, 2011.

[50] P. X. Joris, L. H. Carney, P. H. Smith, and TCT. Yin. Enhancement of neural synchronization in the anteroventral cochlear nucleus I. Responses to tones at the characteristic frequency. *J Neurophysiol*, 71:1022–1022, 1994.

[51] P. X. Joris and TCT. Yin. Responses to amplitude-modulated tones in the auditory nerve of the cat. *J Acoust Soc Am*, 91(1):215–232, 1992.

[52] P.X. Joris and P.H. Smith. The volley theory and the spherical cell puzzle. *Neuroscience*, 154(1):65–76, June 2008.

[53] T Kawase, B. Delgutte, and Liberman C.M. Antimasking effects of the olivocochlear reflex. II. Enhancement of auditory-nerve response to masked tones. *J. Neurphys*, 70(6):2533–2549, 1993.

[54] M. G. Kenward and J. H. Roger. Small sample inference for fixed effects from restricted maximum likelihood. *Biometrics*, pages 983–997, 1997.

[55] N.Y.S. Kiang. Curious oddments of auditory-nerve studies. *Hear Res*, 49(1):1–16, 1990.

[56] G.R. Kidd, C.S. Watson, and B. Gygi. Individual differences in auditory abilities. *J Acoust Soc Am*, 122(1):418–435, July 2007.

[57] S.J. Kramer and D.C. Teas. Forward masking of auditory nerve (N1) and brainstem (wave V) responses in humans. *J Acoust Soc Am*, 72(3):795–803, 1982.

[58] S.G. Kujawa and M.C. Liberman. Adding insult to injury: Cochlear nerve degeneration after "temporary" noise-induced hearing loss. *J Neurosci*, 29(45):14077–14085, November 2009.

[59] G. Kumar, F. Amen, and D. Roy. Normal hearing tests: is a further appointment really necessary? *J R Soc Med*, 100(2):66–66, 2007.

[60] R.E. Lasky. The effect of forward masker duration, rise/fall time, and integrated pressure on auditory brain stem evoked responses in human newborns and adults. *Ear and Hearing*, 14(2):95–103, 1993.

[61] R.E. Lasky and R. L. Allen. emporal masking of auditory evoked brainstem responses in human newborns and adults. *Hear Res*, 6(3):315–334, 1982.

[62] H. Levitt. Transformed up-down methods in psychoacoustics. *J Acoust Soc Am*, 49(2):467–477, 1971.

[63] C. M. Liberman. Auditory-nerve response from cats raised in a low-noise chamber. *J Acoust Soc Am*, 63(2):442–455, 1978.

[64] C. M. Liberman. Morphological differences among radial afferent fibers in the cat cochlea: an electron-microscopic study of serial sections. *Hear Res*, 3(1):45–63, 1980.

[65] C. M. Liberman. Single-neuron labeling in the cat auditory nerve. *Science*, 216(4551):1239–1241, 1982.

[66] C. M. Liberman. Physiology of cochlear efferent and afferent neurons: direct comparisons in the same animal. *Hear Res*, 34(2):179–191, 1988.

[67] C. M. Liberman. Central projections of auditory-nerve fibers of differing spontaneous rate. I. Anteroventral cochlear nucleus. *J Comp Neurol*, 313(2):240–258, 1991.

[68] L. D. Liberman and C. M. Liberman. Dynamics of cochlear synaptopathy after acoustic overexposure. *J Assoc Res Otolaryngol*, 16(2):205–219, 2015.

[69] L. D. Liberman, H. Wang, and C. M. Liberman. Opposing gradients of ribbon size and AMPA receptor expression underlie sensitivity differences among cochlear-nerve/hair-cell synapses. *J Neurosci*, 31(3):801–808, 2011.

[70] H. H. Lim, C. Yit, and C. M. Graeme. Forward masking patterns produced by intracochlear electrical stimulation of one and two electrode pairs in the human cochlea. *J Acoust Soc Am*, 86(3):971–980, 1989.

[71] Edward Lobarinas, Richard Salvi, and Dalian Ding. Insensitivity of the audiogram to carboplatin induced inner hair cell loss in chinchillas. *Hear Res*, 302:113–120, 2013.

[72] E. A. Lopez-Poveda and P. Barrios. Perception of stochastically undersampled sound waveforms: a model of auditory deafferentation. *Front Neurosci*, 7, 2013.

[73] C. A. Makary, J. Shin, S. G. Kujawa, C. M. Liberman, and S. N. Merchant. Age-related primary cochlear neuronal degeneration in human temporal bones. *J Assoc Res Otolaryngol*, 12(6):711–717, 2011.

[74] O.N. Markand. Brainstem auditory evoked potentials. *J Clinical Neurophys*, 11(3):319–342, 1994.

[75] R. Meddis and L.P. O'Mard. A computer model of the auditory-nerve response to forward-masking stimuli. *J Acoust Soc Am*, 117(6):3787–3798, 2005.

[76] J.R. Melcher and N.Y. Kiang. Generators of the brainstem auditory evoked potential in cat. III: Identified cell populations. *Hear Res*, 93:52–71, 1996.

[77] Curt Mitchell, David S Phillips, and Dennis R Trune. Variables affecting the auditory brainstem response: audiogram, age, gender and head size. *Hearing research*, 40(1):75–85, 1989.

[78] D.R. Moore, S. Rosen, D.E. Bamiou, N.G. Campbell, and T. Sirimanna. Evolving concepts of developmental auditory processing disorder (APD): a British Society of Audiology APD special interest group 'white paper'. *Int. J Audiol.*, 52:3–13, 2013.

[79] M. Muller and Robertson D. Relationship between tone burst discharge pattern and spontaneous firing rate of auditory nerve fibres in the guinea pig. *Hear Res.*, 57:63–70, 1991.

[80] O. D. Murnane, B. A. Prieve, and E. M. Relkin. Recovery of the human compound action potential following prior stimulation. *Hear Res.*, 124:182–189, 1998.

[81] A. R Møller and P. J Jannetta. Neural generators of the auditory brainstem response. The auditory brainstem response. *J Acoust Soc Am*, pages 13–31, 1985.

[82] B.A. Nayagam, M.A. Muniak, and D.K. Ryugo. The spiral ganglion: connecting the peripheral and central auditory systems. *Hear Res.*, 278(1):2–20, 2011.

[83] S. T. Neely, M.P. Gorga, and W. Jesteadt. Latency of auditory brain-stem responses and otoacoustic emissions using tone-burst stimuli. *J Acoust Soc Am*, 83:652–656, 1988.

[84] P. C. Nelson and L. H. Carney. A phenomenological model of peripheral and central neural responses to amplitude-modulated tones. *J Acoust Soc Am*, 116(4):2173–2186, 2004.

[85] P. C. Nelson, M. S. Zachary, and Young E. D. Wide-dynamic-range forward suppression in marmoset inferior colliculus neurons is generated centrally and accounts for perceptual masking. *J Acoust Soc Am*, 29(8):2553–2562, 2009.

[86] D. Oertel, R. Bal, S.M. Gardner, P.H. Smith, and P.X. Joris. Detection of synchrony in the activity of auditory nerve fibers by octopus cells of the mammalian cochlear nucleus. *Proc Natl Acad Sci U S A*, 97(22):11773–11779, 2000.

[87] A.R. Palmer and Russellm I.J. Phase-locking in the cochlear nerve of the guinea-pig and its relation to the receptor potential of inner hair-cells. *Hear Res*, 24(1):1–15, 1986.

[88] L. Parkkonen, N. Fujiki, and J. P. Mäkelä. Sources of auditory brainstem responses revisited: contribution by magnetoencephalography. *Hum Brain Mapp*, 30(6):1772–1782, 2009.

[89] J. Pinheiro and D. Bates. *Mixed-effects models in S and S-PLUS*. Springer-Verlag, New York, NY, 2000.

[90] Christopher J Plack, Andrew J Oxenham, and Richard R Fay. *Pitch: neural coding and perception*. New York: Springer, 2005.

[91] C.J. Plack, D. Baker, and G. Prendergast. Perceptual consequences of "hidden" hearing loss. *Trends Hear*, 18, 2014.

[92] C.J. Plack and A. J. Oxenham. Basilar-membrane nonlinearity and the growth of forward masking. *J Acoust Soc Am*, 103(3):1598–1608, 1998.

[93] D. W. Purcell, S. M. John, B. A. Schneider, and T. W. Picton. Human temporal auditory acuity as assessed by envelope following responses. *J Acoust Soc Am*, 116(6):3581–3593, 2004.

[94] S. Puria. Measurements of human middle ear forward and reverse acoustics: Implications for otoacoustic emissions. *J Acoust Soc Am*, 113(5):2773–2789, 2003.

[95] E. M. Relkin and J. R. Doucet. Recovery from prior stimulation. I: Relationship to spontaneous firing rates of primary auditory neurons. *Hear Res.*, 55(2):215–222, 1991.

[96] E. M. Relkin and J. R. Doucet. Recovery of the compound action potential following prior stimulation: evidence for a slow component that reflects recovery of low spontaneous-rate auditory neurons. *Hear Res.*, 83(1):183–189, 1995.

[97] E. M. Relkin and R. L. Smith. Forward masking of the compound action potential: thresholds for the detection of the NI peak. *Hear Res.*, 53:131–140, 1991.

[98] E. M. Relkin and Turner C. W. A reexamination of forward masking in the auditory nerve. *J Acoust Soc Am*, 84:584–591, 1988.

[99] W.S. Rhode, Geisler C., and D. Kennedy. Auditory nerve fiber response to wide-band noise and tone combinations. *J. Neurophysiol*, 41:692–704, 1978.

[100] W.S. Rhode and P.H. Smith. Characteristics of tone-pip response patterns in relationship to spontaneous rate in cat auditory nerve fibers. *Hear Res.*, 114:159–168, 1985.

[101] Filip Munch Rønne, Torsten Dau, James Harte, and Claus Elberling. Modeling auditory evoked brainstem responses to transient stimuli. *J Acoust Soc Am*, 131(5):3903–3913, 2012.

[102] D. Ruggles and B.G. Shinn-Cunningham. Spatial selective auditory attention in the presence of reverberant energy: Individual differences in normal-hearing listeners. *J Assoc Res Otolaryngol*, 12(3):395–405, June 2011.

[103] D.K. Ryugo. Projections of low spontaneous rate, high threshold auditory nerve fibers to the small cell cap of the cochlear nucleus in cats. *Neurosci.*, 154(1):114–126, 2008.

[104] B. G. Schaalje, J. B. Mcbride, and G. W. Fellingham. Adequacy of approximations to distributions of test statistics in complex mixed linear models. *J Agricult, Biol, Environ Stats.*, 7(4):512–524, 2002.

[105] R. Schaette and D. McAlpine. Tinnitus with a normal audiogram: physiological evidence for hidden hearing loss and computational model. *J Neuro.*, 31(38):13452–13457, 2011.

[106] R. A. Schmiedt, J. H. Mills, and F. A. Boettcher. Age-related loss of activity of auditory-nerve fibers. *J Neurophysiol*, 76(4):2799–2803, 1996.

[107] Yevgeniya Sergeyenko, Kumud Lall, M Charles Liberman, and Sharon G Kujawa. Age-related cochlear synaptopathy: an early-onset contributor to auditory functional decline. *J Neurosci*, 33(34):13686–13694, 2013.

[108] S. A. Shamma, M. Elhilali, and C. Micheyl. Temporal coherence and attention in auditory scene analysis. *Trends Neurosci*, 34(3):114–123, 2011.

[109] M. Sharma. *Translational Perspectives in Auditory Neuroscience: Hearing Across the Life Span-Assessments and Disorders.* International journal of audiology, 2013.

[110] C. A. Shera. Mechanisms of mammalian otoacoustic emission and their implications for the clinical utility of otoacoustic emissions. *Ear and hear*, 25(2):86–97, 2004.

[111] S.E. Shore. Influence of centrifugal pathways on forward masking of ventral cochlear nucleus neurons. *J Acoust Soc Am*, 104(1):378–389, 1998.

[112] H. Simon, R.D. Frisina, and J.P. Walton. Age reduces response latency of mouse inferior colliculus neurons to AM sounds. *J Acoust Soc Am*, 116(1):469–477, 2004.

[113] G.C. Stamper and T.A Johnson. Auditory Function in Normal-Hearing, Noise-Exposed Human Ears. *Ear Hear*, 2014.

[114] M. A. Stellmack, A. J. Byrne, and N. F. Viemeister. Extracting binaural information from simultaneous targets and distractors: Effects of amplitude modulation and asynchronous envelopes. *J Acoust Soc Am*, 128(3):1235–1244, 2010.

[115] O. Strelcyk and T. Dau. Relations between frequency selectivity, temporal fine-structure processing, and speech reception in impaired hearing. *J Acoust Soc Am*, 125(5):3328–3345, May 2009.

[116] Kinga Szydlowska and Michael Tymianski. Calcium, ischemia and excitotoxicity. *Cell calcium*, 47(2):122–129, 2010.

[117] A.N. Temchin, R.C. Nola, and M.A. Ruggero. Threshold tuning curves of chinchilla auditory nerve fibers. II. Dependence on spontaneous activity and relation to cochlear nonlinearity. *J Neurophys*, 100(5):2899–2906, 2008.

[118] S. Verhulst, H. M. Bharadwaj, G. Mehraei, C. A. Shera, and B. G. Shinn-Cunningham. Functional modeling of the human auditory brainstem response to broadband stimulation. *J Acoust Soc Am*, 138(3):1637–1659, 2015.

[119] S. Verhulst, T. Dau, and C.A. Shera. Nonlinear time-domain cochlear model for transient stimulation and human otoacoustic emission. *J Acoust Soc Am*, 136(6):3842–3848, 2012.

[120] Neal F Viemeister. Intensity coding and the dynamic range problem. *Hear Res*, 34(3):267–274, 1988.

[121] J. Walton, M. Orlando, and Burkard R. Auditory brainstem response forward-masking recovery functions in older humans with normal hearing. *Hear Re.*, 127(1):86–94, 1999.

[122] J. P. Walton, R.D. Frisina, and L.R. Meierhans. Sensorineural hearing loss alters recovery from short-term adaptation in the C57BL/6 mouse. *Hear Re.*, 88(1):19–26, 1995.

[123] L.A. Westerman and R.L. Smith. A diffusion model of the transient response of the cochlear inner hair cell synapse. *J Acoust Soc Am*, 83(6):2266–2276, 1988.

[124] F.L. Wightman and D.J. Kistler. The dominant role of low-frequency interaural time differences in sound localization. *J Acoust Soc Am*, 91(3):1648–1661, March 1992.

[125] I .M. Winter, N. Itatani, S. Bleeck, and N. Ingham. Enhancement of forward suppression begins in the ventral cochlear nucleus. *J Acoust Soc Am*, 135(4):2347, 2014.

[126] Y. Ye, D.G. Machado, and D.O. Kim. Projection of the marginal shell of the anteroventral cochlear nucleus to olivocochlear neurons in the cat. *J Comp Neurol*, 420:127–138, 2000.

[127] E. D. Young and P. E. Barta. Rate responses of auditory nerve fibers to tones in noise near masked threshold. *J Acoust Soc Am*, 79(2):426–442, 1986.

[128] F.G. Zeng, K.M. Martino, F.H. Linthicum, and S.D. Soli. Auditory perception in vestibular neurectomy subjects. *Hear Res*, 142(1):102–112, 2000.

[129] X. Zhang and L. H. Carney. Analysis of models for the synapse between the inner hair cell and the auditory nerve. *J Acoust Soc Am*, 118(3):1540–1553, 2005.

[130] X. Zhang, M. G. Heinz, I C. Bruce, and L. H. Carney. A phenomenological model for the responses of auditory-nerve fibers: I. Nonlinear tuning with compression and suppression. *J Acoust Soc Am*, 109(2):648–670, 2001.

[131] Muhammad SA Zilany and Ian C Bruce. Modeling auditory-nerve responses for high sound pressure levels in the normal and impaired auditory periphery. *J Acoust Soc Am*, 120(3):1446–1466, 2006.

[132] Muhammad SA Zilany, Ian C Bruce, and Laurel H Carney. Updated parameters and expanded simulation options for a model of the auditory periphery. *J Acoust Soc Am*, 135(1):283–286, 2014.

[133] Muhammad SA Zilany, Ian C Bruce, Paul C Nelson, and Laurel H Carney. A phenomenological model of the synapse between the inner hair cell and auditory nerve: long-term adaptation with power-law dynamics. *J Acoust Soc Am*, 126(5):2390–2412, 2009.